Zeitschrift: IABSE reports = Rapports AIPC = IVBH Berichte
Band: 37 (1982)

Rubrik: Theme 7: Cables, prestressing strands, composite structures

THEME 7

Cables, Prestressing Strands, Composite Structures

Câbles, câbles de précontrainte, constructions mixtes

Kabel, Vorspannlitzen, Verbundbauwerke

Leere Seite
Blank page
Page vide

Fatigue Behaviour of a Composite, Steel-Concrete Girder

Comportement à la fatigue d'une poutre mixte acier-béton

Ermüdungsverhalten eines Stahl-Beton-Verbundträgers

P.C. BHASIN
Ministry of Shipping and Transport
New Delhi, India

D.S. PRAKASH RAO
Structural Engineering
Research Centre
Roorkee, India

M.G. TAMHANKAR
Structural Engineering
Research Centre
Roorkee, India

S.P. SHARMA
Structural Engineering
Research Centre
Roorkee, India

SUMMARY
Tests were carried out to determine the behaviour of a steel-concrete composite girder, with basket type shear connectors, under pulsating loads. Shear connector capacity was calculated according to various codes of practice and compared with the test results. The girder was only loaded beyond the computed elastic limit after one million cycles had been applied below yield. Full composite action was exhibited up to failure.

RESUME
Des essais ont été effectués pour déterminer le comportement d'une poutre mixte, acier-béton, avec des connecteurs de type „basket", sous charges pulsatives. La résistance ultime des connecteurs a été calculée selon différentes normes et comparée aux résultats d'essais. La poutre a été sollicitée au delà de la limite élastique calculée après avoir subi un million de cycles de charges en dessous de la plastification. L'effet mixte complet a été observé jusqu'à la rupture.

ZUSAMMENFASSUNG
Der Beitrag behandelt dynamische Versuche an einem Verbundträger mit halbkreisförmigen Schubdübeln. Der Schubwiderstand der Dübel wurde unter Anwendung verschiedener Normen berechnet und mit den Versuchsresultaten verglichen. Nach einer Ermüdungsbelastung von einer Million Lastwechsel im elastischen Bereich wurde der Versuchsträger zyklischen Belastungen oberhalb des rechnerischen elastischen Bereichs unterworfen. Es wurde volles Verbundverhalten bis zum Bruch beobachtet.

1. INTRODUCTION

Steel concrete composite construction is extensively used in buildings as well as bridge superstructures. Of late, the composite construction is finding application in long span bridges too. The second Hooghly bridge in Calcutta, India when completed is expected to be the longest composite structure with its 457 m cable stayed main span. The interface connection between concrete and steel forms an important feature of the design in composite structures. Basically the connection has to ensure composite action through the longitudinal shear at the interface at all the stages of loading. This feature assumes added importance in bridge structures subject to varying loads in their life time. Several tests are reported on composite beams. However, most of them pertain to the stud connectors and under static loads. Tests are carried out on basket type connector shown in Fig.1 to determine its capacity in longitudinal shear. The test results are compared with the values predicted by various codes of practice.

These results are verified to check the integral action between steel beam and concrete slab in a composite girder. The girder was subjected to one million loading cycles, the amplitude varying upto the working load, then subjected to cyclic loading beyond elastic limit and loaded to failure.

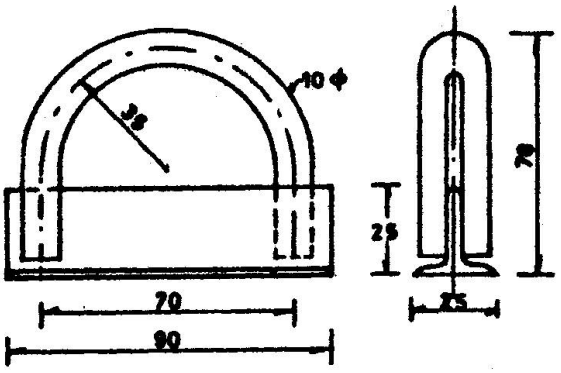

Fig.1 Basket type shear connector

2. STRENGTH OF SHEAR CONNECTORS

2.1 Specifications in various codes of practice

Emperical or semi-emperical formulae are available in several codes of practice to assess the capacity of the shear connectors subject to longitudinal shear. However, the formulae are not usually of general nature and have rather limited applications. These formulae have to be necessarily conservative to prevent the failure in longitudinal shear before the advent of the flexural failure of the structure. Specifications for standard tests are also not available in many codes of practice.

BS 5400, Part 5 [1] and CP 117 Part 1 [2] specify tests on standard specimen. The lowest value of the failure load of three standard specimen is to be taken for design purposes. The specified live load factor against connector failure is to be at least 2.5 as per CP 117 and the average force on shear connectors should not exceed 80% of the ultimate capacity as per CP 117 as well as BS 5400. The Canadian Standard [3] specifies a factor of safety as a function of the live load and dead load shears and moments. The AASHO specifications [4] incorporate a factor in the strength formula to account for the number of loading cycles. However, these are available only for channels and studs. The German code of practice [5] insists on making computations with the ultimate load factors even for constructional loads. The shear stress on the possible failure plane around the shear connector should not exceed the values specified in the code. The capacity of the shear connector is estimated by considering the enlarged area of the connector upto the next connector at an angle $\tan^{-1} 1/5$. These values are to be reduced by a factor 2/3 for structures subjected to dynamic loads like bridges. The concrete cover requirements according to the German standard are rather liberal. Whereas the British code requires a

minimum cover of 25 mm at the top of the connector, the German standard allows the studs to be flush with the concrete surface if corrosion is not a problem. The Indian Roads Congress code of practice [6] provides a formula to estimate the strength of the shear connector based on the strength of concrete and as a function of the cube root of the ratio of area of failure plane and the enclosed area of the connector.

2.2 Tests on the shear connector

Tests on standard specimen based on BS 5400 were carried out to assess the ultimate capacity of the basket type shear connectors. One shear connector was welded to each side of the central steel I-section. The slip of the central steel girder relative to the concrete blocks during the push out tests on the specimen S1, S2 and S3 is shown in Fig.2. Mould oil was applied on the steel girder surface to prevent the bond at the interface. All the three specimen exhibited more or less the same load displacement characteristics in the initial stages. The specimen S2 and S3 were subjected to about 30,000 cycles of load varying from 20 to 80 kN before conducting the test to failure. The fourth specimen S4 did not show any change in load displacement characteristics after 50,000 cycles of load varying from 38 to 80 kN. The typical failure of the specimen is shown in Fig.3. The failure in S2 and S3 was through crushing of concrete whereas the shear connector gave way in S1. The changes in concrete block in the vicinity of the shear connectors was sought to be monitored by measuring ultrasonic pulse velocity through the blocks and the steel section. However, this was not successful as the ultrasonic tester was showing erratic readings and hence not pursued further.

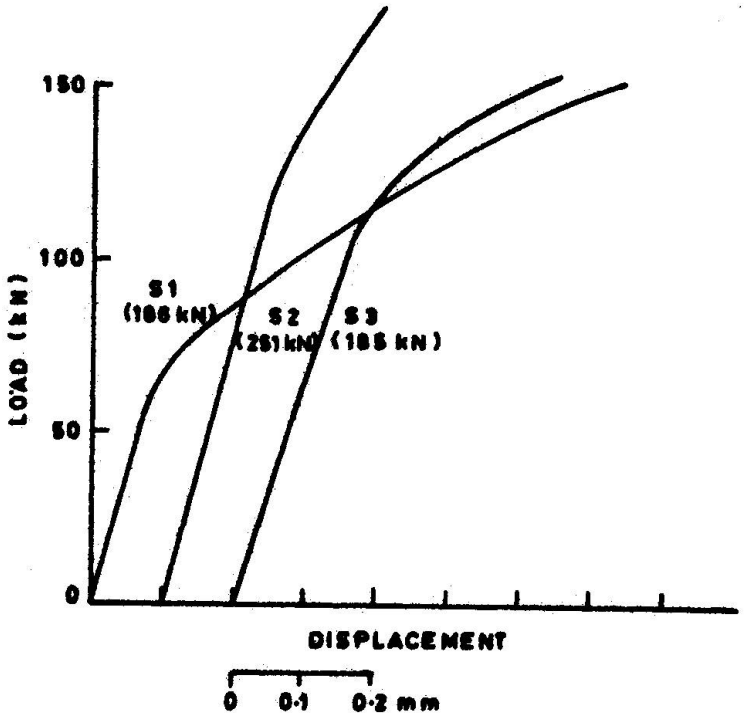

Fig.2 Load displacement curves of the standard specimen S1,S2 and S3. The figures in the brackets indicate the failure load

The capacity of the shear connectors computed according to various codes of practice is given in Table 1 for comparison. It can be seen that there is wide disparity in the values predicted by various codes of practice. The IRC code of practice appears to be the most conservative, whereas the values computed as per the German code appear to be on higher side than the test results.

Table 1 Strength of the shear connector based on various codes of practice

S.No.	Code of practice	Allowable load (kN) during working	at ultimate
1	BS 5400 [1]	37.0	74.0
2	CSA Standard [3]	41.8	-
3	DIN 1078 [5]	-	123.9*
4	IRC Code [6]	25.6	63.9
5	Laboratory tests (as per BS 5400)	-	92.5

* 82.6 kN for structures subject to dynamic loads, such as bridges

3. DESIGN OF THE TEST BEAM

The test beam was designed based on working stress method for a live load of 150 kN over two points as shown in Fig.4. The average strength of three concrete cubes of 150 mm cast along with the beam was 17 N/mm^2. The yield strength of the steel girder was assumed to be 260 N/mm^2 and the allowable strength as per IRC code of practice was 140 N/mm^2. The top slab had a nominal reinforcement of 6 mm bars at 160 mm in the transverse direction and 8 bars of 6 mm in the longitudinal direction, Fig.4.

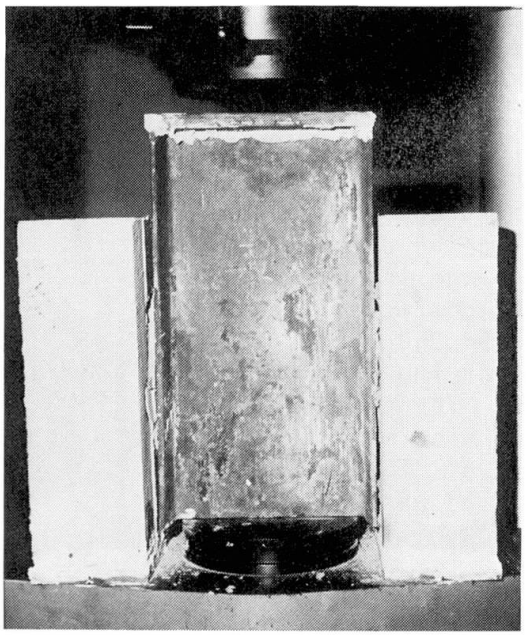

Fig.3 Typical failure at the interface of the standard specimen

The steel girder was greased well so that the bond between steel and concrete was effectively prevented. The integral action was possible only through the shear connectors provided at 160 mm spacing throughout the length of the girder. The ratio of Young's modulii of elasticity for steel and concrete was assumed to be 9 for calculation purposes. It may be mentioned, however, that variation in the value of the

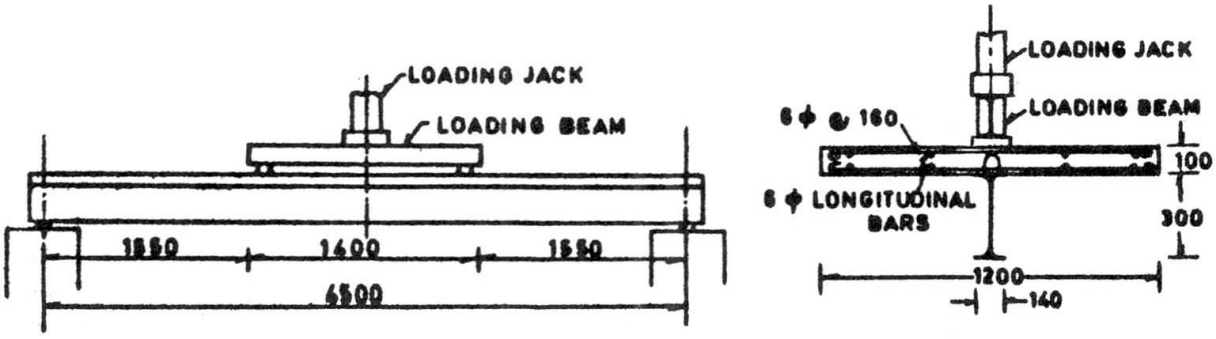

Fig.4 Longitudinal-and cross-sections of the composite girder

Young's modulus of concrete affects the computed stresses and deflections to a small degree.

4. TESTS ON THE COMPOSITE GIRDER

The composite girder was tested under static load at the start of the test as well as periodically during the fatigue loading. The deflections of the girder were measured by means of dial gages. These values compared well with the predicted deflection profile. The girder was then subjected to one million cycles of load varying from 40 to 150 kN at a frequency of 250 cycles per minute. This range of loading produces an average computed force varying from 19 kN to 36 kN on the shear connectors. The upper limit of the average force on the shear connectors is more than the value predicted by the IRC code but close to the value as per BS 5400. This range of loading was adopted to simulate the effects of force on shear connectors in a bridge structure which will be subjected to a constant force under dead load and a varying force due to live loads. The test set up is shown in Fig.5.

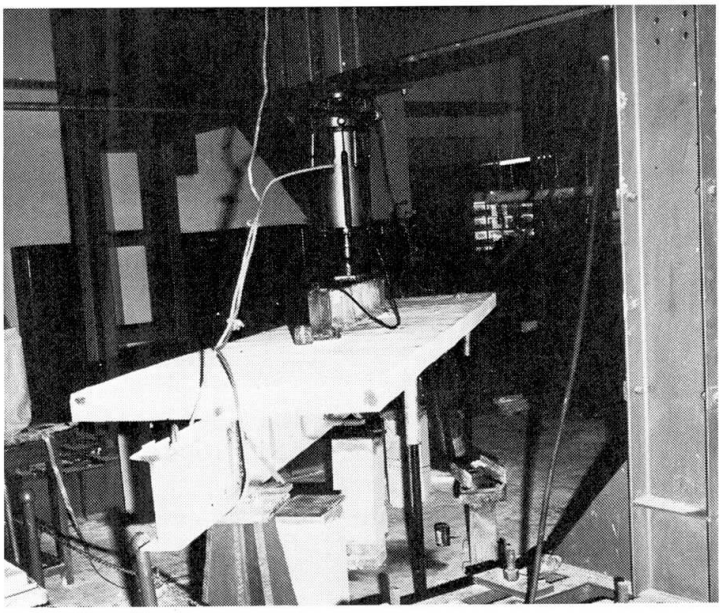

Fig.5 Test set up showing the girder and the pulsator

The deflections of the girder at mid span and one metre from the supports are shown in Fig.6 at the start of the test and after application of the cyclic load. The cyclic load does not seem to alter the behaviour of the beam appreciably. The concrete slab did not show any signs of distress at the interface.

The girder was then repeatedly loaded beyond the computed elastic limit as shown in Fig.7. The first load cycle of 250 kN produced a residual mid span deflection of about 0.2 mm compared to the elastic deflection of 5.1 mm under 150 kN at the end of one million cycles

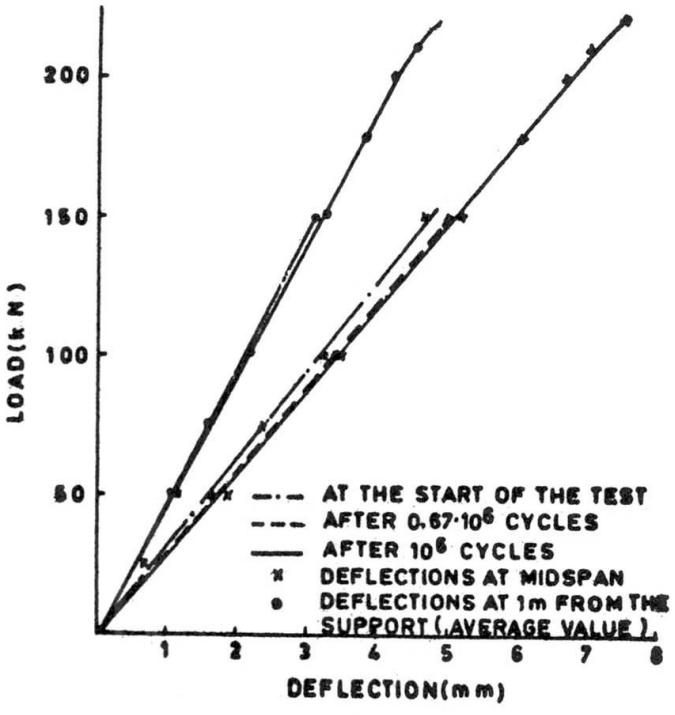

Fig.6 Load deflection curves of the girder

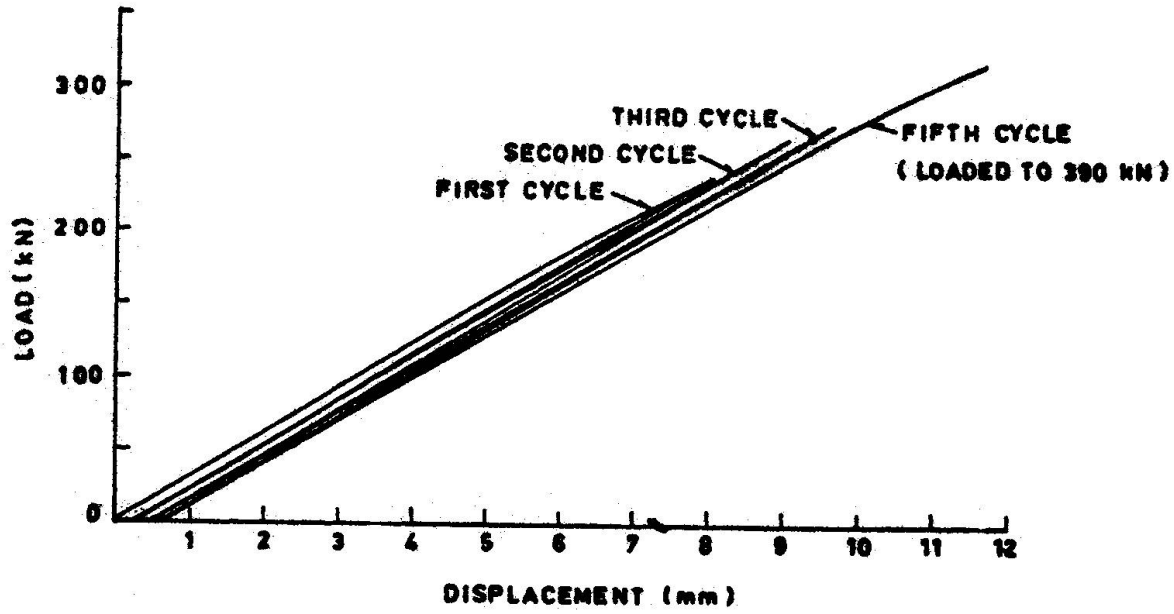

Fig.7 Mid span load deflection curves of the girder during cyclic loading beyond elastic limit

of loading. The residual mid span deflection was almost zero after another three cycles upto 270 kN.

The horizontal displacement of the concrete slab relative to the steel beam was monitored during the cyclic loading by means of dial gages set up at the ends of the girder, Fig.8. The relative displacements were very small in the beginning but grew at a large rate beyond 200 kN load. However, the recovery was almost full when the load was removed. During subsequent loadings the behaviour was similar, indicating that the average behaviour of the shear connectors was still elastic.

During the ultimate load test the left end of the slab started showing larger relative displacement than the other end. The right end of the slab showed no increase in the displacement between 200 kN and about 300 kN when the displacement started increasing at a larger rate than initial. The left end showed a steady increase upto about 310 kN when the relative displacement showed an increasing rate. The failure of the girder took place at 435 kN with the concrete in the vicinity of the shear connectors at the left end giving way. The concrete slab split in the longitudinal direction over the interface and the girder could not take any more load, Fig.9.

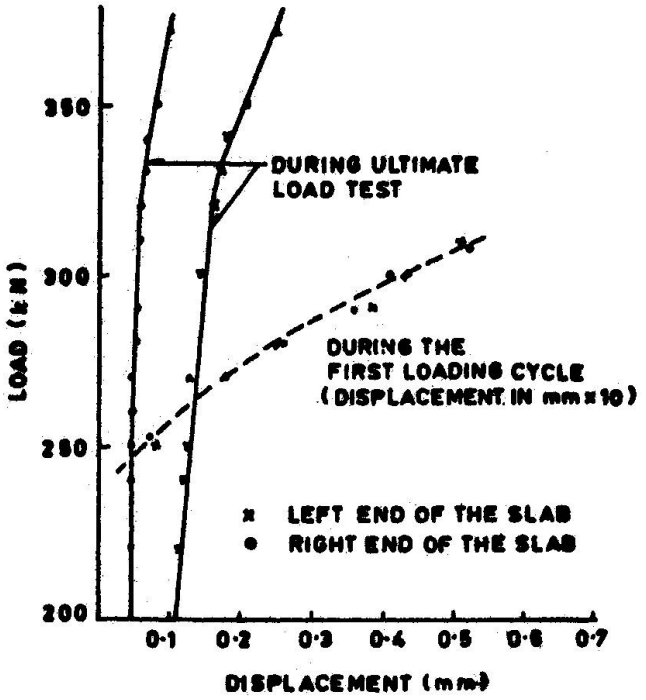

Fig.8 Horizontal displacement of the concrete slab relative to beam

5. DISCUSSION

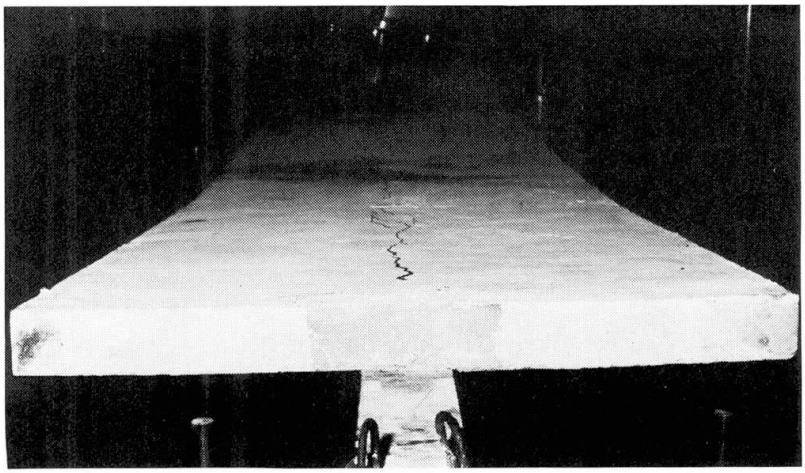

Fig.9 Longitudinal cracks on the concrete slab surface along the line of shear connectors at the ultimate load

The chief objective of the tests was to study the behaviour of basket type shear connectors under fatigue load by simulating the conditions in a composite bridge deck. The capacities of the shear connector at working and ultimate loads as per various codes of practice differ considerably from each other. The codes of practice usually refer to limited types of connectors and actual tests are required for other types. The capacity of the shear connector was adopted from the standard tests in this case. The composite girder exhibited usual behaviour even after one million cycles of loading and subsequent cyclic loading beyond computed elastic limit. This indicates that the shear connectors behaved well though the integral action was solely through shear connectors as the bond between steel beam and concrete slab had been destroyed by application of grease. The final failure was brought about by the splitting of the concrete slab along the line of shear connectors. The average load on the shear connectors at the failure stage works out to be about 170 kN, almost double that of the standard test value. It is likely that the capacity of the shear connector gets influenced by the presence of other connectors apart from the interaction between longitudinal shear and flexural compression. Influence of the connector spacing is taken into account by the German code of practice [5]. However, the average load per connector is still higher than the value computed as per the German code, Table 1. Further investigations into these aspects are necessary.

6. ACKNOWLEDGEMENT

The tests reported here were carried out at the Structural Engineering Research Centre, Roorkee, India.

REFERENCES

1. BS 5400, Steel, Concrete and Composite Bridges, British Standards Institution, 1979.

2. CP 117, Composite Construction in Structural Steel and Concrete, Part I, British Standards, 1965

3. CSA Standard S6-1966, Design of Highway Bridges, Canadian Standards Association

4. AASHO, Standard Specifications for Highway Bridges, adopted by the American Association of State Highway Officials, 1973

5. Beton-Kalender, Part II, Wilhelm Ernst & Sohn, Berlin, 1979, pp.354-382

6. IRC, Standard Specifications and Code of Practice for Road Bridges, Section VI, The Indian Roads Congress, 1966

Leere Seite
Blank page
Page vide

Comportement à la fatigue des poutres mixtes préfléchies

Ermüdungsverhalten vorverformter Doppelverbundträger

Fatigue Behaviour of Composite Preflexed Beams

G. FIRQUET
Directeur Technique
PREFLEX SA
Bruxelles, Belgique

RESUME

Les poutres mixtes préfléchies, judicieusement présollicitées lors de leur fabrication, présentent l'avantage que les amplitudes de variation des contraintes sous charges variables y sont beaucoup plus faibles que dans les poutres non présollicitées. Par une analyse de l'évolution des contraintes dans chacun de ces deux types de poutres, on montre l'incidence de cette réduction sur la résistance à la fatigue. La description de deux essais en laboratoire et l'analyse du comportement des poutres d'un ouvrage réel étayent l'argumentation alors que la conclusion montre l'économie obtenue par l'emploi de ce type de poutres.

ZUSAMMENFASSUNG

Vorverformte Verbundträger, sinnvoll vorbelastet während ihrer Herstellung, haben den Vorteil, dass die Spannungsdifferenz zwischen ruhender und voller Belastung im Vergleich mit dem nicht vorverformten Träger wesentlich verringert wird. Mit einer Spannungsuntersuchung beider Arten Träger wird diese Auswirkung auf den Ermüdungswiderstand dargelegt. Die Ergebnisse zweier Dauerversuche und der Bericht über das Verhalten eines ausgeführten Bauwerks untermauern die Berechnungen. Die Schlussfolgerungen zeigen die Wirtschaftlichkeit solcher Träger.

SUMMARY

Composite beams properly preflexed during their fabrication offer the advantage that the range of stress variation under live loads is much smaller than in non-preloaded beams. The resulting effect on the fatigue resistance is shown by analysis of the development of stresses in both types of beam. This analysis is supported by the description of two laboratory tests and the examination of the behaviour of real beams in situ. The conclusion shows the economies made possible by these types of beams.

1. INTRODUCTION

Dans le début des années 1950, lors des recherches en vue de la mise au point d'un nouveau type de poutres élancées associant l'acier et le béton et bien qu'à cette époque le problème de la résistance en fatigue n'était pas encore à l'ordre du jour comme il l'est aujourd'hui, Monsieur A. Lipski, Ingénieur-Conseil à Bruxelles, inventeur de la poutre PREFLEX,a créé une poutre dont la résistance en fatigue dépasse largement celle des poutres mixtes déjà connues.

Par le procédé de fabrication lui-même, il a obtenu une réduction sensible de la variation des contraintes tout en continuant à utiliser au maximum la capacité de l'acier utilisé.

Ce procédé consiste en une mise en charge d'un profilé métallique suivie de l'exécution du béton d'enrobage de sa semelle tendue, les charges appliquées n'étant relâchées qu'après durcissement de ce béton.

2. DESCRIPTION DU PROCEDE

La poutrelle nue, posée sur ses deux appuis d'extrémité est soumise à des charges dont la position et l'intensité sont choisies de telle sorte que le diagramme des contraintes de traction à la fibre extrême tendue soit l'enveloppe de celui des contraintes de service (Fig. 1-a)

Dans cet état chargé, la semelle tendue de la poutre est enrobée de béton (Fig. 1-b) puis, lorsque le béton a atteint une résistance suffisante, les charges appliquées sont enlevées. La poutre revient partiellement vers sa position de départ tandis que le béton entourant sa semelle tendue se met en compression (Fig. 1-c).

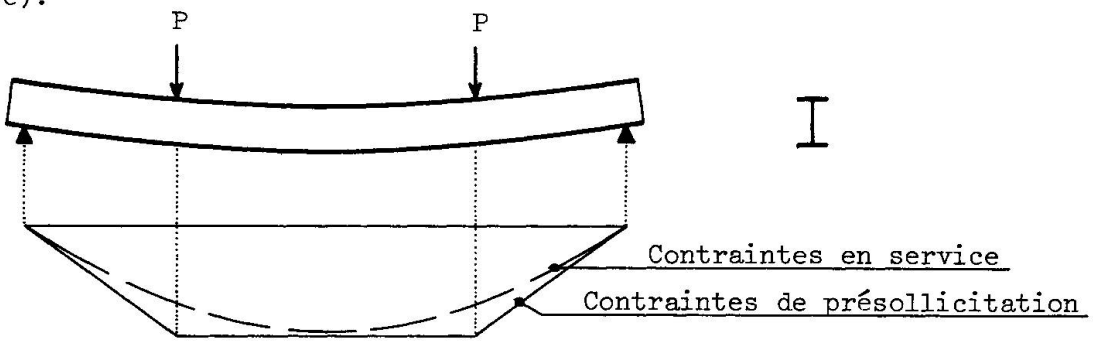

Fig. 1-a

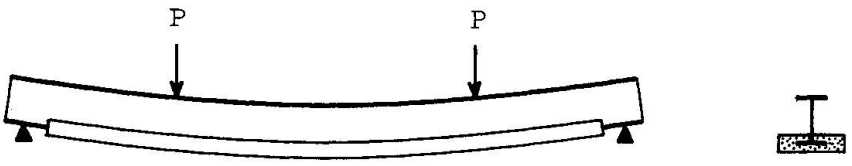

Fig. 1-b

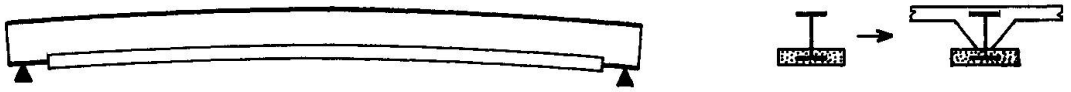

Fig. 1-c

Après la mise en place de la poutre dans l'ouvrage, son enrobage est éventuellement complété par du béton entourant l'âme et par l'exécution d'une dalle collaborante au niveau de la semelle comprimée.

3. COMPARAISON DES EVOLUTIONS DES CONTRAINTES

Dans l'exposé qui suit, nous nous référons à un cas concret : une poutre de pont route, en acier AE 355 D, qui servira à établir une comparaison au point de vue fatigue entre une poutre préfléchie et une poutre identique mais non présollicitée.

Les sollicitations maxima auxquelles cette poutre doit résister en service sont les suivantes :
- Moment dû au poids propre du tablier : M_1 = 2.733 KNm
- Moment dû aux surcharges fixes : M_2 = 783 KNm
- Moment dû aux surcharges mobiles : M_3 = 2.565 KNm

3.1 Evolution des contraintes dans la poutre préfléchie

Le diagramme de la figure 2 donne, en trait plein, l'évolution des contraintes de traction à la fibre extrême tendue à mi-portée de la poutre

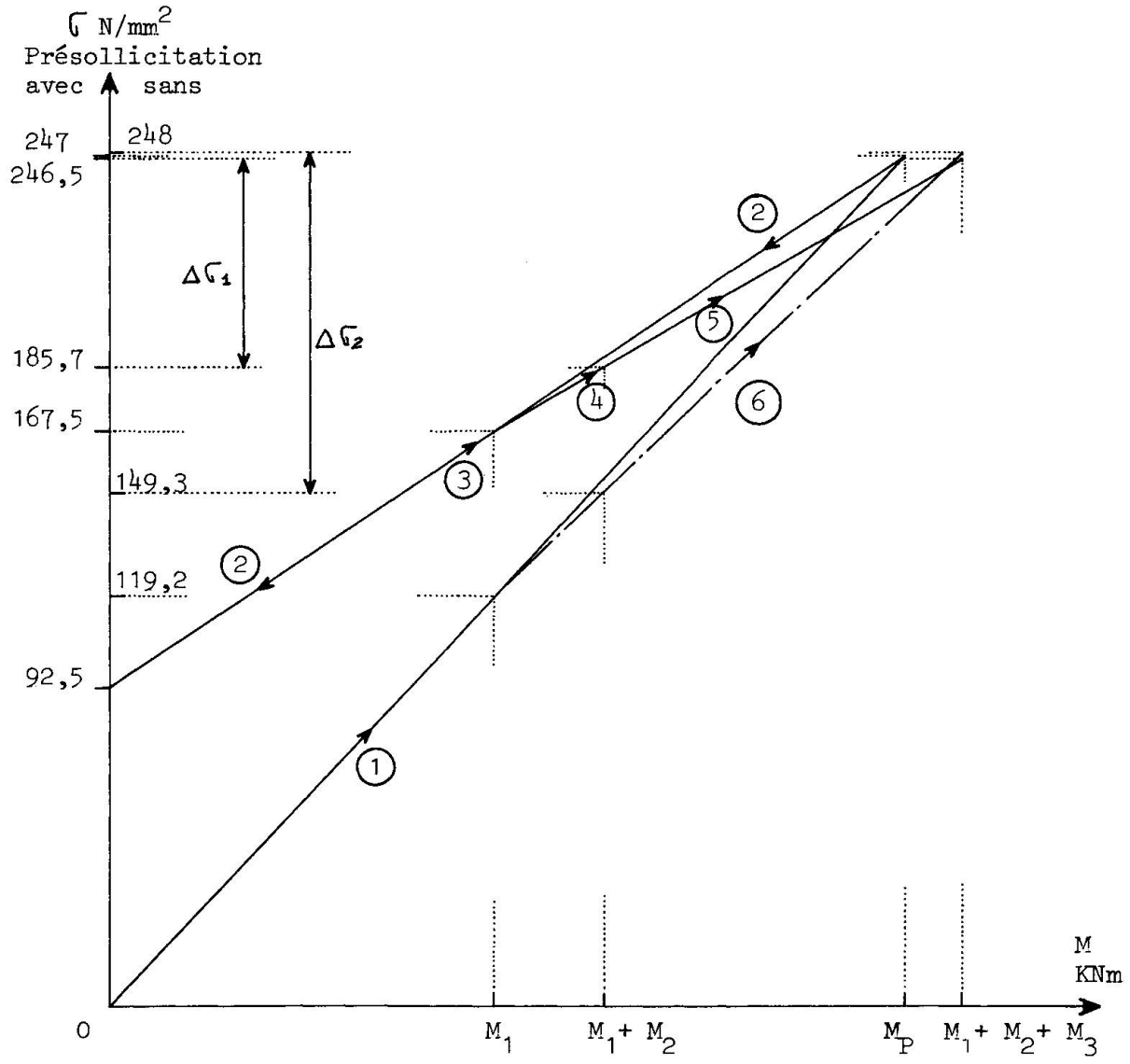

Fig. 2

La poutre non enrobée est tout d'abord soumise à un moment de préflexion M_p = 5664 KNm choisi de façon telle que la contrainte induite dans l'acier soit égale à la contrainte de service résultant, pour cet ouvrage, du profil choisi, soit 247 N/mm^2.* Lors de la mise en charge, le point représentatif de la contrainte parcourt la droite (1) du diagramme.

Après durcissement du béton d'enrobage de la semelle tendue, les charges de préflexion sont annulées, la contrainte évolue le long de la droite (2) pour atteindre la valeur de 92,5 N/mm^2 sous charge nulle.

Sous l'effet du poids propre de la poutre et de celui du béton d'enrobage, le point représentatif remonte le long de la droite (2) jusqu'au point correspondant au moment M_1; la contrainte vaut alors 167,2 N/mm^2

A partir de ce point, la droite $\sigma = f(M)$ s'écarte de la droite (2) puisque la présence de la dalle collaborante a modifié les caractéristiques de la section. Aux sollicitations précédentes s'ajoutent d'abord l'effet des surcharges fixes (Moment M_2, trajet (4)) faisant passer la contrainte à 185,7 N/mm^2 puis finalement celui dû aux surcharges mobiles (Moment M_3, trajet (5)) qui nous amène à la contrainte maximum de service : 246,5 N/mm^2. L'amplitude maximum de variation des contraintes sous surcharges mobiles vaut $\Delta\sigma_1$ = 60,8 N/mm^2.

3.2 Evolution des contraintes dans la poutre non préfléchie

Le point représentatif de l'état $\sigma = f(M)$ se déplace d'abord le long de la droite (1) jusqu'au point d'abscisse M_1 correspondant à une contrainte de 119,2 N/mm^2. Compte tenu de la présence de la dalle de compression, il suit ensuite la droite (6) . Nous voyons que sous l'ensemble des charges fixes, σ vaut 149,3 N/mm^2 et que la contrainte maximum vaut 248 N/mm^2. L'écart de contrainte dû aux surcharges mobiles vaut donc ici $\Delta\sigma_2$ = 98,7 N/mm^2.

3.3 Comparaison des deux types de poutres

On remarque immédiatement la différence fondamentale entre les deux systèmes de poutre. Si la contrainte maximum de service est quasi la même dans les deux cas, il n'en va pas de même en ce qui concerne l'amplitude de la variation de contrainte qui n'atteint que 60,8 N/mm^2 pour la poutre préfléchie alors qu'elle monte à 98,7 N/mm^2 soit 62% de plus pour la poutre non présollicitée.

Si on reporte ces valeurs sur les courbes $\Delta\sigma$ – N telles qu'elles apparaissent dans les normes suisses par exemple, on trouve les nombres de cycles maxima suivants :

- Poutre préfléchie : Détail constructif E : Ne = 1,6 x 10^6
  D : Ne = 3,3 x 10^6 (à comparer aux 2 x 10^6 cycles imposés pour les routes principales)
  A_0, A_1, B, C : on se trouve sous la limite d'endurance, donc pas de problème de fatigue.
- Poutre non présollicitée : Détail constructif E : Ne = 0,375 x 10^6
  D : Ne = 0,700 x 10^6
  C : Ne = 1,50 x 10^6
  A_0, A_1, B : même conclusion que ci-dessus.

*N.B. Il est à noter que les normes belges autorisent pour les poutres préfléchies une contrainte maximum de service égale à 0,8 x Re.

La démonstration est nette, si besoin en était, du meilleur comportement en fatigue des poutres préfléchies.

Pour obtenir, avec une poutre non préfléchie, la même résistance en fatigue, il faudrait diviser toutes ses contraintes de traction dans le rapport 98,7/60,8 = 1,62.
C'est-à-dire qu'il faudrait renforcer sa section de façon telle que son module de résistance soit multiplié par ce même facteur, ce qui abaisserait sa contrainte maximum de service à 153 N/mm^2. Ce serait là bien mal utiliser un acier ayant une limite d'élasticité de 355 N/mm^2.

4. ESSAIS EN LABORATOIRE

Plusieurs essais de résistance à la fatigue ont été faits par divers laboratoires officiels pour confirmer le bien-fondé des conclusions tirées de la comparaison de l'évolution des contraintes dans chaque type de poutre.

4.1 Essai de Bruxelles

Une poutre HE 750, préfléchie, d'une portée de 14,50 m, complètement enrobée de béton et munie de butées d'adhérence soudées sur les semelles tendues et comprimées résiste aux sollicitations suivantes :

- 2.000.000 cycles de sollicitations entre 0,4 et 1 fois la charge de service.
- 1.180.000 cycles de sollicitations entre 0,85 et 1,5 fois la charge de service.

Aucune altération des qualités de résistance et d'élasticité de la poutre n'a été relevée au cours de l'essai.

Il est utile d'ajouter qu'il s'agissait d'une poutre en grandeur réelle analogue à celles devant servir à la couverture d'un tunnel destiné à supporter un trafic lourd (surcharge utile 25 KN/m^2).

4.2 Essai de Stuttgart

Une poutre HE 260 A complètement enrobée a subi sans dommage significatif les mises en charge suivantes :

- 2.030.000 cycles de mises en charge à la charge de service avec une amplitude de variation des contraintes de 46 N/mm^2.
- 2.053.000 cycles de mises en charge à 1,25 fois la charge de service avec une amplitude de variation des contraintes de 57,5 N/mm^2.

Elle fut ensuite soumise à une nouvelle mise en charge dynamique poussée jusqu'à 1,5 fois la charge de service avec un écart des contraintes de 69 N/mm^2.

La rupture due à 4 cratères de soudage situés dans la même section transversale (les détails de soudage ont été modifiés suite à cet essai) est intervenue après 1.277.000 cycles supplémentaires de mise en charge.

5. EXAMEN D'UN OUVRAGE REEL

Une série de poutres préfléchies ont été utilisées dans la construction d'une rampe pour tramways. Elles n'ont reçu aucun enrobage de béton à l'exception du béton précomprimé entourant leur aile tendue. Chaque passage d'un essieu sur une poutre y provoquait un accroissement de 29,9 N/mm^2 de la contrainte de traction; le croisement de deux essieux sur une même poutre augmentait cette contrainte de 59,8 N/mm^2.

Le décompte du nombre de passages de véhicules sur la rampe permet d'affirmer qu'au moment de sa mise hors service, suite à des transformations de l'ouvrage dont elle faisait partie, chaque poutre avait subi environ 13.000.000 de mises en charge totales (deux essieux) et 26.000.000 de mises en charge partielles (un essieu).
Après démontage de la rampe, les poutres ont été réutilisées comme éléments porteurs couvrant un tunnel construit à cet endroit en-dessous de la voirie.

6. CONCLUSIONS

Les considérations théoriques, les constatations faites lors des essais en laboratoire et les observations sur des ouvrages réels, en service depuis de nombreuses années montrent l'intérêt au point de vue comportement à la fatigue du recours à des procédés de fabrication qui réduisent l'amplitude des variations de contraintes en service.

Depuis la mise au point du procédé PREFLEX en 1951, plus de 300 ouvrages d'art, ponts-rails et ponts-route, ont été construits rien qu'en Belgique avec ce type de poutres, sans qu'aucun désordre ne se soit jamais produit. Il est d'ailleurs à souligner que dans les colloques consacrés à l'entretien et à la gestion des ouvrages d'art, il n'a jamais été question de ponts construits avec des poutres préfléchies.

La comparaison établie dans le paragraphe 3 montre clairement que le procédé de préflexion confère aux poutres une résistance en fatigue beaucoup plus grande par rapport à celle des poutres non préfléchies et, dans la plupart des cas, l'auteur de projet peut ignorer les réductions de contrainte imposées par la considération des phénomènes de fatigue. Il est libre d'utiliser des aciers de meilleure qualité au maximum de leur résistance, avec toute l'incidence que cela a sur l'économie du projet.

Fatigue Strength of Concrete-Filled Grillage Decks

Résistance à la fatigue des tabliers en grille de poutres enrobées de béton

Ermüdungsfestigkeit von ausbetonierten Stahlgitterrosten

Y. MAEDA
Professor
Osaka University
Suita, Osaka, Japan

S. MATSUI
Assistant Professor
Osaka University
Suita, Osaka, Japan

K. KUSHIDA
Head of Design Section
Kobe Steel Co., Ltd
Wakihama, Kobo, Japan

SUMMARY

Although the concrete-filled, steel grillage is a popular form of highway bridge deck, there is little information available on its fatigue strength. With this in mind, three sets of fatigue tests were carried out. The test procedure and results are presented and the fatigue strength of I beams in the floor, including the effect of the infill concrete, is discussed. On the basis of the discussion the fatigue security of an actual bridge is evaluated and some recommendations made for floor design.

RESUME

Bien que les tabliers de ponts-routes mixtes constitués d'une grille de poutres métalliques enrobées de béton soient très répandus, il y a actuellement peu d'information sur leur résistance à la fatigue. Dans cet esprit, trois séries d'essais de fatigue ont été effectués. Ce rapport présente le dispositif d'essai et les résultats, ainsi qu'une discussion sur la résistance à la fatigue des poutres en double-té incorporée dans le tablier, en incluant l'effet du béton. Sur la base de cette discussion, on évalue la sécurité à la fatigue des ponts existants et on propose quelques recommandations pour le dimensionnement de ce type de tabliers.

ZUSAMMENFASSUNG

Obwohl Fahrbahnplatten aus Beton aus gegossenen Stahlrosten weit verbreitet sind, ist noch wenig Information über ihr Ermüdungsverhalten vorhanden. Aus diesem Grund wurden drei Serien Ermüdungsversuche durchgeführt. Die Versuchsdurchführung sowie die Resultate werden vorgestellt und die Ermüdungsfestigkeit der in der Fahrbahnplatte einbetonierten I-Trägern diskutiert. Basierend auf diesen Ergebnissen wird einerseits die Sicherheit gegenüber Ermüdung einer bestehenden Brücke bestimmt und andererseits werden Empfehlungen für die Dimensionierung solcher Fahrbahnplatten vorgeschlagen.

1. INTRODUCTION

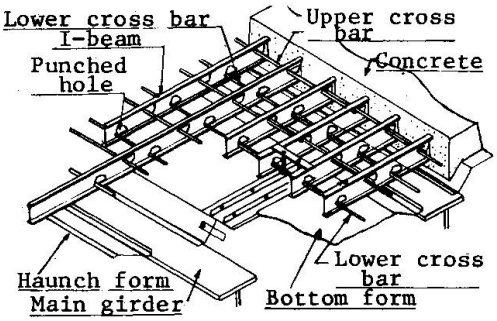

Fig.1 Sketch of floor.

Concrete Filled Steel Grating Floor is one of composite bridge decks. It has a large load-carrying capacity in spite of the thinner thickness than conventional RC-slabs[1]. The inner steel grid consists of specially rolled small I-beams and cross bars. The steel grid pannel as illustrated in Fig.1 is completely prefabricated at a shop. In Japan, a lot of serious damages of RC-slabs have been reported with a recent remarkable increase in traffic. Under these circumstances, the grating floors are getting to be frequently used not only for newly constructed bridges, but also for the replacement of damaged RC-slabs as seen in Fig.2, which shows the past records of use. The floor has already been recognized officially as a useful bridge deck. A design method, though it is yet in draft, is also proposed officially[2,3]. However, the authors have noticed that a more reasonable design method than the present proposed has to be established for the floors. There are two main problems to be considered, such as interaction between a steel grating and concrete from the point of plate behavior and fatigue strength of the floors. Regarding the former one, the authors have derived reasonable design bending moment formulas considering their orthotropic plate effects which would be caused by concrete cracking [4].

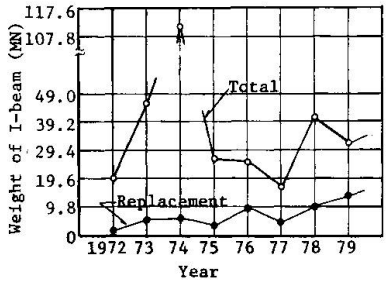

Fig.2 Past records of use of I-beams for bridge decks.

This paper covers discussions on fatigue of the floors. Fatigue fractures have been occasionally found in steel I-beams under large loading in our past labolatory tests. Generally, places of the fracture may be predicted to be located in the neighbor of edges of the loaded area as shown in Fig.3. Both bending and shear force in this region are very high. In addition, the I-beam has punched holes in the web, through which cross bars are placed, as shown in Fig.1. At the corner of the hole located in the region, a high stress occurs under simultaneous action of primary bending and secondary bending due to shear force as indicated in Fig.4. Furthermore, the effect of stress concentration due to the web opening is added to the previous stress. Accordingly, some points around the corner seem to be a crack initiation point. From the above experiences, three series of fatigue tests, such as isolated steel I-beam tests, concrete -encased I-beam tests and full-sized deck tests, were carried out. The first series are to clarify structural behaviors and fundamental fatigue features of the steel I-beams. The second series are to investigate the effects of concrete on the fatigue strength. The last are aimed at finding out the relation between the beam-type and the deck-type specimens. Through the tests the evaluation of the fatigue safety of the floor can be made.

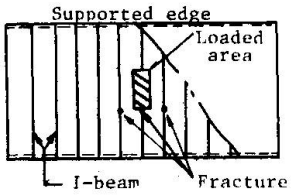

Fig.3 Cracking points in a deck.

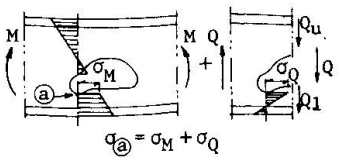

Fig.4 Stress at the corner of a hole.

2. DESCRIPTION OF SPECIMENS AND TEST PROCEDURES

2.1 Isolated Steel I-beam Tests

The two types of hole arrangements within an I-beam are typical for the practical usage. The first type has holes in a line along the lower side of the web. It is available in case upper cross bars are placed on the I-beams as shown in Fig.5(a). The second one has holes in a zigzag along the both sides of the web. It is use-

ful for thin decks because the upper cross bars also have to be placed through the web as seen in Fig.5(b). The first is named S-type and the second is W-type.

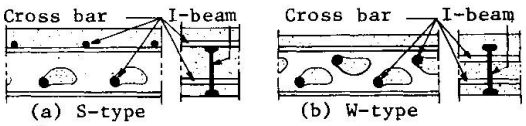

Fig.5 Types of I-beam.

Configurations of all the specimens are indicated in Fig.6. In the shop fabrication, cross bars are tack welded to I-beams so that the panel can have sufficient stiffness during its transportation and erection. Therefore, the influence of the welding on the fatigue strength at the welded points of the web is expected. The specimens of S-DB and W-DB in which 10 cm long deformed bars are welded, are also tested. Material properties of the I-beams are the same as those of structural carbon steel SS41 designated by the Japanese Industrial Standards. The static coupon tests of the steel showed 311 MPa, 483 MPa, 199 GPa, and 25.3 %, respectively, for its yielding stress, tensile strength, Young's modulus and elongation.

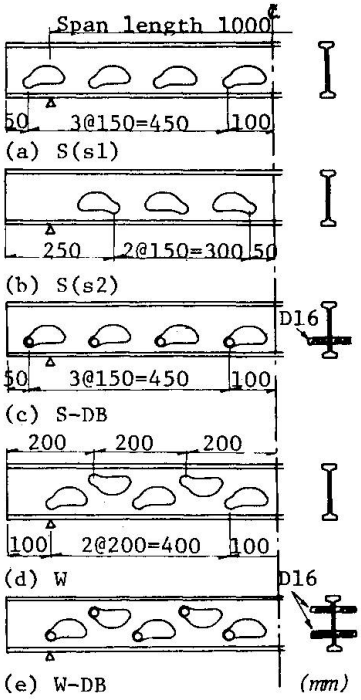

Fig.6 Isolated I-beam specimens.

A test apparatus for the beam-type specimens is illustrated in Fig.7. The span length is exactly 1.0 m. A great number of strain gauges of 2 mm or 5 mm gauge length were placed to measure strain distributions.

If the same repetition of loading is continued after the initiation of a crack, the crack will easily propagate to the bottom surface of the lower flange, and the I-beam loses its load-carrying capacity. Hereafter, such a phenomenon is called the fracture of an I-beam. The above mentioned test procedure gives only one kind of information for a single specimen. Therefore, the authors devised a procedure to obtain many data from a single specimen in order to save the time and the number of specimens by repairing each cracked hole. A repairing method by H.T.-bolts as shown in Fig.8 gave the most favorable results for the crack propagation arrest. As a matter of course, it was proved that the repairing scarcely gave an influence on the stress distribution at the adjoining cracking points. Thus, three or four data related to the life of initiation of a crack can be obtained from a single specimen. Afterward, one of the H.T.-bolts on the cracked points were released, and the repetition of the loading was continued until the fracture of the I-beam has been observed. By such a procedure, a remaining fatigue life up to the fracture can be also obtained.

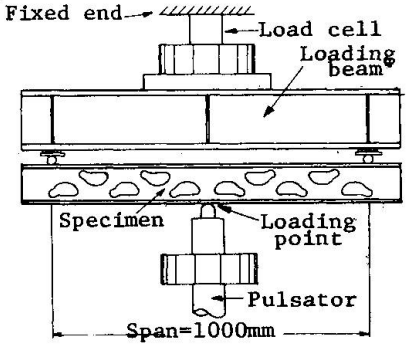

Fig.7 Test apparatus of beam test.

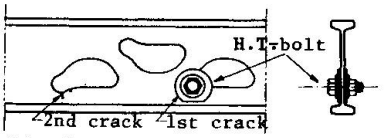

Fig.8 Repairing by H.T.-bolt.

2.2 Concrete -Encased I-beam Tests

The encased I-beam are essentially of S-, W-, S-DB-,and W-DB-types. The specimens are classified into three groups having the symbols of NC, NCC and COM as seen in Fig.9. NC means a specimen in which an I-beam is completely encased in concrete. NCC means a completely cast beam, but has artificial cracks in concrete up to the neutral axis of the composite section. These cracks are created by inserting thin plastic plates of 1 mm thickness and are uniformly distributed along the span with 10 cm to 15 cm intervals. COM means a composite beam which consists of one I-beam and concrete section only in the compression side.

In this series, the fatigue life is defined by the number of cycles of loading when a fracture of the I-beam has just occurred. It is named a fracture life.

2.3 Full-Sized Deck Tests

Two types of specimens as shown in Fig.10 were prepared. The decks are supported so that the two opposite edges can be simply supported and the other two be free. The deck span is 1.8 m. A single load is applied through a rectangular plate of 20 cm in length and 50 cm in width, which corresponds to the contact area of a rear wheel specified in the Specifications for Highway Bridges in Japan.

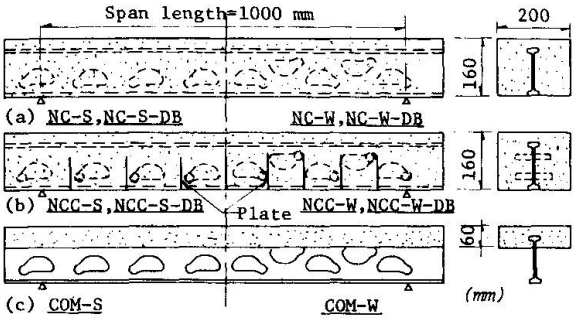

Fig.9 Concrete -encased I-beam specimens.

Since it is impossible to repair a cracked I-beam in a deck, a loading point is changed alternatively after each occurrence of fracture in the I-beam to obtain several data from a single specimen. In a deck specimen, since its load-carrying capacity does not decrease with only one fracture in the I-beam beneath a loading point, the fracture time of the I-beam was detected accurately by an electric instrument.

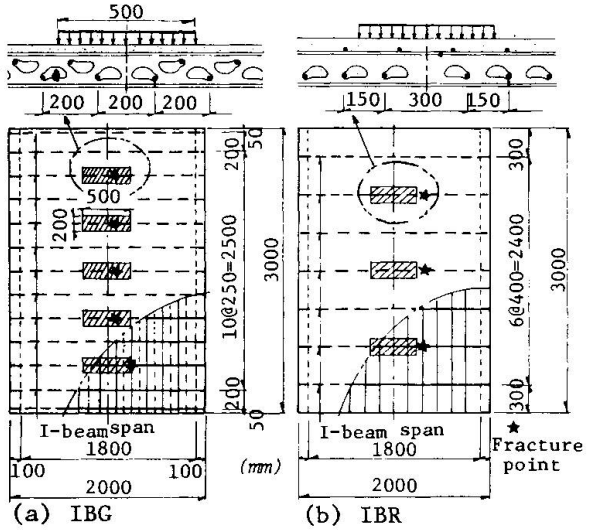

Fig.10 Deck specimens.

3. TEST RESULTS AND DISCUSSIONS

3.1 Fatigue Crack Patterns

Fig.11 shows patterns of fatigue cracks observed at the prototype I-beams. All cracking points in the tensile region are labeled by circled alphabets as seen in Fig.12. Hereafter, these labels will be used for explanations. When the circular part of a hole faces to a support, the first crack occurs at ⓐ of the nearest to a loading point. Then, fatigue cracks successively appear at the same part of outer holes with decreasing stresses. In the specimen S(s2), an initial cracks occurs at the point ⓑ, because stresses at ⓑ are higher than at ⓐ. In W-type specimen, the point ⓑ and ⓓ are also cracking points under a large load, since large stresses due to shear forces occur around these points. In W-DB-type which has deformed bars, fatigue cracks appear at the toe ⓒ of weld instead of ⓓ owing to the effects of heat and notch due to welding. The I-beams of the composite beams or decks showed the fracture of flanges caused by a crack from ⓐ as already shown in Fig.10.

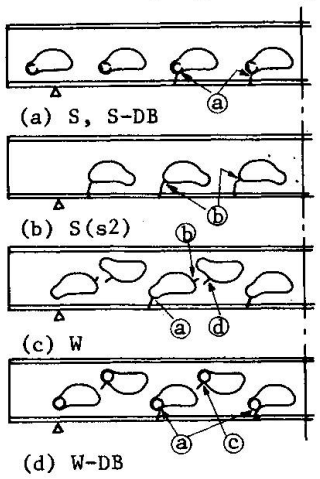

Fig.11 Fatigue crack pattern

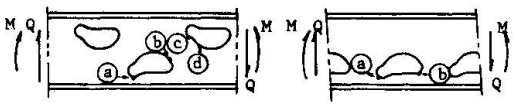

Fig.12 Labeling of cracking points.

3.2 Stress and Strain Distributions

Fig.13 shows a typical strain distribution measured at the lower flange of an I-beam. The zigzag distribution indicates how large an influence of secondary bending due to shear force is in an I-beam having web holes. Fig.14 is an example of stress distribution in the web of W-type beam by FEM. A large tensile stress appears in the neighbor of the points ⓐ, ⓑ, ⓒ and ⓓ. Especially, the stress at the point ⓐ is extremely high proving

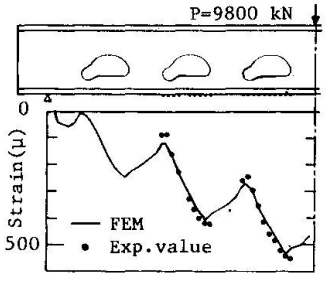

Fig.13 Distribution of strain on the bottom surface of a tensile flange of S-type beam.

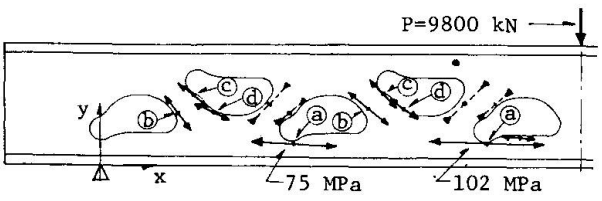

Fig.14 Principal stress distribution in the web of W-type beam.

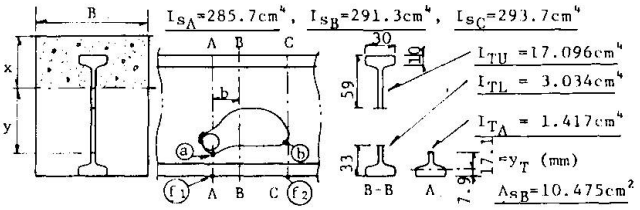

Fig.15 Cross sectional properties of the I-beam at a hole.

that the first crack would start at this point.
As a result of the detailed investigation, the following simplified formulas for normal stresses can be derived for the points ⓐ, ⓑ, ⓕ1 and ⓕ2 in Fig.15.

For an isolated I-beam,
$$\sigma_x = \alpha \frac{M}{I_S} \cdot y + \beta \frac{y_T}{I_T} \cdot \frac{I_{TL}}{I_{TU} + I_{TL}} \cdot b \cdot Q \qquad (1)$$

For an encased I-beam,
$$\sigma_x = \alpha \frac{M}{I_V} \cdot y + \beta \frac{y_T}{I_T} \cdot \frac{A_S}{\frac{B\,x}{n} + A_S} \cdot \frac{I_{TL}}{I_{TU} + I_{TL}} \cdot b \cdot Q \qquad (2)$$

where,
- α, β : the coefficients of stress concentration due to the web opening,
- b : the distance from the inflexion point of secondary bending moment at a hole due to shear force to the referring point, and is at the tests 2.5 cm and 5.5 cm for the points ⓐ, ⓕ1 and ⓑ, ⓕ2 , respectively,
- I_S, I_V : the moments of inertia of I-beam and composite beam at the referring cross section, respectively,
- I_{TU}, I_{TL} : the moments of inertia of the upper and lower T-sections at the inflexion point, respectively,
- I_T : the moment of inertia of the lower T-section at the referring point,
- y, y_T : the distance from the neutral axis to the referring point for the whole section and for the lower T-section, respectively,
- M : the bending moment at the referring point,
- Q : the shear force at the inflexion point,
- A_S : the cross sectional area of an I-beam at the inflexion point,
- B : the width of concrete section,
- x : the effective concrete depth at the inflexion point,
- n : the modular ratio of E_S/E_C.

The coefficients of stress concentration for each specimen and the above mentioned sectional properties are listed in Table 1 and in Fig.15, respectively. The coefficient at the bottom surface of the flange becomes 1.0 except in W-type. The value of β for W-type becomes 0.4 due to the effect of a diagonal portion of the web, because the behavior of W-type is similar to a Warren truss. The effect appears also on β-value at ⓐ. Comparing with the results obtained by FEM, proof of the accuracy of Eqs. (1) and (2) is shown in Fig.16 and 17. In a concrete -encased I-beam specimen, an amplitude of the zigzag strain distribution becomes smaller, because the concrete section can carry some part of the shear force as known in Eq.(2). Eq.(2) is also applicable to deck specimens. However, M and Q in the deck have to be deter-

Table 1 Coefficient of stress concentration

I-beam	Point	α	β
S	a	2.14	2.47
S-DB	b	1.08	1.95
	$f_{1,2}$	1.00	1.00
W	a	2.19	1.35
W-DB	a	2.10	1.52
W,W-DB	$f_{1,2}$	1.00	0.40

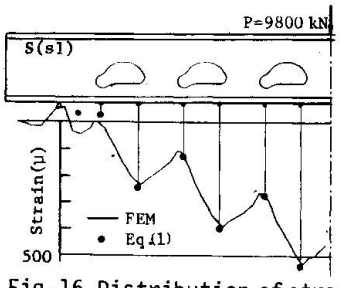

Fig.16 Distribution of strain on the bottom surface of S-type beam.

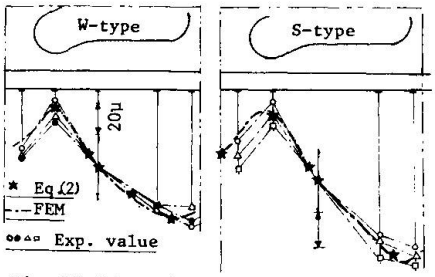

Fig.17 Distribution of relative strains on the bottom surface of the flange under a hole of an encased I-beam.

mined by an orthotropic plate theory. In a deck, since a wheel load is well distributed in the transverse direction, the influence of the second term in Eq.(2) becomes much smaller than that of encased beam specimen due to a decrease in the shear force.

3.3 S-N Relations

All the data from the fatigue tests and the resulting S-N curves obtained by the method of least square are shown in Figs.18 to 21. The vertical axis shows the magnitude of stress range at a cracking point given by the Eq.(1) or Eq.(2). Investigating these figures, the following features are able to be pointed out:

(1) From Fig.18, the effect of welding can be seen comparing features for S and W with those for S-DB and W-DB, respectively. The reduction of fatigue lives due to welding is remarkable. Especially, an abnormally large size tack welding gives worse results as seen in W-DB-type.

(2) Fig.19 is a diagram to show how long the remaining fatigue life is. It is worth to note that the remaining life after a crack has been initiated, is nearly equal to the initial crack life.

(3) The results from the deck tests are compared with the ones from the isolated I-beam tests in Fig.20. The test results in the decks, which are plotted at the fracture lives of I-beams, lie properly on S-N curves obtained for the fracture life of beam specimen within experimental errors. Such a good agreement gives the proof that M and Q in the decks can be evaluated accurately by the orthotropic plate theory. Also, the results from the deck tests have been modified considering cumulative damages due to the above mentioned multi-point loadings.

(4) The results in Fig.21 were prepared for discussions in the next section.

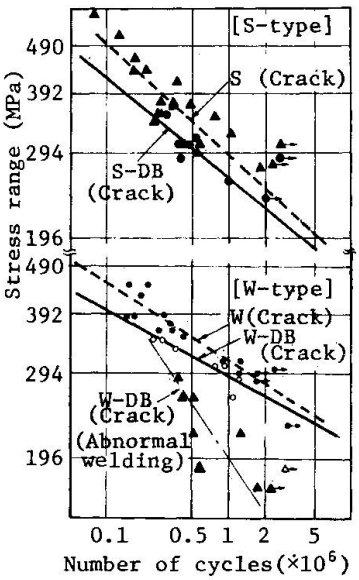

Fig.18 S-N relations for isolated I-beams.

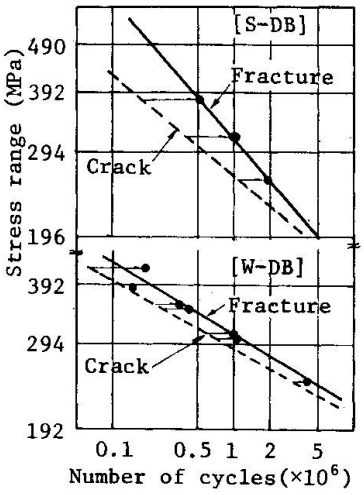

Fig.19 S-N relations for fracture life.

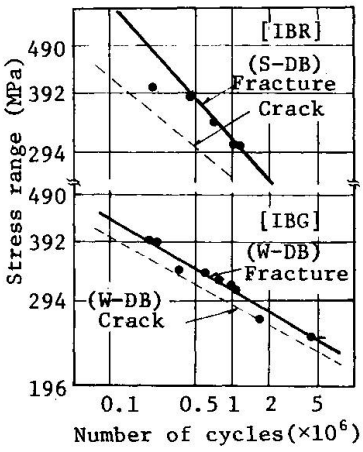

Fig.20 S-N relations for deck specimens.

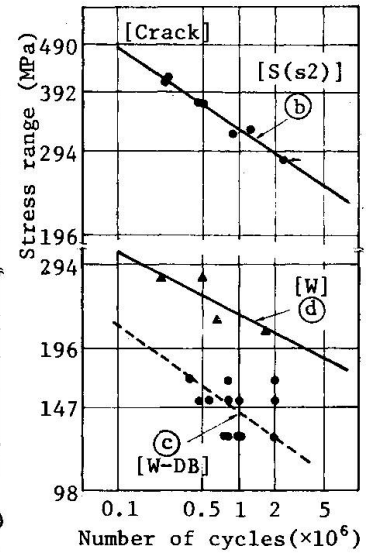

Fig.21 S-N relations at ⓑ in S-type, and at diagonal portions of web in W-type.

3.4 Fatigue Diagrams

It is difficult directly to find the difference between S-type and W-type in the S-N diagrams. Comparing these two types in term of fatigue diagrams, the difference is then clearly detected. The fatigue diagrams at 2×10^6 cycles are obtained using Eqs.(1) and (2) as shown in Fig.22. The results lead to the following discussions:

(1) Since W-type has more holes than S-type, the former has less stiffness than the latter. However, in reality, the fatigue strength of W-type is much larger than that of S-type. It depends on the decrease of α and β as discussed in Section 3.2.

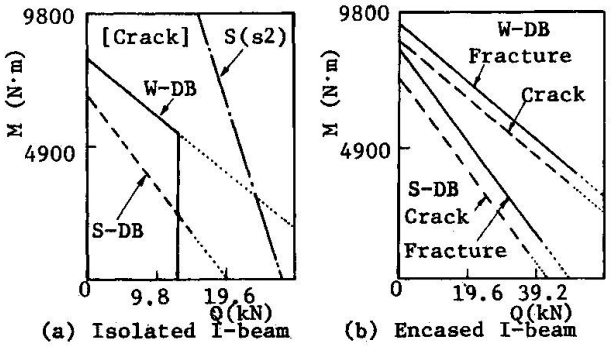

Fig.22 Fatigue diagrams at 2×10^6 cycles.

(2) One limit of the values of shear force exists in an isolated I-beam of W-type. In case the shear force becomes larger than the limit, a crack will occur in a diagonal portion of the web.
(3) The fatigue strength at the point ⓑ in S(s2)-type is much larger than that at the point ⓐ in S-type. Therefore, if an I-beam has holes facing in the same direction, the first crack will be sure to be initiated at the point ⓐ.
(4) Even though the fracture life is two times as large as the crack life, the difference of fatigue diagrams between fracture and crack is not so large.
(5) The effect of concrete on the fatigue life is extremely great. It depends not only on stresses decreasing due to the composite action, but also on a decrease in shear force due to a share with concrete.

4. EVALUATION OF FATIGUE SAFATY OF ACTUAL FLOORS

4.1 Procedure for Derivation of Safety Factor

Using the above mentioned S-N curves, it is possible to evaluate the fatigue safaty of actual floors under traffic load. Now, the fatigue safety of five decks, of which the span length are 1.5, 2.0, 2.5, 3.0 and 3.5 m, is derived under the combination of the following conditions: (a) Employed I-beam: S-DB and W-DB, (b) Traffic load spectrum: two actually measured spectra of rear axle loads of NHW and UEW as listed in Table 2, where, NHW means a spectrum on a national highway in Japan and UEW means one on an urban expressway in Japan[5]. (c) Probability functions of passing positions of vehicle wheels on a road surface: two actually measured functions of NHW and UEW as shown in Table 3. (d) Daily traffic volumes of vehicles on a single lane: 10,000, 15,000 and 20,000. (e) Design life of bridges: 50 years.

Table 2 Axle load spectra

Weight (kN)	NHW (%)	UEW (%)
0 ~ 20	73.03	79.54
20 ~ 39	10.61	9.60
39 ~ 59	8.09	6.16
59 ~ 78	3.32	2.21
78 ~ 98	2.12	1.35
98 ~118	1.60	0.78
118 ~137	0.849	0.238
137 ~157	0.210	0.079
157 ~176	0.091	0.028
176 ~196	0.038	0.028
196 ~235	0.034	0.012
235 ~274	0.0071	0.006
274 ~314	0.00092	-----

Table 3 Probability function of passing position of vehicles

	Mean value	Standard deviation	L=width of one lane
NHW	0.73 L	0.09 L	Left wheel, Right lane mark
UEW	0.77 L	0.065 L	

The fatigue safety is evaluated by the following processes: (a) Calculate N_{eq} of Eq.(3) based on the Miner's linear damage hypothesis. (b) Find the fatigue stress (σ_f) corresponding to the cycles N_{eq} on a S-N curves. (c) Obtain the maximum stress (σ_d) acting at a referring point under a specified axle load including impact with a plate analysis. (d) Finally calculate the safety factor given by the ratio of σ_f to σ_d. Fig.23 is a block diagram of the procedure for the explanation.

$$N_{eq} = N_t \int_{T_{min}}^{T_{max}} \left(p(T) \cdot \left(\frac{T}{156.8}\right)^{1/K} \right) dT \cdot \int_0^L \left(p(x) \cdot Inf(\sigma)^{1/K} \right) dx \quad (3)$$

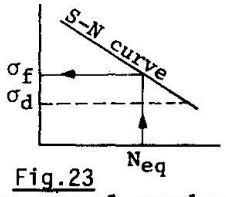

Fig.23

where,
N_{eq} : the effective number of cycles which is converted from the total number of traffic loading cycles N_t by the cumulative damage law,
N_t : (design life in year of the bridge) × 365 days × (daily traffic volume),
T : the rear axle load of a vehicle in the unit of kN,
156.8 : the specified rear axle load in the unit of kN,
p(T) : the axle load spectrum,
p(x) : the probability function of passing position of wheels,
Inf(σ) : the influence value of stresses along a referring I-beam with regard to a referring point,
K : the absolute value of a slope of a S-N curve.

4.2 Results, Discussions and Recommendations

Discussions on the fatigue safety have to be done with optimum cross sections

designed by the conventional formula[2]. Table 4 gives an optimized design cross section of each deck. The maximum design stress in the bottom flange of I-beams is almost equal to the allowable stress. Figs.24 to 26 show the resulting safety factors regarding the referring point apart 10 cm from the midspan of each deck. Each figure leads to the following discussions:

(1) Generally, W-type seems to have sufficient fatigue strength as seen in Fig.24. S-type is not suitable for a deck whose span is less than 2.3 m.

(2) Both load spectra and daily traffic volumes significantly influence on the safety. Therefore, NHW spectrum still has to be used for the assessment of fatigue. The daily traffic volume of 20,000 is probably the largest in Japan. However, it may be desirable to use the number for the fatigue design of decks.

(3) Two safety curves associated with the fracture life and crack life are illustrated in Fig.26 for a comparison. The difference between the two safety factors can not be observed in S-type, because the slope of the S-N curve for the fracture life becomes larger than that for the crack life. So, in an actual design it seems to be desirable to use the crack life even for W-type.

Table 4 Cross section of decks and design stress

	Span length				
	1.5m	2.0m	2.5m	3.0m	3.5m
t (cm)	16	17	18	19	20
B (cm)	28.5	23.5	19.5	17.0	15.0
σ (MPa)	133	136	137	136	137

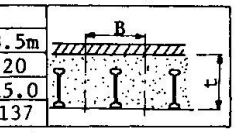

σ_a=137.2 MPa

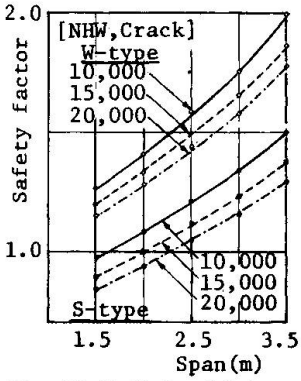

Fig.24 Safety factors for crack life.

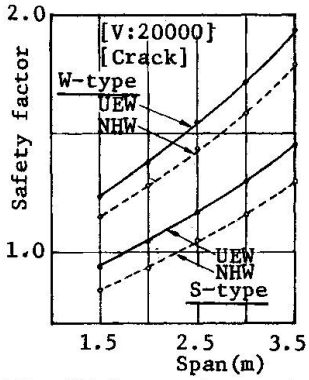

Fig.25 Comparison of load spectra used for safety factor.

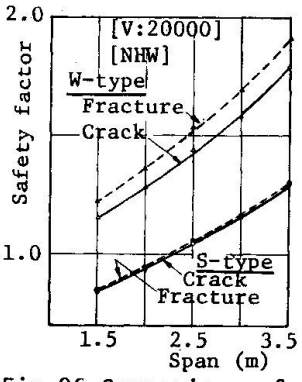

Fig.26 Comparison of fatigue life used for safety factor.

5. CONCLUSIONS

Through three of tests, the effect of cracks and the fatigue safety of Concrete Filled Grating Floors were made clear. The followings are concluded from the present study:

(1) Fatigue strength of the floors is governed by that of encased I-beams.
(2) I-beams of W-type are more reliable than those of S-type.
(3) The floors designed by the present design method have generally sufficient fatigue strength.
(4) The fatigue safety of the floors is influenced by vehicle loads, position spectra, and traffic volumes.
(5) The fatigue safety of the floors has to be evaluated by the initiation lives of cracks
(6) Eqs.(1) and (2) are useful stress formulas for I-beam having holes.

REFERENCES

1. Y.MAEDA and S.MATSUI: Experimental Study on Structural Behaviors and Load-Carrying Capacity of Full-Sized Steel Grating Floors, Trans. of JSCE, 1978.
2. JRA: Design Manual for Steel Highway Bridges, Japan Road Association, 1979. *(in Japanese)*
3. The Surveying Committee for Highways: Rept. on the Design and Construction of I-beam Grating Floors, Japan Road Public Corporation, 1980. *(in Japanese)*
4. S.MATSUI and Y.MAEDA: Structural Behaviors and Design of Concrete Filled Steel Grating Floors, 1st Annual Conf. of JCI, 1979. *(in Japanese)*
5. T.KUNIHIRO et al.: Study on Design Live Loads - Actual Traffic Loads and Application to Bridge Design -, Rept. of the Public Works Reseach Institute, Minst. of Const., 1971. *(in Japanese)*

Concrete Placing Methods and Fatigue of Shear Studs

Mise en place du béton et fatigue des goujons soumis à l'effort tranchant

Einfluss der Betoneinbringung auf das Ermüdungsverhalten von Schubdübeln

S. AKAO
Prof. Dr. -Ing.
Osaka Institute of Technology
Osaka, Japan

A. KURITA
Assistant Prof.
Osaka Institute of Technology
Osaka, Japan

H. HIRAGI
Assistant Prof.
Setsunan University
Osaka, Japan

SUMMARY
In many steel-concrete composite applications, other than ordinary beams and girders for bridges or buildings, water "bleeding", in the fresh concrete, has an important effect on fatigue and static strength of shear studs. This strength behaviour is discussed with relation to the means and direction of concrete placing and examined by way of push-out tests.

RESUME
Dans de nombreuses constructions mixtes acier-béton, autres que les poutres ordinaires utilisées dans les ponts ou les bâtiments, l'eau de resuage dans le béton frais a une influence importante sur la résistance statique et à la fatigue des goujons soumis à un effort tranchant. Ce comportement de la résistance est discuté en relation avec la mise en place du béton et est examiné au moyen d'essais "push-out".

ZUSAMMENFASSUNG
In vielen Anwendungsbereichen der Verbundbauweise hat das Ausscheiden von Wasser aus frischem Beton einen grossen Einfluss auf die dynamische und statische Festigkeit der Schubdübel. Eine Ausnahme bilden dabei gewöhnliche Balken und Träger des Brücken- und Hochbaus. Der Einfluss der Art und Richtung der Betoneinbringung auf das Festigkeitsverhalten wird aufgezeigt und mit "Push-Out" Versuchen untersucht.

1. INTRODUCTION

Since 1956, many valuable results of studies on the design of the stud shear connectors have been reported [1]. The purpose of these studies is mainly to facilitate the application of stud shear connectors for the ordinaly composite steel beams or girders in bridges and buildings, and as matter of cource, the problems of the effect of water bleeding in concrete to the bearing surface of stud connectors were not discussed (only in the push-out tests by J.W.Fisher et al. [2], the effect was considered). When the stud connectors are applied in various steel-concrete composite constructions such as the concrete encased steel beams and girders or columns, and in steel-concrete mixed structural systems [see Fig.1], the problems of the above effect become very important. In these cases, because, there are several placing directions of concrete relating with the shearing directions of stud connectors. In this paper, therefore, the static and fatigue behaviors of studs in relation to the placing directions of concrete are studied.

2. TEST SPECIMENS AND CONDITIONS

The specimens were of the push-out type. As shown in table 1, the specimens were classified into four types denoted by A, B, C and D. To unify the properties of concrete for four types of the specimens, it was necessary to make all type specimens at a time. The web plate of H-shape steel in A and B type were separated at the time of concrete placing. In order to ensure the natural bond between concrete and flanges of H-shape steel, the steel surfaces were not covered with a layer of cup grease which was employed in the previous studies [1], prior to concrete placing. Fig. 2 shows details of specimens, in which four studs are embeded in each slab.

The push-out tests of each type were carried out dividing into five series. Dimensions of studs and properties of concrete in each series are listed in table 2. Experimental parameters in series 1 to 3 and series 3 to 5 are heights of stud and strengths of concrete, respectively. H-shape steel and stud materials of all specimens were structural carbon steel of SS41 designated by JIS.

In static loading tests, the load was intermittently released to observe the residual slips. Slip between H-shape steel and concrete portions was measured by four dial gages (1/1000 mm) and four displacement meters (1/100 mm) at the level of the studs. On the other hand, in fatigue tests, the frequency of repeated loading was 5.5 Hz., and minimum shear stress level of stud was kept constant of 15 N/mm^2. Relative slip between steel and concrete was observed by two non-contact type displacement meters.

3. STATIC TEST RESULTS AND PROPOSED DESIGN FORMULAE

Load-residual slip curves of push-out specimens are shown in Fig. 3. In this figure, it is clearly indicated that the residual slips for C-type specimens are extremely large in comparison with the specimens of other types at early stage of loading. This seems to be influenced by the bleeding of water in concrete to the bearing surface of studs.

The measured values of the ultimate loads of studs are protted in Fig. 4, and the design values in AASHTO, BS and DIN are also illustrated. On the ultimate loads of the 100 mm height studs, the values by the AASHTO specification give good agreement with test data.

From the static test results, the static strength of studs are proposed as

follows:
The nominal static strength of the stud at the ultimate limit state is given by;

For all-types, $P_d = 0.126\ d\ h\ \sqrt{f_{ck}}$ (kN) (1)

And the static strength at the serviceability limit state is given by;

For A, B and D-types, $P_s = 0.50\ P_d$ (kN) (2)

For C-type, $P_s = 0.35\ P_d$ (kN) (3)

These formulae can be applied in the range of $h/d = 3.0$ to 5.0. The coefficient in equations (2) and (3) were determined on an assumption that a serviceability limit state of studs is defined as the load at a residual slip of 0.5 mm. Where , the load-residual slip relationship generally became nonlinear as shown in Fig. 3.

4. FATIGUE TEST RESULTS AND CONSIDERATIONS

Fig. 5 shows a typical example of the relationship between number of cycles of loading and relative slip at the stress range of 150 N/mm^2 in series 3. Fatigue life of B-type is extremely short than the other types, and fatigue failure occurs when relative slip reaches about 1.0 mm.

$\Delta\tau$-N relationships in five test series are summarized in Fig. 6. In all test series, it is recognized that the fatigue lifes of B-type specimens are clearly shortest. But in series 5, namely, at high level of concrete strength as 40 N/mm^2, these tendency is not so remarkable. As the reason of decrease of the fatigue life on B-type specimens, it is considered that water bleeding in fresh concrete gives bad effects at the contact surface between the H-shape steel flanges and the slabs, especially around the bottom of the welded studs.

From the test results, the fatigue strengths of all type studs at cycles of $N = 2 \times 10^6$ are estimated, and are protted in Fig. 7. As the matter of course, the correlation between the fatigue strength and the concrete strength is observed. It can be observed that the stud heights have no effect to fatigue strength.

$\Delta\tau$-N relations of each type specimens included from series 1 to 3 are shown in Fig. 8. The recommended design values of CEB-ECCS-FIP-IABSE Joint Committee on Composite Structures [7] are also illustrated in Fig. 8. The code gives very conservative values to the studs such as A-type specimens. But, it satisfactorily coincides with the B-type studs.

For the reliability analysis of the studs under the repeated loading, the coefficients of $\Delta\tau$-N relations and parameters of Weibull distribution of each type stud in series 1 to 3 are given in table 3. Design ranges of shear stress of the studs under constant amplitude loading can be calculated from the equations in table 3 if the reasonable probability of fatigue failure and the number of load cycles are specified. On the other hand, the fatigue life of the studs subject to random loading can be also determined by Miner's linear cumulative damage rule.

5. CONCLUSIONS

Throughout the push-out tests by using forty specimens in static and eighty

specimens in fatigue, some remarkable results which support the assumption were obtained. The conclusions are as follows:

1) Water bleeding in fresh concrete gives a bad effect both to C-type studs in static behavior and to B-type studs in fatigue strength.

2) In standard push-out test method such as British Standards, the placing direction of concrete at the time of making the specimens should be noted.

3) One of the reason of the scatter of fatigue test results in previous studies [1]-[3] is considered due to the difference of concrete placing directions.

In the future, it is necessary to test also the studs have the height of 100 mm over. And the interaction problems of the studs under the shear and tension would be the subject for further study.

ACKNOWLEDGEMENTS

This work was sponsored by the Central Reseach Laboratory of Osaka Institute of Technology and Nippon Stud Welding Co., Ltd. The authors are thankful for the assistance given by our many colleagues of Osaka Institute of Technology and Setsunan University.

NOTATIONS

P_d = design shear strength at ultimate limit state, (kN)
P_s = design shear strength at serviceability limit state, (kN)
d = diameter of the stud, (cm)
h = overall height of the stud, (cm)
f_{ck} = characteristic cylinder strength of concrete at age considered (N/cm^2).

REFERENCES

[1] for examples,
Viest, I.M.: "Investigation of Stud Shear Connectors for Composite Concrete and Steel T-Beams," Journal of the ACI, Vol.27, No.8, 1956, pp.875-891,
Thürlimann, B.: "Composite Beams with Stud Shear Connectors," Bulletin No. 174, Highway Research Board, 1958, pp.18-38,
Thürlimann, B.: "Fatigue and Static Strength of Stud Shear Connectors," Journal of the ACI, Vol.30, No.12, 1959, pp.1287-1302,
King, D.C., Slutter, R.G. and Driscoll, Jr. G.C.: "Fatigue Strength of 1/2-Inch Diameter Stud Shear Connectors," Highway Research Record, No.103, 1965 , pp.78-106.
[2] Fisher, J.W. et al.: "Shear Strength of Stud Connectors in Lightweight and Normal-Weight Concrete," AISC Engineering Journal, Vol.8, No.2, 1971, pp.55-64.
[3] Mainstone, R.J. and Menzies, J.B.: "Shear Connectors in Steel-Concrete Composite Beams for Bridges; Part 1: Static and Fatigue Tests on Push-Out Specimens," Concrete, Vol.1, No.9, 1967, pp.291-302.
[4] AASHTO: "Standard Specifications for Highway Bridges," 12th ed., 1977.
[5] BSI: "BS 5400, Part 5, The Design of Composite Bridges," 1979.
[6] DIN: "Richtlinien für Stahlverbundträger," 1980.
[7] ECCS: "Composite Structures," The Construction Press, 1981.

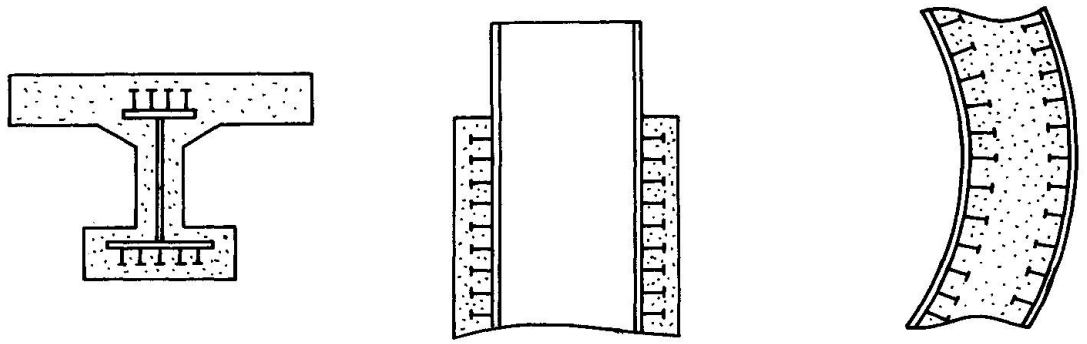

(a) Preflexed beam (b) Composite column (c) Composite shell

Fig. 1 Applications of stud shear connectors in various steel-concrete composite constructions

Table 1 Classification of specimens

Type	Placing direction of concrete
A	
B	
C	
D	

Table 2 Dimensions of studs and properties of concrete in five test series

Series	Stud			Concrete	
	Height h (mm)	Diameter d (mm)	h/d	Ave. Slump (cm)	Ave. Strength (N/mm^2)
1	40	19	2.11	16	34.2
2	70	19	3.68	18	32.2
3	100	19	5.26	17	31.3
4	100	19	5.26	15	37.7
5	100	19	5.26	12	46.0

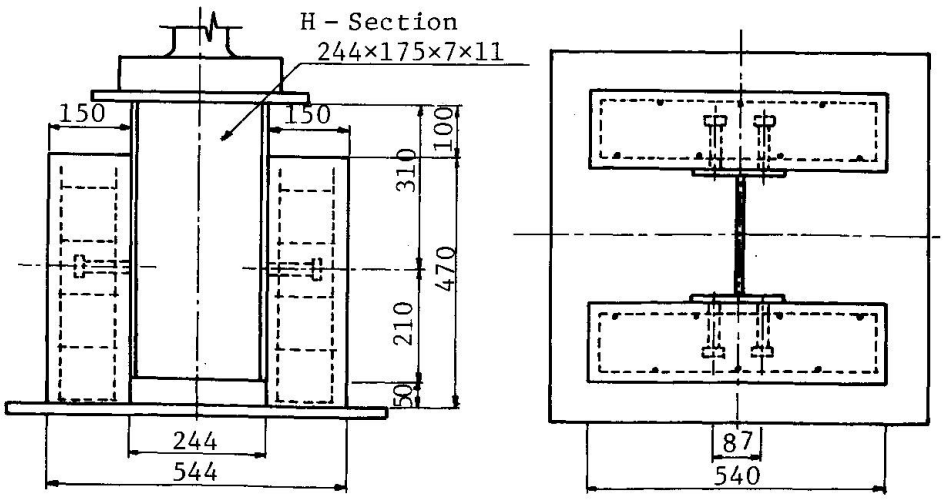

Fig. 2 Details of specimens

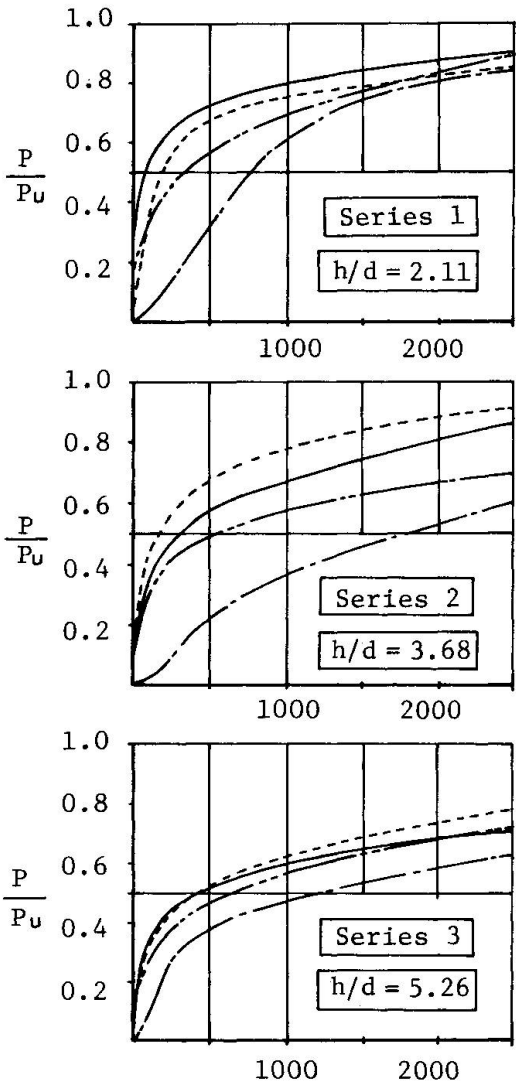

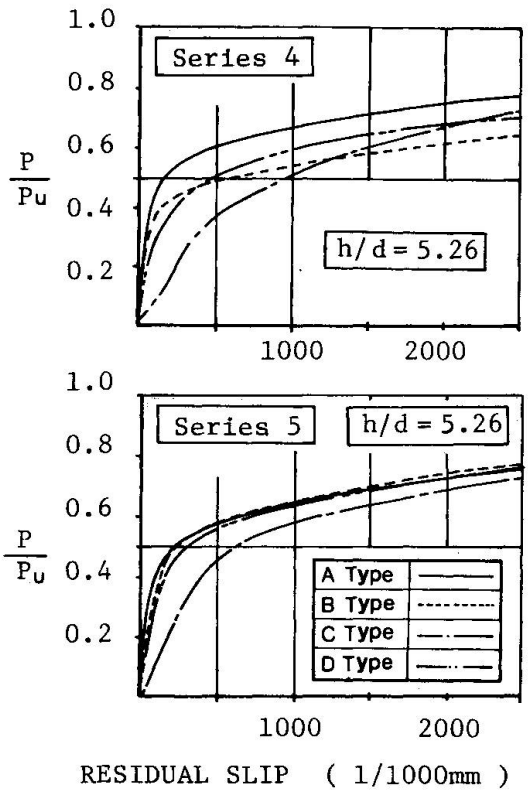

Fig. 3 Load-residual slip curves

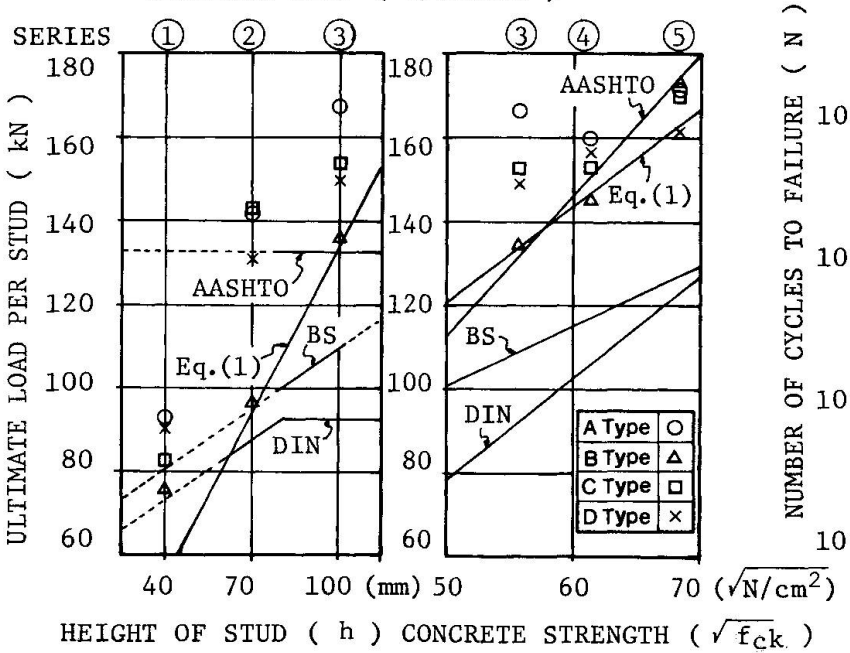

Fig. 4 Ultimate load versus height of stud and concrete strength

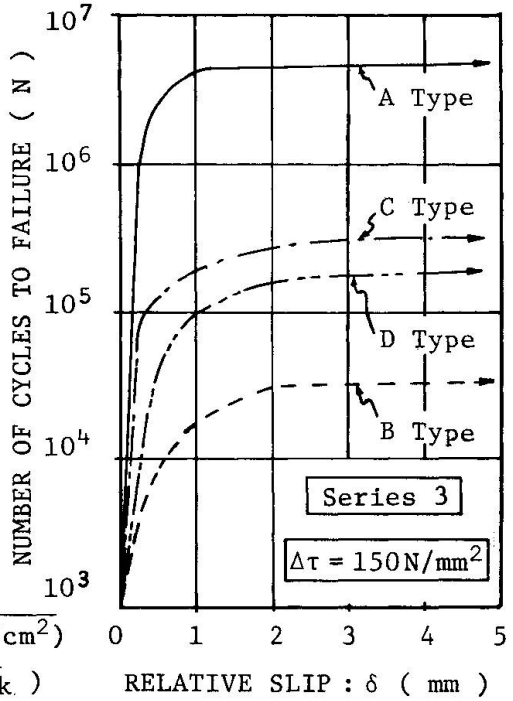

Fig. 5 N-δ curves

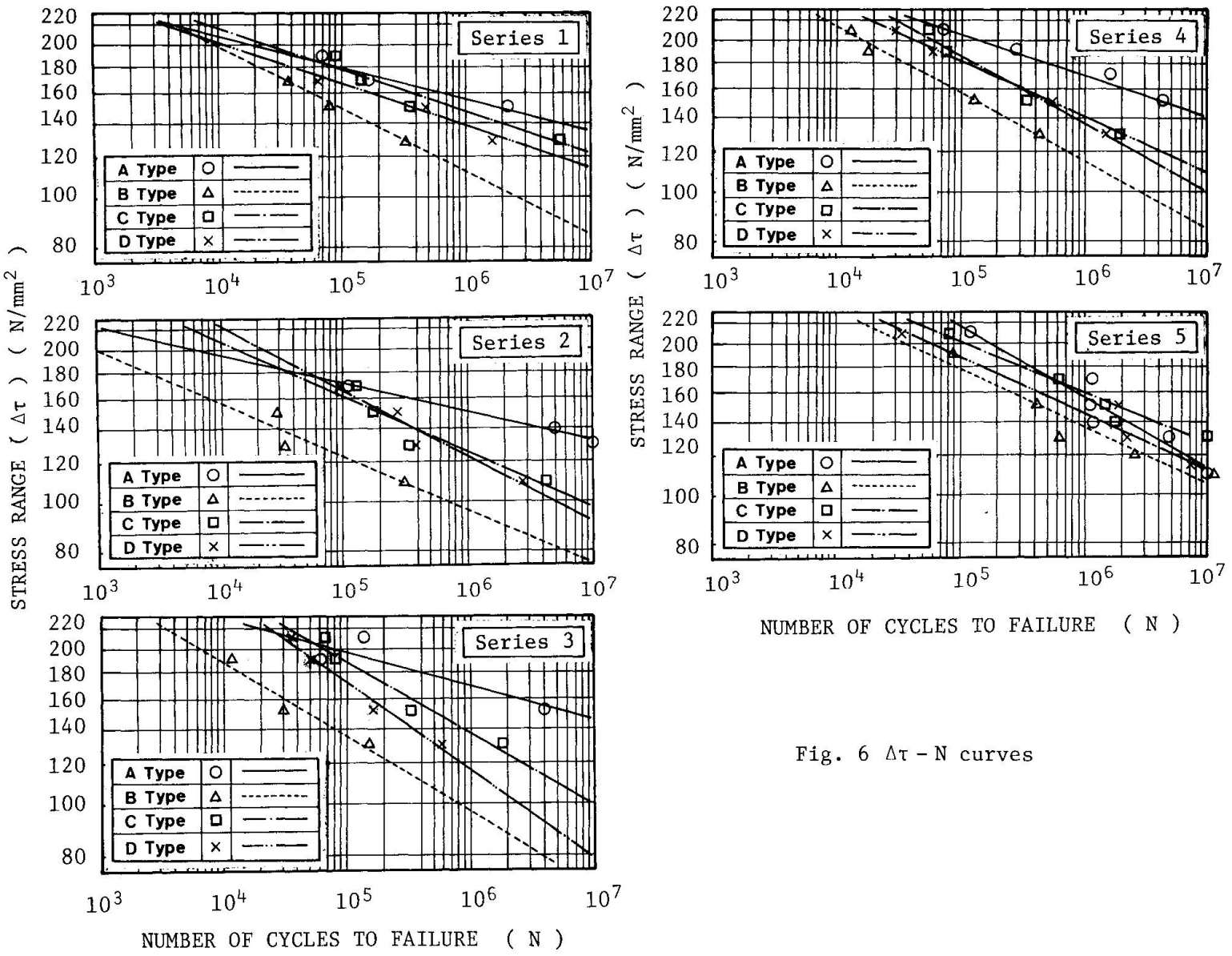

Fig. 6 Δτ - N curves

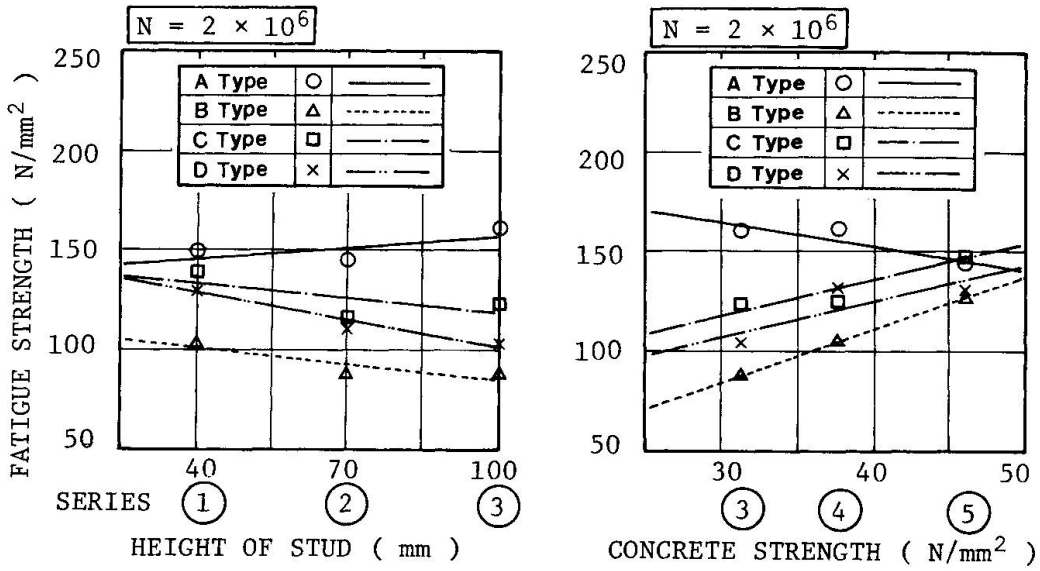

Fig. 7 Estimation of fatigue strength at $N = 2 \times 10^6$

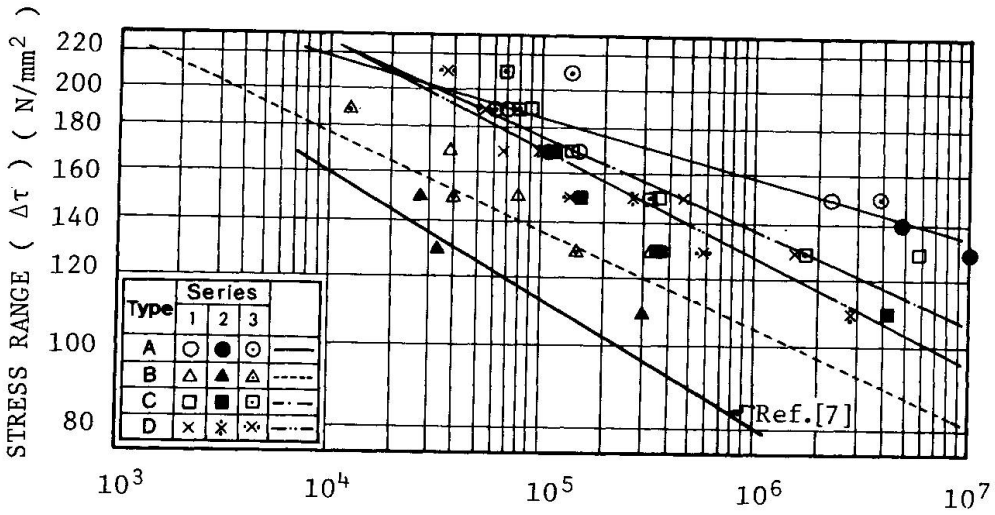

Fig. 8 Δτ - N relations in series 1 - 3

Table 3 Statistical properties in series 1-3

Type	Δτ-N Relation		Probability of failure		
	Coefficient		Parameter		
	a	b	Shape(m)	Scale(β)	Location(χ_o)
A	37.621	14.384	3.706	1.596	-1.446
B	23.672	8.749	3.784	1.222	-1.109
C	25.375	9.073	3.803	1.271	-1.154
D	22.658	7.918	4.814	0.972	-0.900
Remark	$\log_{10} N = a - b\log_{10}\Delta\tau$ Δτ : Stress range		$P = 1.0 - \exp\{-[(\chi-\chi_o)/\beta]^m\}$ P : Probability of failure χ : Deviation		

Fatigue Strength of Grouted Tubular Steel Connections for Offshore Structures

Résistance à la fatigue des assemblages scellés au mortier de tubes en acier pour les structures "offshore"

Ermüdungsfestigkeit von mit Mörtel vergossenen Stahlrohrfüssen bei „Offshore"-Konstruktionen

C.J. BILLINGTON
Wimpey Laboratories Ltd.
Hayes, Middlesex, England

I.E. TEBBETT
Wimpey Laboratories Ltd.
Hayes, Middlesex, England

SUMMARY
Grouted connections form the primary structural connections between large steel jacket structures and their foundation piles and are essential to the integrity of the offshore installation. These connections are subjected to cyclic loading due to environmental conditions during grouting, curing and subsequent life. This paper describes and presents the results from tests simulating cyclic loading during early life and long term fatigue loading. Results include relationships of the S-N form and measured displacements. Implications for design and offshore construction are discussed and recommendations are made.

RESUME
Les scellements au mortier constituent les principales liaisons structurales entre les grandes structures en tubes minces et leurs piles de fondation, et sont essentiels pour l'intégrité d'une installation „offshore". Ces liaisons sont soumises à des charges cycliques dues aux conditions environnantes aussi bien durant l'opération de scellement que pendant la cure et la période d'utilisation postérieure. Cet article décrit et présente les résultats d'essais simulant des chargements cycliques à un âge jeune ainsi que les sollicitations de fatigue au cours du temps. Les résultats sont constitués de relations de la forme S-N et des déplacements mesurés. On discute des conséquences pour le dimensionnement des constructions „offshore" et des recommandations sont faites.

ZUSAMMENFASSUNG
Die wichtigsten Verbindungen zwischen der Stahlkonstruktion und den Fundationspfählen werden bei „Offshore"-Bauten mit Zementmörtel sichergestellt. Diese Verbindungen sind während des Vergiessens mit dem Mörtel, während der Erhärtung sowie während der Nutzungsdauer Wechselbelastungen ausgesetzt. Der Beitrag beschreibt die Resultate von dynamischen Versuchen, die die Belastungen im Anfangsstadium sowie die spätere Ermüdungsbelastung simulieren. Es werden die gemessenen Verschiebungen sowie Wöhlerkurven vorgestellt. Vorschläge für die Bemessung von „Offshore"-Konstruktionen werden unterbreitet und Folgerungen daraus abgeleitet.

1. INTRODUCTION

Cement grouted connections are used between large steel jacket structures and their foundation piles. Adequate static strength and long term integrity of these connections, which due to environmental conditions are subjected to continuous dynamic loading throughout their life, are essential. The UK Department of Energy has funded a comprehensive experimental programme at Wimpey Laboratories to generate design data for grouted connections. This paper presents the results of investigations into the behaviour of connections subjected to cyclic loads.

2. EARLY AGE CYCLIC LOADING TESTS

2.1 Objective

During grouting, relative axial displacements between the pile and sleeve can exist due to wave action, particularly for the first piles to be grouted. Reduced scale tests have investigated subsequent ultimate strength and performance. These tests were carried out at real time wave frequency.

2.2 Details of programme

A total of eight tests were carried out using tubular geometries which represent approximately 1/5th scale of prototype connections on major North Sea installations. The grouted length (L) was equal to two pile diameters. Three specimens were plain pipe, the remainder having mechanical shear connectors in the form of weld beads. Two different cementitious grout mixes were used: an Oilwell 'B' mix in general use for structural grouting applications in the North Sea and a High Alumina Cement (HAC) mix which may be used when an early high strength is required.

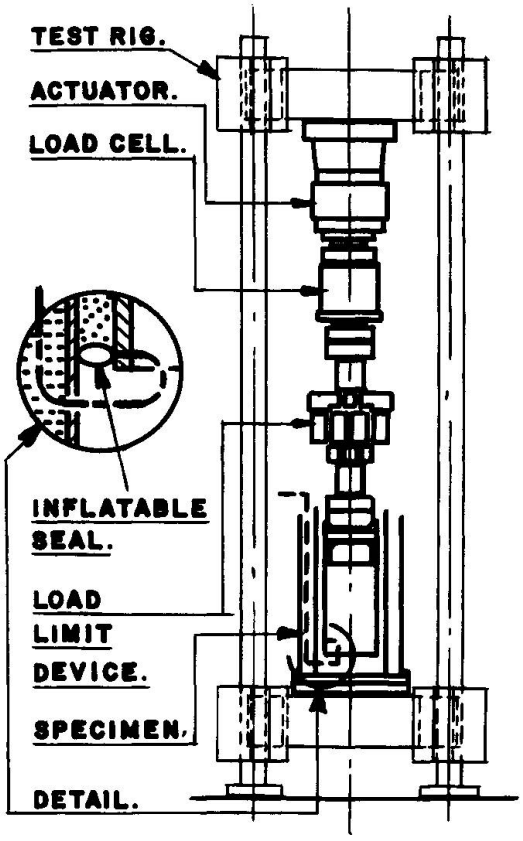

Fig. 1 Early age cyclic load arrangement

2.3 Input displacement and load limits

The applied cyclic loading was designed to represent the effects of a 7.5 m wave on a typical jacket. For the example structure this produces a relative movement of $\pm$ 0.0035D before grouting or an equivalent bond stress of 0.06 N/mm^2 when the grout is set. The frequency of input was 0.1 Hz (approximate North Sea wave frequency) and a sinusoidal wave form was used. One test was carried out with input displacement of $\pm$ 0.0017D.

2.4 Test arrangements

The cyclic loading was applied by a servo hydraulic actuator within a stiff frame as shown in Figure 1. The actuator was operated in displacement control and an adjustable load limiting device was placed in series with the actuator. The input load was measured by load cell in series with the actuator and load limit device. Relative displacement of the tubulars was measured by independent transducers. Data from the load cells and displacement transducers were recorded on an X-time plotter.

2.5 Test procedure

The surfaces of specimens to be in contact with grout were shotblasted and the tubulars were then assembled concentrically. An inflatable rubber tube was used to effect a grout seal and tubular concentricity at the lower end. The specimen was placed in a cooling jacket and the whole assembly was placed in the test rig, as shown in Figure 1.

Water at 8°C representing North Sea temperatures was circulated through the cooling jacket. The cyclic movement was then introduced, the grout seal checked and the annulus filled with seawater. Grout was then injected into the bottom of the annulus displacing the seawater. Grout cubes were also cast and cured at 8°C for determination of grout compressive strength on completion of the test. Cycling was continued for a number of days after grouting with continuous monitoring of load and displacement. On completion, the specimen was subjected to ultimate load test using the procedures described in Reference 3.

2.6 Test results

2.6.1 Displacement and loads during curing

Typical displacement-time and load-time results are given in Figure 2. During the setting period the displacement reduces quickly with a corresponding increase in load. Thereafter the results indicate generally stable conditions, although some further reduction in displacement may occur. The shapes of the displacement and load cycles show very small elastic movements at the lower load range with larger rapid movements on or shortly after load reversal.

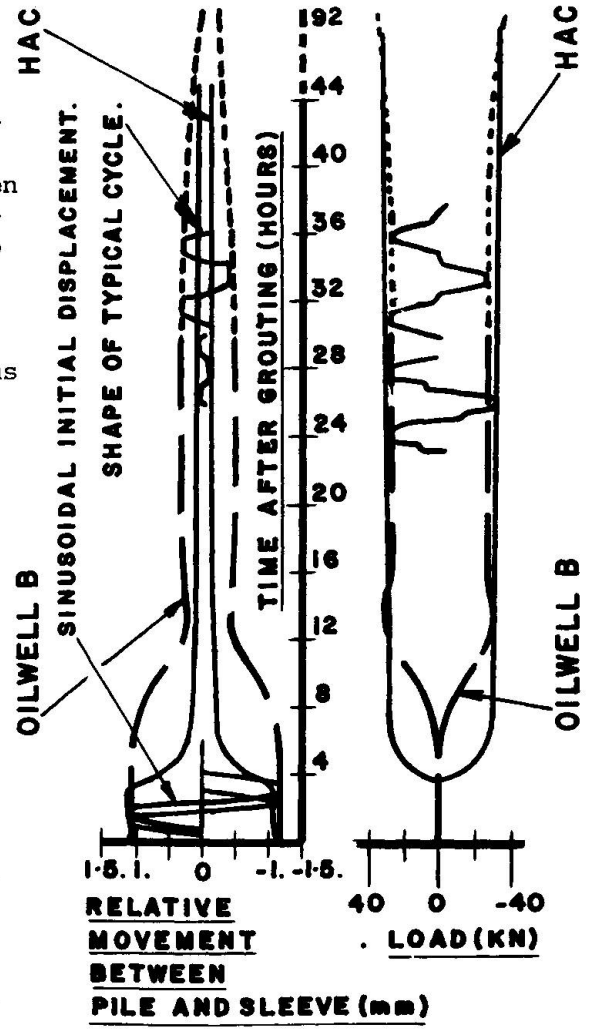

Fig. 2 Load-time and displacement-time graphs

2.6.2 Setting times & residual displacements

Initial set, as determined from the displacement-time graphs, occurred 3 hours after grouting for HAC specimens and 7 hours for Oilwell 'B' specimens. The HAC specimens reached a stable condition (minimum displacement, maximum load) by 8 hours after grouting, whereas Oilwell 'B' specimens did not reach this condition for approximately 24 hours.

All specimens exhibited a reduction in displacement during grout setting. However, displacements were not completely eliminated. Typical residual displacements were:-

Specimen type	Displacements as multiple of pile diameter	
	Input	Residual
Oilwell 'B' with shear connectors	± .0035	± .0003
Oilwell 'B' plain pipe	± .0035	± .0002
HAC with shear connectors	± .0035	± .0004
HAC plain pipe	± .0035	± .0018
Oilwell 'B' with shear connectors	± .0017	± .0001

For a ± 0.0035D input displacement it is found that residual displacements of the order of 10% of the input displacement occur except for HAC plain pipe specimens which exhibit much larger residual displacements (50%). This behaviour was not observed during some preliminary work carried out at approximately 1/20th scale and indicates that reduced scale tests may not fully represent prototype behaviour. For ± 0.0017D input displacement, very small residual displacements are recorded, these being comparable with typical elastic displacements.

2.6.3 Static strength after cycling

Plain pipe specimens gave average strengths 19% greater than predicted by the general formula (1) and specimens with shear connectors gave 10% greater strengths than predicted. Given the degree of scatter in the strength of grouted connections, these increases are not considered significant.

2.6.4 Stiffness during static loading tests

The general shape of the load-displacement curve was as expected. However the stiffness of the specimen and the displacement at which ultimate load was achieved were significantly greater than those recorded for comparable specimens not subjected to early age cyclic loading. Typical results are:

Specimen type	Displacement at ultimate load (mm)	
	Static only	After early age cycle
Oilwell 'B' with shear connectors	8	18
Oilwell 'B' plain pipe	18	45
HAC with shear connectors	8	15
HAC plain pipe	18	30

Similarly, at working load (one sixth of ultimate) the stiffness is significantly reduced by early age cycling.

3. FATIGUE TESTS

3.1 Objective

This programme was designed to investigate the performance of grouted connections under long term sinusoidal loading and to determine whether a relationship of the S-N form exists for such connections.

3.2 Details of programme

A total of thirteen specimens, including both plain pipe connections and connections with shear connectors, were tested. A single tubular geometry identical to that used for the early age investigation was used. To eliminate the effects of early age cycling and to enable the test on any one specimen to be carried out under near uniform grout compressive strength, specimens were prepared under zero load and cured for a minimum of 28 days at 8°C. In this case the grouted length of specimens with weld beads was restricted to give L/D = 1 because of load capacity limitations. Plain pipe specimens had L/D = 2.

3.3 Applied loading

Ten of the thirteen specimens were subjected to fully reversible sinusoidal loading at single amplitude. The magnitude of applied loads are expressed here

as a proportion of the estimated ultimate strength of the connection (based on grout compressive strength determined from 76 mm cubes subjected to identical curing regime) and varied between $\pm$ 0.2 and $\pm$ 0.6 times ultimate strength. Initially tests were conducted at the extremes of this range to determine general trends in the results and establish the failure mechanism. High load tests giving short lives were carried out at 0.1 Hz and longer life tests at 3 Hz.

One specimen was subjected to unidirectional loading with zero minimum load and up to a maximum of + 0.8 times ultimate strength. Since failure of the grouted connection did not occur, this was subsequently tested under static conditions. Similar results were found for the plain pipe specimens under fully reversible load and these were also subsequently tested under static conditions.

3.4 Test arrangements

The cyclic loading was applied by a 1000 kN capacity servohydraulic actuator in a test arrangement similar (except with no load limit device) to that shown in Figure 1. The actuator was operated in force control with displacement and force responses monitored as load-deflection graphs on an X-Y plotter.

3.5 Specimen preparation

After shotblasting of surfaces to be in contact with the grout the tubulars were assembled concentrically on a timber and rubber base designed to seal the annulus and centralise the tubulars at the lower end. The specimen was placed in a large curing tank containing water at 8°C and the annulus filled with water. Grout was then injected from the lower end of the annulus displacing the seawater. Grout cubes were also prepared and cured in an identical environment; these were used to determine grout compressive strength at start and completion of the fatigue test.

3.6 Test results for specimens with shear connectors subjected to reversible loading

3.6.1 S-N relationships

For each specimen an estimate of the ultimate bond strength (f_{bue}) was calculated from measured grout compressive strengths and grouted lengths. The applied bond stress amplitude (f_{ba}) was also calculated.

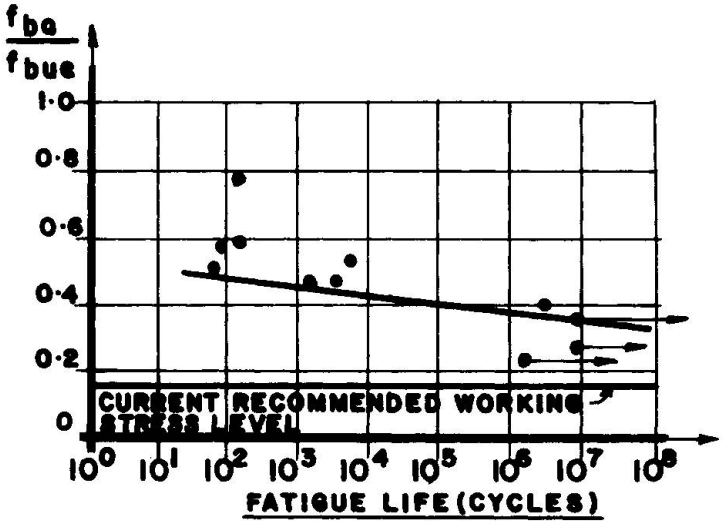

Fig. 3 Fatigue test results in S-log N form

The available test results are presented in S-log N form in Figure 3 in log S - Log N form in Figure 4.

The results form two groups: one group with lives in the range 10^1 to 10^4 cycles and the second group with lives in excess of 10^6 cycles. In the second group only one specimen actually failed, two others having been tested to 10^7 cycles without apparent deterioration.

The results indicate a value for f_{ba}/f_{bue} of 0.4 below which no failure occurs at less than 10^7 cycles (and possibly failure does not occur at all). Above

f_{ba}/f_{bue} of 0.4 a linear relationship has been found to describe the lower bound to the test results. Figures 3 and 4 also indicate the maximum permitted bond stress used in current design. This gives a safety factor of 6 on mean strength giving i.e $f_{ba}/f_{bue}=0.166$, which is less than half the identified endurance limit.

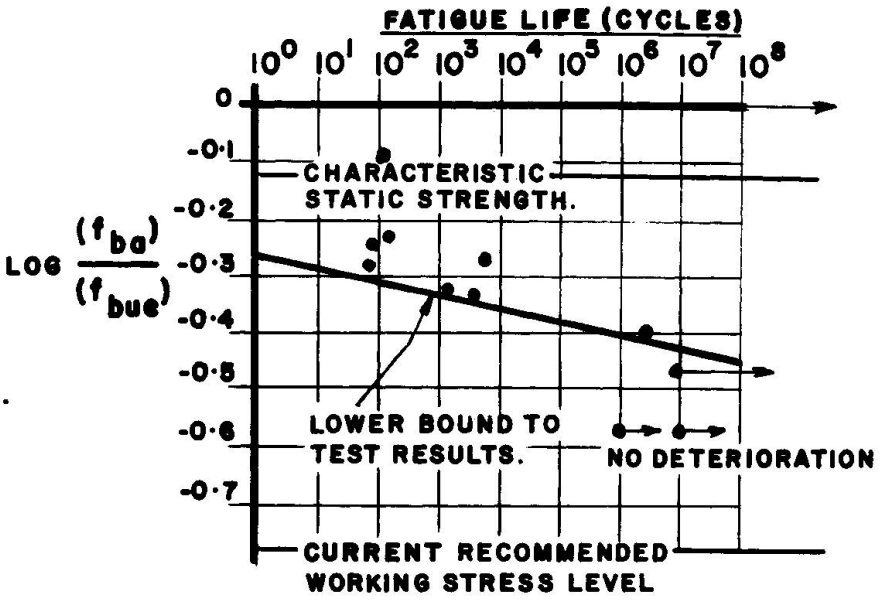

Fig. 4 Fatigue test results in log S - log N form

3.6.2 Measured displacements, hysteresis loops and form of failure

The connections failed by fatigue of the grout rather than of the steel tubulars. For specimens with f_{ba}/f_{bue} less than 0.4, a linear load-displacement is found throughout the applied load range with no measurable hysteresis loop. For more highly loaded specimens the maximum loads cause departure from the linear load-displacement relationships and since the load was fully reversible a significant hysteresis effect is present. A typical hysteresis plot showing the complete life for a specimen with approximately 80 cycle life is given in Figure 5.

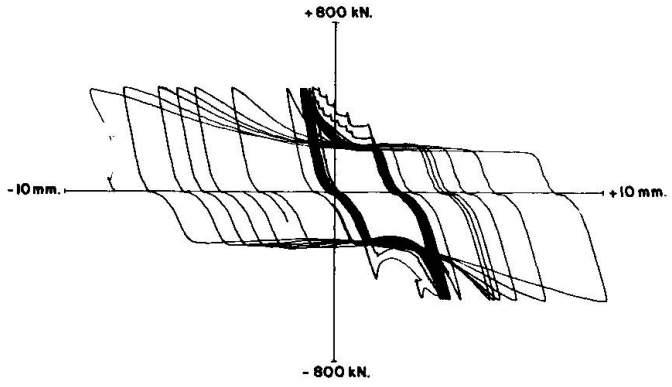

Fig. 5 Hysteresis of connection with mechanical shear connectors

When the measured displacement amplitudes for each cycle are plotted as shown in Figure 6, it can be seen that failure is sudden, with no loss of stiffness occurring before approximately the final five percent of the life. The form of failure of the more highly loaded specimens and the absence of any significant hysteresis effect when f_{ba}/f_{bue} is less than 0.4 can be understood by reference to the known failure mechanism under static loads (3). Only when the peak loads are sufficient to create a void adjacent to the weld bead can impact occur on load reversal leading to fatigue failure.

3.7 Test results for specimens with shear connectors subjected to unidirectional loading

One specimen with shear connectors was subjected to cyclic loading between zero and a maximum tensile load. This was initially subjected to approximately 10^6 cycles of load at cyclic stress varying between zero and 0.8 times estimated ultimate load without deterioration. A single large load well into the non-linear region was then applied. A further application of 2.8×10^6 cycles of fatigue loading was then applied without deterioration of the connection. The specimen was then subjected to ultimate load test to confirm the estimated bond strength.

The displacements under the single application of static load were sufficient to generate voids behind the shear connectors. However, since the load was not reversible impact effects did not occur and no further deterioration of the connection was recorded.

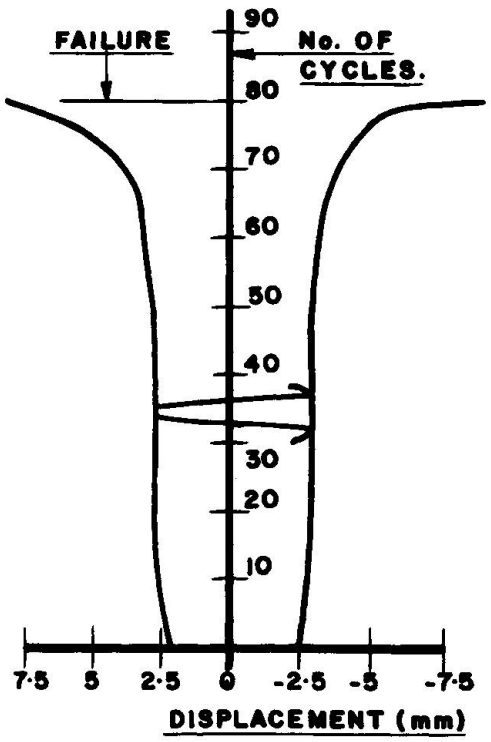

Fig. 6 Displacement amplitude against number of cycles for connection with mechanical shear connectors

3.8 Test results for plain pipe specimens

A programme of tests to determine an S-N relationship for plain pipe specimens was originally envisaged and three specimens were prepared for testing under reversible loading. The first specimen was subjected to a total of 10^5 cycles of load at 0.1 Hz over a range of maximum loads up to 0.5 times the estimated strength with no deterioration of the connection. The specimen was then subjected to 3 x 10^6 cycles of load at 3 Hz between 0 and 0.63 times estimated strength, again with no deterioration.

The mode of failure of a statically loaded plain pipe connection does not involve significant degradation of the grout such as that which occurs adjacent to a shear connector and it is generally found that the post ultimate strength of a plain connection is close to the original value until very large displacements have been introduced. The load-displacement characteristics of a plain pipe connection are also different in that failure is more sudden with very little non-linear behaviour before sudden slip of the connection. This and the results of the fatigue tests lead to the conclusion that fatigue of the grout was only likely to occur at very high bond stresses (perhaps greater than 0.8 times bond strength) and further testing was not undertaken in this programme. The two specimens already prepared were subjected to static loading to obtain improved estimates of ultimate strength.

4. CONCLUSIONS AND DESIGN IMPLICATIONS

4.1 Early age cyclic loading

(1) For the input displacements tested, the ultimate strength of a grouted connection subjected to cyclic movement during grouting and curing is comparable to that of specimens cured without movements.

(2) The test results indicate a significant reduction in stiffness both at working load and at ultimate load compared with specimens cured without movement. This has the following implications for design -

- unequal distribution of loads between piles in a group if the piles are not all grouted at the same time

- the designer may choose to limit environmental conditions in which grouting may proceed to keep displacements/applied loads to a level where significant residual displacements under cyclic load do not occur. Alternatively temporary mechanical devices could be used to restrict movements

- residual displacements may affect the long term fatigue performance

(3) Specimen size may influence test results and it is recommended that full scale tests are carried out to confirm the above conclusions.

4.2 Long term fatigue loading

(1) Grouted connections can fail by fatigue of the grout rather than of the steel tubulars. Failure is sudden with no loss of stiffness occurring until approximately the final five percent of life.

(2) An S-N relationship can be identified for grouted connections with mechanical shear connectors subjected to reversible loading.

(3) There would seem to be a stress range endurance limit (at approximately 0.4 times ultimate strength) below which failure does not occur and which has negligible influence on the life when subsequently subjected to higher stress ranges.

(4) Whilst the above endurance limit is greater than permissible stresses used in static design, fatigue has only been investigated for short connections (L/D = 2). In practice, connections are much longer (L/D between 8 and 16). Static design formulae are derived by factoring ultimate load which, because of the inherent ductility, occurs after complete redistribution of elastic peak stresses. Situations may arise where elastic peak stresses lead to local fatigue failure; the residual capacity and capacity for redistribution would be low and progressive failure might result. Further testing of longer specimens is required.

(5) Plain pipe connections and connections subject to unidirectional loads are less susceptible to fatigue failure than connections with shear connectors subjected to reversible loading.

(6) The interaction of early age cyclic loading (during grouting and curing) and long term fatigue loading has not been investigated. The effect of impact due to the presence of voids adjacent to weld beads is such that the subsequent fatigue performance of connections subjected to reversible loading may be affected by early age cyclic loading and this requires further investigation.

REFERENCES

1. Billington C.J and Tebbett I.E. The basis for new design formulae for grouted jacket to pile connections. Paper OTC 3788 of Offshore Technology Conference, Houston, Texas, May 1980.

2. Department of Energy. Offshore Installations : Guidance on design and construction, London 1977.

3. Tebbett I.E and Billington C.J. Model studies of grouted connections for offshore structures. Paper 7 of I.Struct.E/BRE Seminar on The Use of Physical Models in the Design of Offshore Structures, Watford, November 1979.

Méthode de dimensionnement des câbles à la fatigue

Methode zur Bemessung von Drahtseilen auf Ermüdung

Design Selection of Wire Ropes Based on Fatigue

UGO ROSSETTI
Professor
Politecnico Torino
Torino, Italie

RESUME
Le calcul des câbles est actuellement effectué à l'aide d'un coefficient de sécurité fixe rapporté à l'effort de traction. La méthode illustrée, inspirée d'une conception probabiliste de la sécurité, considère comme critère de calcul l'endommagement par fatigue-usure et l'hypothèse de Miner en employant une courbe d'endurance appropriée ainsi qu'un spectre réaliste des charges en service.

ZUSAMMENFASSUNG
Die Dimensionierung von Drahtseilen erfolgt heute mit einem Sicherheitskoeffizienten bezogen auf die Zugkraft im Seil. Die vorgeschlagene Methode beruht auf einem probabilistischen Sicherheitskonzept. Die Schädigung durch Ermüdung und Abnützung dient als Bemessungskriterium unter Anwendung der Palmgren-Miner-Hypothese mit einer Ermüdungsfestigkeitskurve des Seils und einem realistischen Betriebslastspektrum.

SUMMARY
At present, wire ropes are designed on the basis of a fixed safety coefficient related to the axial load. The method proposed considers the fatigue-wear damage as a design criterion. It is based on a probabilistic safety concept and uses Miner's hypothesis applied to a realistic endurance curve of the rope and an appropriate service load spectra.

1. INTRODUCTION

Le câble d'acier constitue une structure assez compliquée dont le calcul rigoreux est sans aucun doute un problème extrèmement lourd même en présence d'hypothèses simplificatrices.
En réalité le câble est aussi à considérer comme une machine transmettant une énergie à distance, avec les problèmes dynamiques des machines: donc structure et machine à la fois.
Le projet des câbles et la vérification de leur sécurité sont effectués par des Règles basées sur une limite fixe de l'effort axial maximum rapportée à l'effort de rupture statique sur brin droit; sur des rapports minimaux du diamètre de la poulie ou galet avec le diamètre du câble, et/ou des fils; sur une durée maximale de vie fixée à priori par les Normes; sur un contrôle périodique des ruptures des fils extérieurs et/ou sur des inspections périodiques magnéinductives. (*)
Quant aux essais de réception, ils sont purement statiques (traction, flexion, torsion des fils et traction sur brin droit) en dépit du fait que les câbles sont soumis, au passage sur poulies et galets, à des contraintes dynamiques donnant lieu à des phénomènes de fatigue et d'usure.
D'autre part le principal critère de dimensionnement prévu par les Règles est le coefficient statique de sécurité à traction, qui n'a aucune liaison directe avec les effort répétés subis par les câbles. Les autres critères se rapportent plutôt à la surveillance périodique ou bien fixent une durée de vie (5, 10, 15 ans) dont il n'est pas facile trouver une justification rationelle.
Cette situation trouve une explication dans la difficulté d'une part de déterminer les actions appliquées au câble en mouvement, d'autre part de calculer les contraintes dans les fils sous ces actions et enfin de mettre au point des essais de réception reproduisant mieux les conditions de service.
Par ailleurs, au cours des dernières années de concepts nouveaux se sont développés (dommage cumulatif en fatigue, spectres de charge, critères "safe-life" et "fail-safe", méthodes probabilistes aux états limites, évaluation statistique des actions et des résistences) que nous nous sommes proposés d'employer pour présenter une méthode nouvelle de calcul des câbles et de vérification de leur sécurité, compte tenu aussi des récents remarquables progrès dans le domaine des recherches d'endurance sur câbles.
Ces recherches ont non seulement permis d'améliorer nos connaissances sur cette structure si compliquée qui est le câble, mais aussi

---

(*) Nous nous rapportons ici aux câbles de téléphériques à passagers ou aux câbles de levage de mines ou ascenseurs: pour les autres cas les règles sont simplifiées.

d'affirmer que:
a) deux câbles apparemment analogues, présentant des résultats semblables aux essais classiques de réception peuvent donner lieu à des comportements très différents soit à l'essai de fatigue soit en service: ceci parce que la durée d'un câble dépend de plusieurs paramètres que les essais actuels ne sont pas à même de contrôler ou de mettre en évidence, ce qui peut être fait d'une façon synthétique par l'essai de fatigue qui reproduit au mieux les conditions de travail du câble;
b) les durées maximales de vie fixées par les Normes sont en général trop reduites et l'endurance restante du câble, mesurée après dépose avec essai de fatigue, est souvent assez élevée; ceci n'empêche pas d'observer que dans certains cas la durée a été inférieure à celle prévue par les Règles;
c) la courbe de fatigue du câble peut être exprimée par une équation du type Wholer - Weibull mais sans limite de fatigue;
d) les essais en charge progressive et par blocs ont confirmé la validité de l'hypothèse de Miner dans la fatigue des câbles.

2. PRINCIPES DE LA NOUVELLE METHODE

2.1 Etat limite ultime de la structure-câble.

Nous établissons de choisir comme état limite ultime la durée jusqu'à rupture sous sollicitations de fatigue-usure au lieu de la rupture par effort axial statique prise en compte actuellement.

2.2 Etats limite de service

On peut prévoir les états limite suivants: de déformation par allongement axial excessif, de rupture de fils extérieurs (critère fail-safe), de diminution excessive du diamètre.

2.3 Critère de sécurité

La sécurité sera rapportée à l'endurance du câble. Par l'analyse statistique des actions et de la résistance à la fatigue il est possible de mettre au point un critère probabiliste de sécurité.
En première approximation on pourra adopter un critère déterministe en utilisant un coefficient de sécurité fonction des caractéristiques de l'installation: la durée du câble sera calculée en divisant par ce coefficient l'endurance déterminée par notre méthode.

2.4 Actions

Supposons de nous rapporter au câble tracteur d'un téléphérique.
De l'examen du tracé on peut localiser facilement la zone de câble que subit le plus grand nombre de flexions sur poulies et galets: dans les sections correspondantes on devra calculer l'effort axial du câble dans les combinaisons les plus défavorables (charges permanentes, vent, nombre de passagers en montée et en descente).

2.5 Contraintes dans les fils

Les actions donnant lieu à l'effort axial, l'effet de flexion sur poulies et galets ainsi que la pression Hertzienne sur les gorges et les éventuels effets de torsion produisent dans les fils des contraintes dont le calcul rigoreux est assez complexe, compte tenu de la complexité de la "structure-câble".
En accord avec d'autres auteurs [1] [2] nous proposons la formule conventionelle élastique:

$$\sigma_r = \sigma_t + \sigma_f = \frac{T}{A \cos \varphi_1 \cos \varphi_2} + E \frac{\delta}{D} \cos^2 (\varphi_1 \pm \varphi_2) \qquad (1)$$

où:

σ_r = contrainte de référence (MPa)

σ_t, σ_f = contraintes théoriques de traction et de flexion (MPa)

T = effort local de traction [N]

A = aire de la section du câble

φ_1, φ_2 = angles de toronnage et de câblage

δ = diamètre des fils considérés

D = diamètre de la poulie; au cas de flexion ponctuelle sur galet, D = 2R où R est le rayon de courbure minimal déterminé en fonction de la situation locale à l'aide des résultats d'essais préalables de raideur. (°)

2.6 Bloc de charge

Le bloc de charge représente la succession des valeurs de la contrainte de référence correspondantes à une course du câble. Dans cette détermination les valeurs des contraintes de référence sont considérées uniquement en correspondance des passages du câble sur de poulies ou galets; (dans un téléphérique étudié par nous, un bloc typique pourrait être le suivant: 8 valeurs de σ_R sur galets d'un appuis, 12 valeurs de σ_R sur galets d'un autre appuis, 4 valeurs différentes au passage sur les poulies de la station motrice, 8 valeurs sur galets d'un appui en descente).

2.7 Courbe de fatigue du câble

Le courbe de fatigue en flexion-traction est déterminée en Laboratoire par un raisonnable nombre d'essais visant à reproduire autant que possible les conditions de service.

(°) Nous avons mis au point un appareil qui détermine en Laboratoire la "ligne élastique" du câble en correspondance d'un galet chargé par une force transversale P sous divers efforts axiaux. De ces essais de raideur ou tire des abaques permettant d'évaluer la courbure du câble dans les situations de service.

Les contraintes dans les fils lors de l'essai sont calculées par la même formule (1).
L'équation de la courbe de fatigue peut être exprimée, dans sa forme la plus simple, par une rélation du type:

$$\sigma_R^n N = C \qquad (2)$$

où n et C, constantes à déterminer pour chaque câble par voie d'expérience, N = durée en flexions.
Puisque les résultats des essais ont une distribution gaussienne, il est possible d'en effectuer l'élaboration statistique et de définir une courbe de fatigue caractéristique déplacée vers l'axe des σ_R d'après le fractile choisi.

2.8 Calcul de l'endurance du câble

La (2) permet de calculer les durées N_i pour chaque valeur σ_R du bloc de charge et donc l'endommagement pour chaque bloc. Par la loi de Miner il est alors possible de calculer le nombre de blocs correspondant à la rupture par fatigue du câble en service, soit l'endurance du câble.

2.9 Sécurité du câble

La vie acceptable du câble sera déterminée en divisant l'endurance par un coefficient approprié (voir 2.3).
Avec un critère semiprobabiliste on pourrait définir les valeurs caractéristiques soit du bloc de charge, soit de la courbe de fatigue et appliquer ensuite un opportun coefficient de sécurité à la durée ainsi calculée.

2.10 Etude d'optimisation

La méthode permet une étude d'optimisation des coûts du téléphérique (diamètres du câble, des poulies et galets; dimensions des structures) en fonction d'une durée optimale du câble compte tenu aussi des états-limite d'exercice, des frais de dépose et de remplacement.

3. OBSERVATIONS

La méthode proposée est sans aucun doute plus rationelle de celle utilisée à présent et constitue un projet de code de calcul basé sur la fatigue (fatigue design code).
Du point de vue pratique il faut toutefois observer que des études ultérieures sont nécessaires soit sur la formule (1) pour le calcul des contraintes dans les fils, soit sur la formule (2) qui exprime la courbe d'endurance, que d'après les critères de la fatigue classique devrait être fonction de l'amplitude $\Delta\sigma$ de la contrainte variable, la contrainte moyenne étant un paramètre mesurant la position de la courbe dans le graphique $\Delta\sigma$ - N.
Quant à l'expression (1) la plupart des auteurs estiment de pouvoir l'utiliser, tout en tenant compte de son caractère conventionnel.

En ce qui concerne la formule (2) il y a au contraire une certaine disparité de points de vue qui a donné lieu à d'autres propositions telles que, par exemple:

Drucker et Tachau (1936): $$\left(\frac{2\ TA}{\sigma_R\ dD}\right)^m N = C \qquad (3)$$

Giovannozzi (1964): $$\sigma_t^n \left(100\ \frac{d}{d+D}\right)^m N = C \qquad (4)$$

Meeuse (1976): $$\left(\sigma_t + \frac{\sigma_f}{2}\right)^m N = C \qquad (5)$$

Luboz (1978): $$\left(\frac{\sigma_f}{2}\right)^m \left(\sigma_t + \frac{\sigma_f}{2}\right)^n N = C \qquad (6)$$

Dans la (3) σ_R est la contrainte de rupture de l'acier des fils, d est le diamètre du câble.
Une discussion de ces formules à été effectuée [3] [4] [5] et se poursuit au sein de l'OIPEEC (Org. Internationale pour l'étude de l'endurance des câbles); ici nous nous bornons à observer que toutes les courbes que l'on obtient par les différentes formules de (2) à (6) s'approchent assez bien des résultats d'expérience dans le domaine des essais de Laboratoire, qui couvrent une partie seulement des situations de service.
Le problème se pose quand on doit extrapoler les courbes pour des situations extrèmes de service: très grands rayons de courbure, soit au passage sur galets, ou très faibles tractions axiales. Dans ces cas les courbes diffèrent entre elles et les calculs du dommage par fatigue et la durée du câble donnent lieu à des différences sensibles dans les résultats. [5]
Des recherches ultérieures ainsi que des observations systématiques sur des câbles en service dont le comportement à fatigue ait été préalablement étudié en Laboratoire pourront éclaircir cet aspect très important pour les câbles travaillant sur galets.
Pour les câbles de levage en général on peut affirmer que la méthode illustrée ne présente pas de problèmes.
En conclusion notre proposition montre la possibilité de préparer un code de règles de réception, calcul et sécurité plus adhérent aux conditions d'emploi des câbles et cohérent avec les progrès récents en d'autres domaines de la technique des constructions.

Bibliographie

[1] GRECO,PERCIABOSO,ANNIBALI: Convegno Internazionale Funiviario. Torino, ottobre 1970
[2] GIOVANNOZZI R.: Comma 1 Research OIPEEC Bulletin 8, 1965
[3] LANZARO, ROSSETTI, TONGHINI: Atti Istituto Scienza Costruzioni Politecnico Torino, n° 390, 1978
[4] CLEMENT Ph.:OIPEEC Bulletin 37, 1980
[5] ROSSETTI U.: Round Table Cracow University, June 1981

Fatigue Crack Propagation in Steel Prestressing Wires

Propagation des fissures dues à la fatigue dans les fils de précontrainte

Ermüdungsrissfortpflanzung in Vorspanndrähten

V. SANCHEZ-GALVEZ
Prof. Dr.
Univ. Politécn. de Madrid
Madrid, Spain

M. ELICES
Prof. Dr.
Univ. Politécn. de Madrid
Madrid, Spain

A. VALIENTE
Prof. Dr.
Univ. Politécn. de Madrid
Madrid, Spain

SUMMARY
This paper presents the results of research carried out to determine fatigue crack growth in steel prestressing wires. Measurements were made by using the compliance method and recording continuously the compliance of the sample by means of a dynamic extensometer. Tests performed at different frequencies, waveforms, stress ratios and load amplitudes show that fatigue crack growth can be described by a Paris law.

RESUME
Cette communication présente les résultats d'une recherche réalisée pour déterminer la vitesse de propagation des fissures de fatigue dans les fils de précontrainte. Les mesures ont été faites au moyen de la méthode de la flexibilité avec un extensomètre dynamique. Les essais qui ont été réalisés à différentes fréquences, formes d'onde, relations de contraintes et amplitude de charge, ont montré que la propagation des fissures dues à la fatigue peut être décrite par une expression de Paris.

ZUSAMMENFASSUNG
Der Beitrag stellt die Ergebnisse einer Untersuchung über das Ermüdungsrisswachstum in Vorspanndrähten vor. Die Messungen wurden mit einem dynamischen Extensometer durchgeführt. Die Versuche, die mit verschiedenen Frequenzen, Wellenformen, Spannungsverhältnissen und Belastungsamplituden durchgeführt wurden, zeigen, dass das Ermüdungsrisswachstum mit einer Gleichung von Paris beschrieben werden kann.

1. INTRODUCTION

In the prestressed concrete industry, steel tendons may be subjected to tensile axial fatigue. But despite the importance of this loading the very few published axial fatigue tests have been made without adequately distinguishing between crack initiation and crack propagation in accordance with most prevailing standards. Recent requirements, in particular the Model-Code [1] issued by CEB (Comite Euro-International du Beton), still specifies for this material an endurance limit from classical Wohler-type or S-N tests. The purpose of this paper is to complement classical approach by applying fracture mechanics techniques to techniques to tendons subjected to axial fatigue. Crack propagation has been measured and is the subject of this paper; work on crack initiation is in progress and will be published later.

2. MATERIALS TESTED

Three steels have been tested; all are eutectoid cold drawn steels, currently used in prestressed concrete structures. Steels A and B were stress-relieved while steel C was stabilized.

Table 1 shows the mechanical properties of all three steels tested. As the material is produced in the shape of wires, the fracture toughness of these steels can not be obtained with compact speciments. Therefore K_C values listed have been determined by testing precracked samples, using single edge notches as starters of surface precracks produced in 3-point bending or in tension.

3. TESTS PERFORMED

Axial loading fatigue tests have been performed in an Instron dynamic testing machine. The observation of crack growth was made by the method of the compliance of the samples. First of all, the compliance of all steels tested has been determined as a function of crack depth by testing in tension several precracked samples with different crack depths. A 12.5 mm. gauge length extensometer provides enough accuracy to achieve a calibration curve compliance vs crack depth.

In fatigue tests, a 12.5 mm. gauge length dynamic extensometer attached to the precracked sample gives a continuous record of the compliance of the sample. A Hewlett Packard data acquisition system has been used to collect and compute compliance data provided by the extensometer and from the calibration curve, to plot the curves of crack depth vs. number of cycles.

All tests have been performed in air at 20°±1°C of temperature and a relative humidity of 50±5%. Load amplitude and frequency have been held constant automatically during the test. Three waveforms have been studied: sinusoidal, triangular and square, and also five frequencies 0.2, 1, 4, 8, 10 and 20 Hz. The stress range was varied from 250 to 610 MPa and R ratio from values below 0.20 to 0.67.

4. EXPERIMENTAL RESULTS

In order to predict fatigue crack growth in prestressing steels it is worthwhile to ascertain whether the experimental results are based upon some general

fatigue crack growth law. Among them, the simplest one is the Paris law [2]:

$$\frac{da}{dN} = C(\Delta K)^n \qquad (1)$$

where da/dN is the crack growth rate, ΔK the stress intensity factor range and C and n constants.

The stress intensity factor for an elliptical crack in the surface of a cylindrical bar in tension is given by the following expression, obtained from a finite element calculation [3] :

$$K = \sigma\sqrt{\pi a}\ \{0.473 - 3.286\ (\frac{a}{D}) + 14.797\ (\frac{a}{D})^2\}^{1/2}\ \{(\frac{a}{D}) - (\frac{a}{D})^2\}^{-1/4} \qquad (2)$$

where a is the crack depth, D the diameter of the wire and σ the remote applied stress.

The stress intensity factor defined by equation (2) has been shown to be a suitable fracture parameter. For each tested material the critical value of this parameter was found to be independent on flaw size. This critical value appears in Table 1 for the three materials as K_C.

From the curves crack depth vs. number of cycles plotted by the system, a numerical differentiation method has been applied to obtain the crack growth rates da/dN at different crack depths. Since the stress range $\Delta\sigma$ was held constant for each test, the stress intensity factor range ΔK can be calculated for these crack depths from equation (2). Then it is possible to plot log. (da/dN) vs. log. (ΔK) and check if there exists a linear relationship as equation (1) predicts.

Steel A has been fully tested to crack the influence of load amplitude, waveform, stress ratio and frequency on the results.

Figure 1 shows the experimental results of crack growth rate vs. stress intensity range in a log. log. plot. for steel A and different load amplitudes. This figure shows that a relationship of the Paris form is able to describe crack growth in prestressing cold drawn steel wires, independently of the stress amplitude applied.

Figure 2 includes also the results obtained at different frequencies, with different waveforms and with different stress ratios. As can be seen, fatigue crack growth in prestressing steel wires is independent of waveform and frequency, as it has been observed for many other alloys [4] . The crack growth also appears independent of stress ratio R. Finally the figure shows the best fit by a straight line in the log. log. plot leading to the following crack growth law:

$$\frac{da}{dN} = 11.08 \times 10^{-12}\ (\Delta K)^{2.3}, \quad \text{where a is in m. and K in MPa } m^{1/2}. \qquad (3)$$

Figures 3 and 4 show the experimental results obtained with steels B and C and the corresponding straight lines fitted. Values of the constants as is shown in those figures are $C = 13.96 \times 10^{-12}$, $n = 2.3$ for steel B and $C = 16.05 \times 10^{-12}$ $n = 2.3$ for steel C. In all cases the correlation coefficient is 0.97.

Values obtained for the constants C and n are very close for the three steels tested within the usual experimental scattering and are in agreement with the experimental results by Ritchie and Knott [5] for material with K_C values similar to those of steels tested.

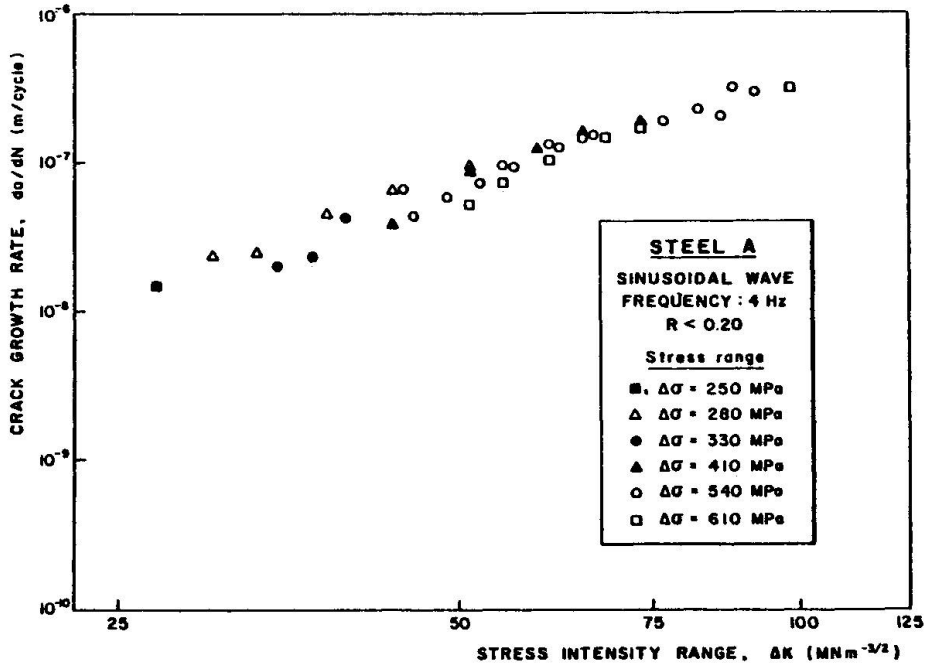

Figure 1. Crack growth rate versus stress intensity range for various stress ranges in steel A.

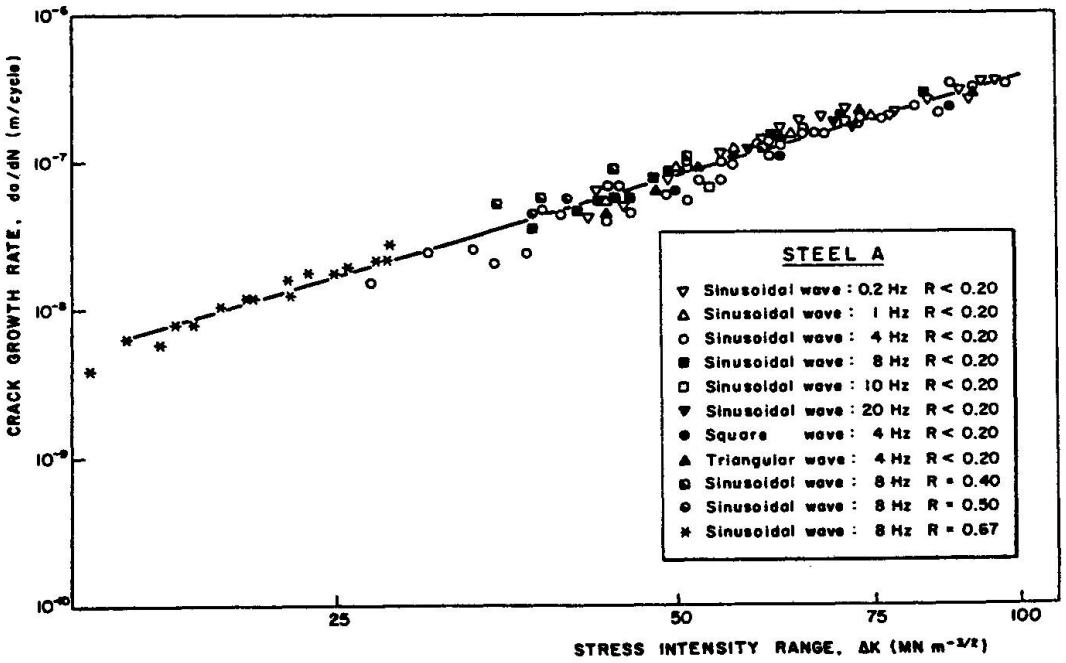

Figure 2. Crack growth rate versus stress intensity range in steel A.

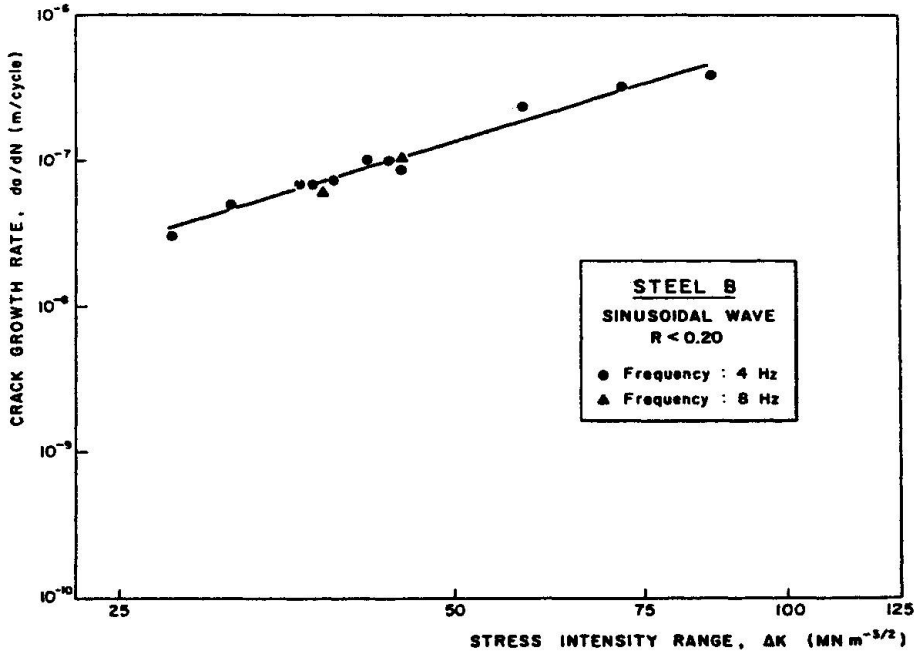

Figure 3. Crack growth rate versus stress intensity range in steel B.

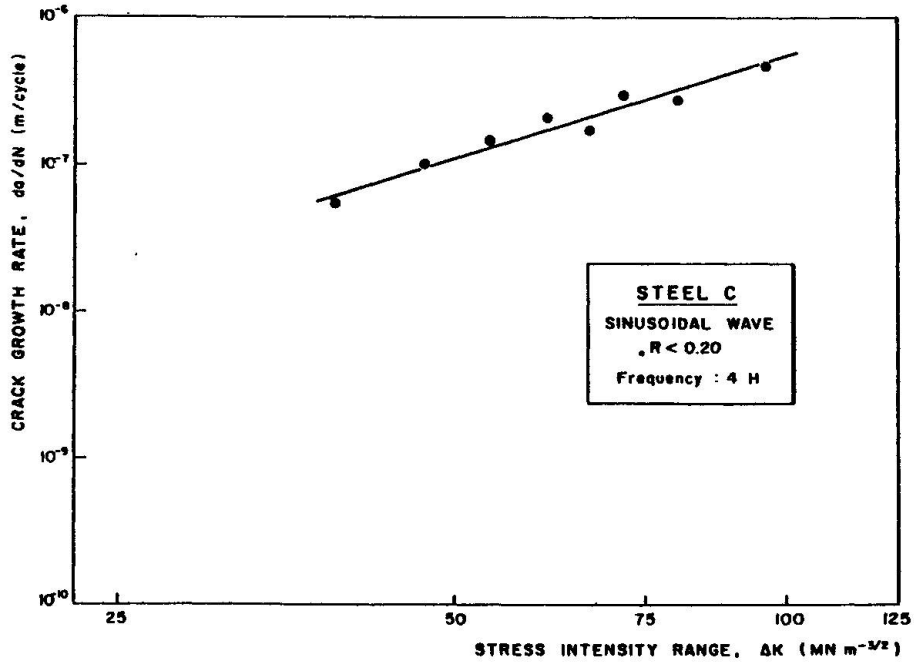

Figure 4. Crack growth rate versus stress intensity in steel C.

Table 1. Mechanical Properties

	Steel A	Steel B	Steel C
Young's modulus (MPa)	2.01×10^5	2.05×10^5	1.81×10^5
0.2% Proof stress (MPa)	1400	1520	1560
Tensile Strength (MPa)	1620	1740	1800
Elongation under max. load (%)	6.5	5.5	6.5
Reduction in area (%)	40	30	35
Fracture Toughness K_c ($MPam^{1/2}$)	108.8	112.3	101.7

5. APPLICATION FOR DESIGN

Two valuables results have been obtained which permit to propose a simple method to predict the life of a prestressing steel wire subjected to cyclic stresses. The first result is that the fatigue crack propagation for these steels follows the Paris law and is independent on stress ratio, frequency and waveform within the abovementioned range. The second one is that the parameters C and n of the Paris law have similar values for all these steels.

If the nominal stress in the wire has a range of variation $\Delta\sigma$, the variation of the stress intensity factor for a crack depth a is given by:

$$\Delta K = \Delta\sigma \sqrt{\pi a}\, M \text{ where} \tag{4}$$

$$M = \{0.473 - 3.286 \left(\frac{a}{D}\right) + 14.797 \left(\frac{a}{D}\right)^2\}^{1/2} \{ \left(\frac{a}{D}\right) - \left(\frac{a}{D}\right)^2 \}^{-1/4} \tag{5}$$

By substituting equation (4) in the Paris law (1) and integrating, the following expression is obtained:

$$N_R = \frac{(\Delta\sigma \sqrt{\pi D})^{-n}}{C} \{F \left(\frac{a_R}{D}\right) - F \left(\frac{a_o}{D}\right)\} \tag{6}$$

in which the subscript R indicates values at fracture, a_o is the depth of preexisting flaws in the wire and F the non dimensional function:

$$F(x) = \int_o^x \left[\sqrt{x}\, M(x)\right]^{-n} dx \tag{7}$$

which has been calculated for n = 2.3 and is plotted in figure 5.

The critical crack depth a_R has to be obtained from equation (2) by equating the stress intensity factor with its critical value K_C, the stress σ being the maximum value of the stress applied.

The method proposed can be succesfully applied to wires with surface flaws of similar size to those used in this work. On the other hand it would be worthwhile to ascertain whether the method could be applied for the life prediction of prestressing wires without any defect except those produced during the steel processing. Therefore the method proposed has been applied to the fatigue tests results carried out on smooth samples by Elices and Sánchez-Gálvez [6].

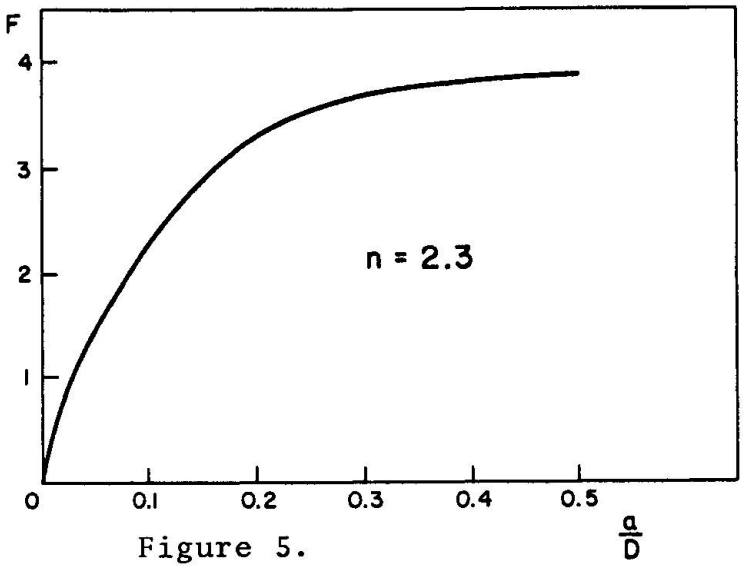

Figure 5.

From all tests results only those tests with stress ranges high enough to ensure that initiation times are negligible as compared with propagation times have been selected.

Table 2 shows for both steels the results of the test (each result is the mean value of four tests) and the predictions obtained from equation (6). To apply this equation a value for a_o has to be assumed.

However figure 8 shows that F (a_o/D) is much smaller that F (a_R/D) for usual values of a_o (below 50 μm) and a_R (which appears in table 2). Therefore f (a_o/D) has been neglected in the calculation. The parameters n and C chosen have been those from the steel A of this work, n = 2.3 and C = 11.10^{-12}.

Table 2 shows that the values of N_R obtained in the tests are in good agreement with the predicted values from the equation (6). Although Linear Elastic Fracture Mechanics (LEFM) has been questioned for such high $\sigma_{max.}$ values, it is hoped that for lower values the agreement should be even better. In consequence this method could be a valuable aid for the designer.

Table 2. Tests results and Predictions

Data of the steels		Steel 1	Steel 2
	Tensile strength (MPa)	1630	1720
	Fracture Toughness K_C (MPam$^{1/2}$)	93.5	82.0
	Diameter (mm)	7	7

Tests results and Predictions

	Δσ (MPa)	$\sigma_{max.}$ (MPa)	a_R (mm)	N_R(measured) 10^5cycles	N_RPrediction) 10^5cycles
Steel 1	330	1300	1.50	3.1	2.8
	410	1380	1.41	1.3	1.7
	330	1460	1.33	2.3	2.7
Steel 2	340	1370	1.23	2.1	2.4
	340	1540	1.03	2.0	2.2

6. CONCLUSIONS

For the first time the crack growth rate in axial loading fatigue for prestressing steel wires has been determined based upon Fracture Mechanics concepts.

Test results show that fatigue crack growth for cold drawn steels can be

described by Paris law. The results are independent of waveform, frequency and stress ratio within the intervals used.

From the tests results it is difficult to ascertain the influence of the heat treatment of the steel on the fatigue crack propagation since the behaviour of all three steels tested has been very similar taking into account the usual scattering of this kind of measurements.

Finally an application to design has been made by predicting the life of wires subjected to axial fatigue. The agreement found with theoretical predictions seems to validate this approach, based on LEFM, although some plasticity should be developed. Starting from known values of K_C, fatigue life under constant amplitude load can be predicted.

REFERENCES

[1] CEB-FIP (1978) Model Code for concrete structures. Paris

[2] PARIS, P.C. and ERDOGAN, F. A critical analysis of crack propagation laws. J. Basic Engng. ASME Series D. 1963, p. 528.

[3] VALIENTE, A. Criterios de fractura para alambres. Ph. D. Thesis. Universidad Politécnica de Madrid. Spain. 1980.

[4] ROLFE, S.T. and BARSON, J.M. Fracture and fatigue control in structures. Prentice Hall. Inc. New Jersey. 1977.

[5] RITCHIE, R.O. and KNOTT, J.F. Mechanisms of fatigue crack growth in low alloy steel. Acta Met., 21, 1973, p. 639.

[6] ELICES, M. and SANCHEZ-GALVEZ, V. Fatiga de alambres de pretensado. Revista de Hormigón y Acero. 1977. p. 85.

Analytical Study for Fatigue of Bridge Cables

Etude analytique de la fatigue des câbles de pont

Analytische Studie über die Ermüdung von freitragenden Brückenkabeln

S. BASU
Senior Mechanical Eng.
Chi Associates, Inc.
Arlington, VA, USA

M. CHI
Chief Engineer
Chi Associates, Inc.
Arlington, VA, USA

SUMMARY

A comprehensive analytical formulation of the fatigue behaviour of highway bridge cables under wind loading is presented in this paper. The formulation includes the deflection and bending stress of highway bridge cables under wind-induced vortex shedding vibrations. The fatigue behaviour of bridge cables resulting from the stress reversals caused by vortex shedding is investigated analytically in this paper using the methodologies of linear elastic fracture mechanics. An attempt is made to compare the results of fatigue life obtained from the formulation with the available experimental data.

RESUME

Une formulation analytique compréhensive du comportement à la fatigue des câbles de ponts autoroutiers soumis aux actions du vent est présentées dans cet article. La formulation inclut la déformation et la contrainte de flexion de ces câbles sous des vibrations dues à des tourbillons alternés de vent. Le comportement à la fatigue des câbles de ponts résultant d'inversions de contrainte produites par des tourbillons alternés est analysé dans cet article par la méthodologie de la mécanique de la rupture linéaire élastique. Un essai de comparaison des résultats de durée de vie obtenus par la formulation avec les données expérimentales disponibles, a été fait.

ZUSAMMENFASSUNG

Der Beitrag behandelt die analytische Formulierung des Ermüdungsverhaltens freier Brückenkabel und -seile unter Windlast. Die Untersuchung berücksichtigt die Deformationen und Biegespannungen infolge der durch Wirbel hervorgerufenen Schwingungen. Das Ermüdungsverhalten unter Wechselbeanspruchung durch die Wirbelwirkung wird unter Anwendung der Methode der linear elastischen Bruchmechanik analytisch behandelt. Es wird der Versuch unternommen, vorhandene experimentelle Ergebnisse über die Lebensdauer unter Ermüdungsbeanspruchung mit der rechnerischen zu vergleichen.

1. INTRODUCTION

Although the concept that a bridge deck can be strengthened by stay cables was first conceived by Fanstus Verantius [1] in Italy, during the early seventh century, the large scale application of this concept to major bridges was quite recent, especially in the U.S.A. The detailed behavior of cable-stayed bridges and the design and construction procedures have been well-established and are available in standard references [1, 2]. However, there are still gaps of knowledge at the present time; for example, there exists no guidelines for stay cable design for prevention of fatigue failure of stay cables due to wind-induced vibrations.

Stay-cables are susceptible to Strouhal vibrations. If the prevailing wind velocities in a geographic location frequently produce resonance conditions in the cable, it is conceivable, or even probable, that the individual wires in the cable may fail due to wind-induced fatigue loadings.

Although a number of fatigue tests of wires and cables are available in the literature, there is a paucity of analysis of wire fatigue through a rational procedure. Even more difficult is the problem to extrapolate the failure of individual wires to the probably failure of the cable as a whole.

This paper entails an initial attempt to fill this gap of knowledge.

2. STRUCTURAL CHARACTERISTICS OF STAY CABLES

The fatigue behavior of stay cables depends, to a large extent, on its structural properties which, in turn, depend on the geometry of the cable configurations. Under the category of helical wire cables, single strand and multiple strand constructions of a wide variety of configurations are possible. Figure 1 shows the two types of cable configurations commonly used in bridge structures. These are: parallel wire cables and helical wire cables.

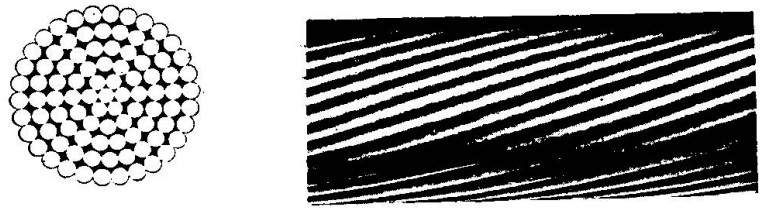

Cable with Helical Wires

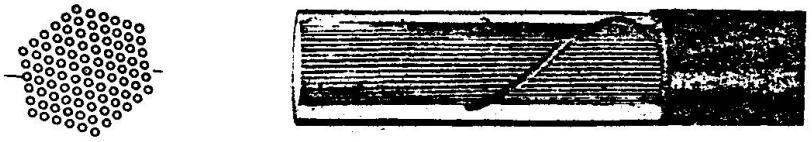

Cable with Parallel Wires

Figure 1. Cable Configurations

Parallel wire cables are made of uncoated, stress-relieved wires which have ASTM designation A421-77BA. Helical wire structural strands are made of zinc-coated steel wires having ASTM designation A586-68, while multiple strand helical cables are manufactured according to ASTM specification A603-70. The mechanical properties of these materials are shown in Table 1.

Table 1. Mechanical Properties of Cable Materials

Material	Zinc Coating Class	Nominal Diameter mm	Minimum Stress at 1% Extension MPa	Minimum Tensile Strength MPa
A 586-68	A	1.016-2.794	1477	1517
		2.820	1576	1517
	B	2.286	1477	1448
	C	2.286	1379	1379
A 603-70	A	1.016-2.794	1477	1517
		2.820	1576	1517
	B	1.016	1477	1448
	C	1.016	1379	1379
A 421-77 (Type BA)		4.978	1407	1655
		6.350	1407	1655
		7.010	1377	1620

When cables are used as structural members, consideration must be given to various factors which determine their load bearing capacities and performance characteristics. One of these factors is the end anchorage which connects a cable to other supporting structural members. End anchorages vary widely in their design and manufacturing techniques and their selection depends on the sizes and properties of the cables to which they are attached. An overview of different cable constructions with particular emphasis on various end anchorages may be found in references [1] and [2]. The reader is also referred to a recent paper on fatigue resistant tendons for cable stayed construction by Birkenmaier [3].

3. FATIGUE ANALYSIS OF STAY CABLES

3.1 Wind-Induced Fatigue Loading

Stay cables used as structural components in bridges are frequently subjected to wind forces which result in vortex shedding. If the vortex shedding frequency is close to any of the natural frequencies of a stay cable, a nonlinear phenomenon known as synchronization or lock-in occurs, and in unfavorable conditions, the cable can undergo large amplitude vibrations.

Recently Basu and Chi [4] investigated the dynamic response of stay cables by considering a simplified vortex excitation model whereby the driving wind force was harmonic with magnitude proportional to the lift coefficient and with frequency equal to the Strouhal frequency. The analytical procedure was used to determine the deflections and bending stresses of stay cables.

Table 2 illustrates typical results of deflections and bending stresses for the main cables of the Intercity Brodge on Columbia River in Pasco-Kennewick, Washington, U.S.A. Properties of the cables are given below:

Length	154 m
Outer diameter of cable	15 cm
Wire diameter	6.35 mm BBR-type
Number of wires	283
Maximum moment of inertia	855 cm^2
Axial stress	745 MPa
Young's modulus	200 GPa

Table 2. Computation of Deflections and Stresses

Mode	Natural Frequency rad/sec	Critical Wind Velocity km/hr	Maximum Deflection mm	Maximum Bending Stress MPa
1	6.5578	2.74	1.082	0.5647
3	19.0608	8.27	1.215	1.7149
5	43.7219	18.98	1.315	3.9064
10	64.5815	28.04	1.093	5.8299
15	96.2724	41.79	1.216	8.8690
29	190.1227	82.52	1.215	18.5110

It is seen that for commonly occurring wind velocities, the magnitude of the maximum bending stress is less than 25 MPa. Moreover, the maximum bending stress is expected to occur at end anchorages. It should be noted that this wind induced bending stress is reversible and cyclic in nature which may cause cables to fail in fatigue.

3.2 Fatigue Life of a Wire

Consider a single wire subjected to wind-induced fatigue loading. The fatigue initiation life of the wire, N_i, is given by the following relationship:

$$N_i = C_1 (\Delta\sigma)^{-\gamma} \tag{1}$$

where $\Delta\sigma$ is the nominal stress range, and where C_1 and γ are two constants which depend, in general, on the material properties. Basu and Chi [4] computed the values of C_1 and γ by a statistical fit of various test data on the fatigue life of high strength steel wires, and found that for wires with average tensile strength of 1650 MPa:

$$C_1 = 1.57 \times 10^{26} \text{ and } \gamma = 7.5$$

The fatigue initiation life of a single wire can therefore be calculated from the knowledge of C_1 and γ.

The fatigue propagation life of a single wire can be determined from the following relationship:

$$\frac{da}{dN} = C_2 (\Delta K)^{\mu} \tag{2}$$

where a is the crack size, ΔK (or equivalently, ΔK_I) is the stress intensity factor range, and C_2 and μ are two parameters which depend, among other things, on material properties. Barsom [5] tested various martensitic steels for fatigue crack propagation and found that:

$$\mu = 2.25 \text{ and } 0.27 \times 10^{-8} \leq C_2 \leq 0.66 \times 10^{-8}$$

for steels having yield strength ranging from 550 MPa to 2000 MPa. We therefore assumed that $\mu = 2.25$ and $C_2 = 0.66 \times 10^{-8}$ for the fatigue propagation in a single wire.

The propagation life can be obtained by the direct integration of Equation (2). For a circumferential crack in a solid cylinder, the stress intensity factor, K_I, can be approximated as follows [4]:

$$K_I = \sigma\{1 + .054\,(\frac{a}{R})^2\}\sqrt{a} \qquad (3)$$

where R is the radius of the wire. Equation (3) may be used to compute the critical crack size, a_o, if the fracture toughness, K_{IC}, and the maximum stress level, σ_{max}, are known. Figure 2 shows the fatigue propagation life of a single wire for various values of initial crack size, a_o, and for a fracture toughness of 100 MPa $\sqrt{m}$.

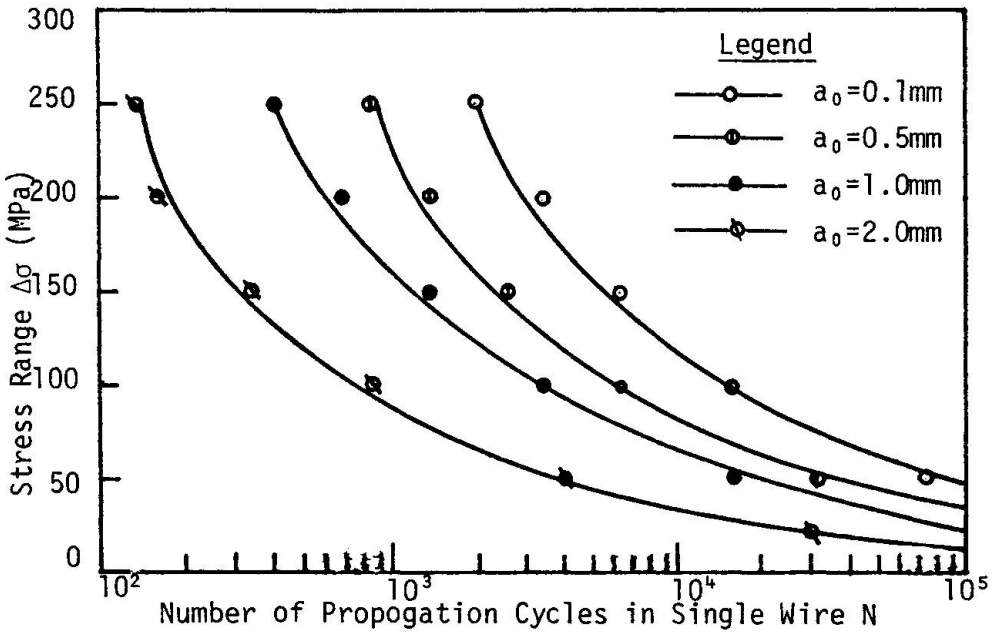

Figure 2. Fatigue Propagation Life of a Single Wire

3.3 Fatigue Life of Cable

Our model for the fatigue failure of a cable is based on the assumption that whenever a wire fails, its load is redistributed equally among the remaining wires. As the number of broken wires increases, the axial stress of unbroken wires would eventually reach the ultimate tensile strength of the wire material at which point the final failure of the cable occurs. Obviously, the number, m, of wires that fail by fatigue before the cable collapses is smaller than n, the number of wires in the cable.

Consider the fatigue life of a single wire is Gaussian distributed with mean life $\bar{N}$ and a standard deviation s. Then the probability of a single wire having a fatigue life of N cycles is given by:

$$\phi(N) = \int_o^N \frac{1}{\sqrt{2\tau}s}\, e^{-\frac{(x-\bar{N})^2}{2s^2}}\, dx^2 \qquad (4)$$

The problem of determining the fatigue life of a cable is now equivalent to computing the probability of failure of m wires out of a bundle of n wires which is given by:

$$P(m,n) = \binom{n}{m}\phi^{m-n}(1-\phi)^m \qquad (5)$$

This type of probabilistic formulation has been developed elsewhere by Andrä and Saul [6] for parallel wire cables. Assuming now that the joint probability distribution, p(m,n) is also Gaussian, the average life of the cable may be calculated.

Figure 3 shows typical plots of the average fatigue life of a 7x1 wire cable in comparison to the fatigue life of a single wire.

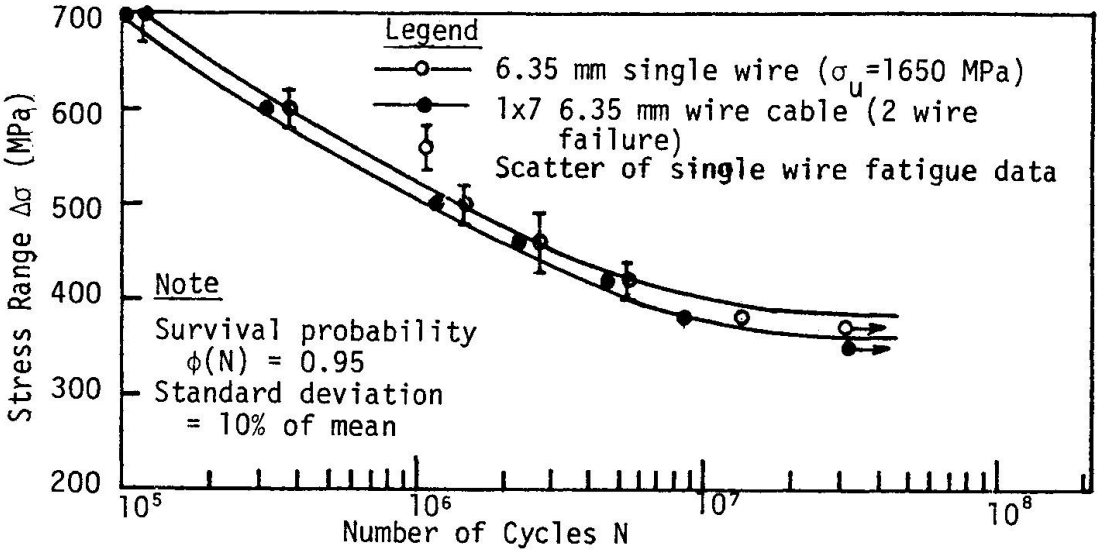

Figure 3. Fatigue Life of Wire and Cable

4. COMPARISON WITH EXPERIMENTAL RESULTS

Fatigue testing of high tension wires and cables have been reported by a number of various authors but the variables in these tests are so different from one another that a direct comparison between the test results and the analytical results are not possible. Only an order of magnitude comparison can be made in a meaningful manner.

Birkenmaier [3] reported test results of dynamic tensile fatigue of 7 mm diameter single wires and wire bundles subjected to 2 million fatigue cycles at different stress ranges. The results are shown in Figure 4. The fatigue limits have also been computed for single wires using the above analytical formulation, and the results are also plotted in Figure 4. The comparison between analytical and experimental results shows a good agreement for single wires.

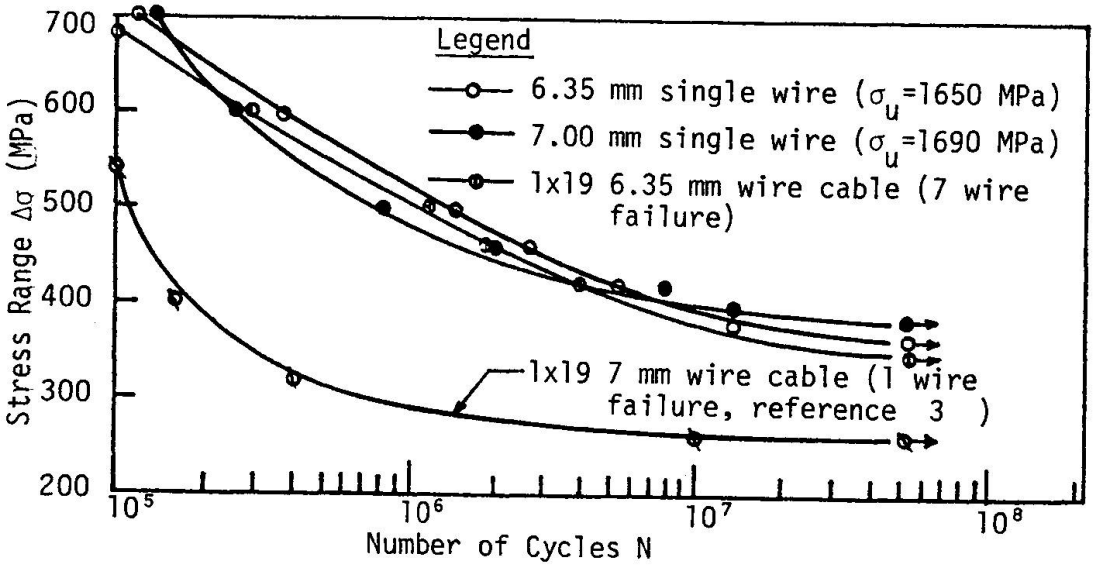

Figure 4. Comparison of Wire and Cable Fatigue Data [3]

5. CONCLUDING REMARKS

The analysis shows that there is a correlation between the fatigue life of a single wire and that of a cable or a wire bundle. In principle, it is now possible to determine the fatigue behavior of stay cables on basis of the structural characteristics and fatigue behavior of single wires. Evidently, a complete understanding and analysis of the same requires an extensive amount of additional research and the present paper may be considered as an initial effort in this direction.

Conversion of units:

1 m = 39.37 in. 1 MPa = 1 N/m^2 = 145 psi 1 GPa = 1 KN/m^2 = 145 ksi
1 MPa $\sqrt{m}$ = 0.91 ksi $\sqrt{in}$.

ACKNOWLEDGEMENTS

The authors wish to acknowledge Mr. Lloyd Cayes of the Federal Highway Administration, Office of Research, and Dr. Walter Podolny of the Office of Engineering for their critical review and comments. The research reported herein was partially supported by the United States Department of Transportation Contract No. DOT-FH-11-9613.

REFERENCES

[1] Leonhardt, F.: Latest developments for cable-stayed bridges for long spans. Saertryk af Bygningsstatiske Meddeleser, Vol. 45, No. 4, 1974.

[2] Podolny, W., Scalzi R.: Construction and Design of Cable-Stayed Bridges. John Wiley & Sons, 1976.

[3] Birkenmaier M.: Fatigue resistant tendons for cable-stayed construction. IABSE Proceedings P-30/80, 1980, pp. 65-79.

[4] Basu, S., Chi, M.: Analytical study for fatigue of highway bridge cables. Report No. FHWA/RD-81/090, July 1981.

[5] Barsom, J.M.: Fatigue behavior of pressure vessel steels. WRC Bulletin 194, Welding Research Council, 1974.

[6] Andrä, W., Saul, R.: Die festigkeit insbesondere dauerfestigkeit langer paralleldrahtbündel. Die Bautechnik, 56 (1979), Hefte 4, pp. 128-130.

Leere Seite
Blank page
Page vide

Zugglieder aus gebündelten und verseilten Drähten

Tension Members in Steel Wire Strand and Rope

Membrures tendues en fils d'acier sous forme de toron et de corde

K. GABRIEL
Dipl. -Ing.
Universität Stuttgart
Stuttgart, BRD

ZUSAMMENFASSUNG

Hergestellt aus verseilten oder gebündelten hochfesten Stahldrähten zeigen die verschiedenen Zuggliederkonstruktionen ein sehr unterschiedliches Gebrauchslast- und Versagensverhalten. Die statisch und dynamisch ermittelten Kennwerte an normalen kurzen Proben werden zur Bestimmung des Zuggliedverhaltens benötigt wie im Bericht dargelegt. Die verschiedenartigen Einflüsse von mechanischen Schädigungen und Reibung auf die Ermüdungsfestigkeit wird erläutert. Sie sind im konstruktiven Entwurf zu berücksichtigen.

SUMMARY

The use of high strength steel wire in either strand or rope form leads to very different service and ultimate load behaviour in tension member structures. To understand the behaviour of these forms of tension members the necessary data from static and dynamic testing of standard, short specimens are presented in this paper. The various influences of mechanical defects and friction effects on fatigue resistance, which must be considered for structural design, are also investigated.

RESUME

L'utilisation de fils d'acier à haute résistance en forme de toron ou de corde conduit à un comportement très différent sous charges de service et de ruine dans les structures à membrures tendues. Pour comprendre le comportement de ces membrures tendues, les indications nécessaires obtenues à partir d'essais statiques et dynamiques sur des échantillons standards courts sont présentées dans cet article. Les diverses influences des dommages mécaniques et du frottement sur la résistance à la fatigue, qui doivent être prises en compte pour le dimensionnement structurel, ont également été examinées.

1. Einleitung

Die Halbzeugform des metallischen Drahtes ist schon seit Jahrhunderten bekannt. Buntmetalle waren die ersten Drahtwerkstoffe, bis sie vom Eisen und vom Stahl zurückgedrängt wurden. Der Stahldraht mit Festigkeiten über 1000 N/mm^2 wurde schon vor hundert Jahren in der Bau- und Fördertechnik verwendet. Die Fördertechnik hat den Stahldraht verseilt und in verschiedenen Konstruktions-und Macharten im Kran-, Berg- und Schiffbau eingesetzt, während der Draht im Brükken-und Spannbetonbau zur Hauptsache in Bündelform Verwendung fand. In der Bautechnik üblich sind heutzutage unlegierte Stahldrähte (vergütet oder patentiert kaltgezogen) mit Durchmessern von 3 bis 7mm und Festigkeiten zwischen 1470 und 1670 N/mm^2. Für Seile werden ausschließlich patentiert kaltgezogene Stahldrähte benötigt, für den Spannbetonbau müssen die patentiert kaltgezogenen Drähte angelassen werden.

Die hohen Festigkeiten der Drähte und wirtschaftliche Herstellungsverfahren haben die Voraussetzung für eine zunehmende Verbreitung der Drähte im Bauwesen geschaffen. Neben dem großen Einsatzbereich des Spannbetonbaues werden gebündelte oder verseilte Drähte immer häufiger als freie Zugglieder verwendet, bis hin zu Tragwerken aus nur auf Zug beanspruchten Bauelementen [1] .Entwicklungsgeschichtlich betrachtet nehmen die rein zugbeanspruchten Tragwerke eine Sonderstellung ein. Mit ihnen erschließt sich zwar eine große Formenwelt (Fig. 1) mit optimaler Materialausnutzung, sie sind aber in der Anwendungsbreite eingeschränkt[4] . In der menschlichen Umwelt mit ihrer Enge, ihren Verkehrsbedürfnissen und der Empfindlichkeit des Menschen auf Schwingungen, ist ein kompakteres, rechtwinkliges und steiferes Tragwerk aus gemischten Traggliedern (Zug-mit Druck-und Biegeelementen) erforderlich. Diese "hybriden" Tragwerke mit Zugelementen, welche sinnvollerweise den Hauptbinder eines weitgespannten Objektes bilden, sind dem Leichtbau zuzuordnen und können demzufolge schwingungsempfindlich sein oder müssen aufgrund des hohen Verkehrslastanteils große Spannungswechsel ertragen. Bei der Wahl des statischen Systems und der Zuggliederkonstruktionsart sowie bei der Durchbildung der konstruktiven Details und des Langzeitschutzes ist daher die Ermüdungsfestigkeit zu beachten [4] .Bisher bekannt gewordene Schäden an Zugelementen waren in den seltensten Fällen allein auf reine Materialermüdung zurückzuführen, immer spielten konstruktive Mängel eine Rolle.

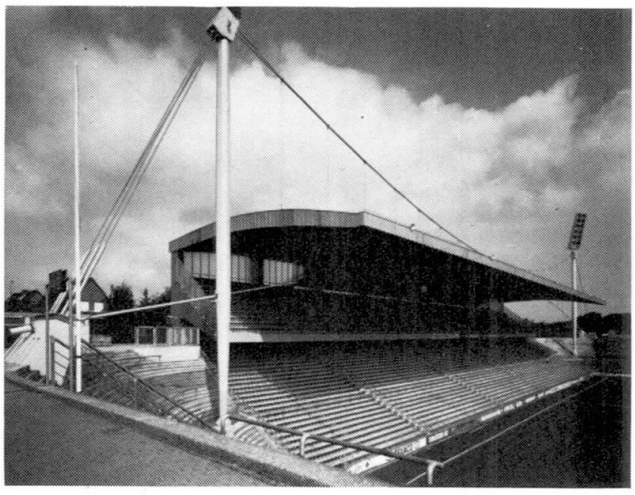

Fig.2 Vorgespannter Seilbinder mit biegesteifer Dachfläche als Beispiel eines hybriden Tragwerkes

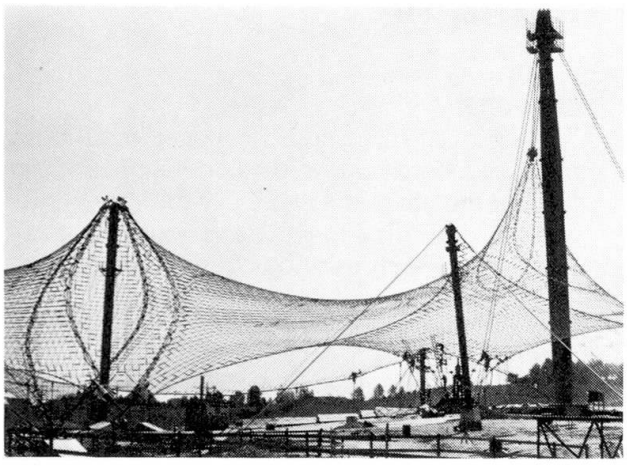

Fig.1 Netzflächen aus Seilen als rein zugbeanspruchtes Tragwerk mit großer Formenvielfalt

2. Systematische und Einzelfehler - Die Streuung der Drahtkennwerte

Abweichungen in der Zusammensetzung der Legierungsanteile, der Größe der Kaltumformung, der Ausbildung des Ziehsteines und der Temperaturbehandlung sind systembedingte Fehler, deren Ausmerzung einen nicht zu vertretenden Aufwand erfordern würde. Sie sind in ihren Auswirkungen zu berücksichtigen [3] . Riefen, Kratzer, Druckstellen und Überwalzungen sind Einzelfehler, die mit Hilfe einer ausreichenden Überwachung ausgemerzt werden sollten. Treten sie trotzdem auf, sind ihre Auswirkungen viel tiefgreifender als die der Fertigungstoleranzen.

In Fig. 3 sind einige mechanische Kennwerte von Seil-und Spanndrähten mit ihren statistischen Daten angegeben, während Fig. 4 die Häufigkeitsverteilung von Ermüdungsbrüchen an teilweise geschädigten Drähten angibt, die über der Lastspielzahl aufgetragen wurden. Die Kennwerte sind an Proben mit ca. 200 mm Länge ermittelt worden [5] .

In den folgenden Betrachtungen werden Einzelfehler ausgeschlossen und es wird davon ausgegangen, daß die systematischen Fehler sich als Streuung einer homogenen Häufigkeitsverteilung erfassen lassen.

Eigenschaften	DIN	ISO	Benennung	$\bar{x}$	s	$\bar{x}$	s
Zugfestigkeit	β_u	R_m	N/mm^2	1771	36	1822	48
Fließgrenze	$\sigma_{0,2}$	$R_{p0,2}$	N/mm^2	1580	39	1372	55
Gleichmaßdehnung	δ_{gl}	A_{gl}	°/oo	34	6	18	4
Reißfestigkeit	β_{riss}	R	N/mm^2	1293	-	1457	-
Steifigkeit	E	E	N/mm^2	206 930	3760	192 744	5200
Prüflänge im stat. Versuch	l	l	mm	100	-	100	-
Schwingfestigkeit bei $2 \cdot 10^6$ Lastwechseln	σ_D	R_d	N/mm^2	log 468 = 2,67	log s_i = 0,05	log 300 = 2,48	log s_i = 0,10
Oberspannung	σ_o		N/mm^2	800	-	1600	-
Probenlänge	l	l	mm	200	-	200	-

Fig.3 Mechanische Eigenschaften von unlegierten Stahldrähten mit ihren statistischen Daten

3. Hintereinanderschaltung und Parallelschaltung

Alle Werkstoffkennwerte werden an handlichen, d.h. kurzen Probestücken ermittelt. Ein Zugelement im Bauwerk soll jedoch eine große Länge haben, um den Aufwand der Verankerungskonstruktionen gering zu halten ($L = n\ l_0$) und wird immer aus mehreren Drähten zusammengesetzt sein ($\Sigma A = m \cdot A_0$). Der Einfluß der Hintereinanderschaltung und der Parallelschaltung auf den Mittelwert und die Streubreite von langen und aus mehreren Einheiten bestehenden Zuggliedern ist der Fig. 5 zu entnehmen [5] . Zu beachten ist dabei, daß nicht alle Kennwertveränderungen den statistischen Begriffen der Hintereinander-und der Parallelschaltung folgen. Während die reinen Verformungskennwerte (Elastizitätsmodul, Proportionalitätsgrenze, Fließgrenze) mit den Faktoren n und m der Parallelschaltung entsprechen, muß bei den Versagenskennwerten (Gleichmaßdehnung, Zugfestigkeit) zwischen der Hintereinanderschaltung n und der Parallelschaltung m unterschieden werden. Auch die Ermüdungsfestigkeit ist ein Versagenskennwert, der allerdings einem spröden Werkstoffverhalten entspricht, auf welchen der oben verwendete Begriff der Hintereinanderschaltung zur Darstellung der Verhaltensweise des einzelnen Drahtes angewendet werden kann. Der Begriff der Parallelschaltung, der im Falle des duktilen Gewaltbruches eine näherungsweise Mittelwertbildung der Festigkeiten erlaubt, ist für die Ermüdungsfestigkeit nicht verwendbar, weil eine Beziehung zwischen dem Einzeldrahtkennwert und dem Bündelkennwert nicht erkennbar ist.

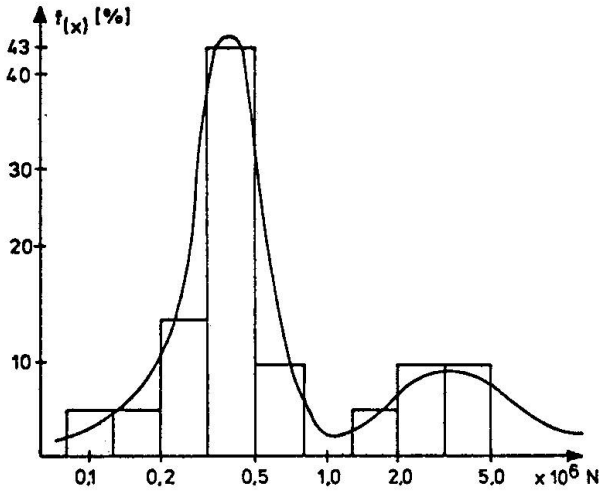

Fig.4 Die Häufigkeitsverteilung von Ermüdungsbrüchen bei gleichartiger Schwingungsbeanspruchung, aufgetragen über der Lastspielzahl

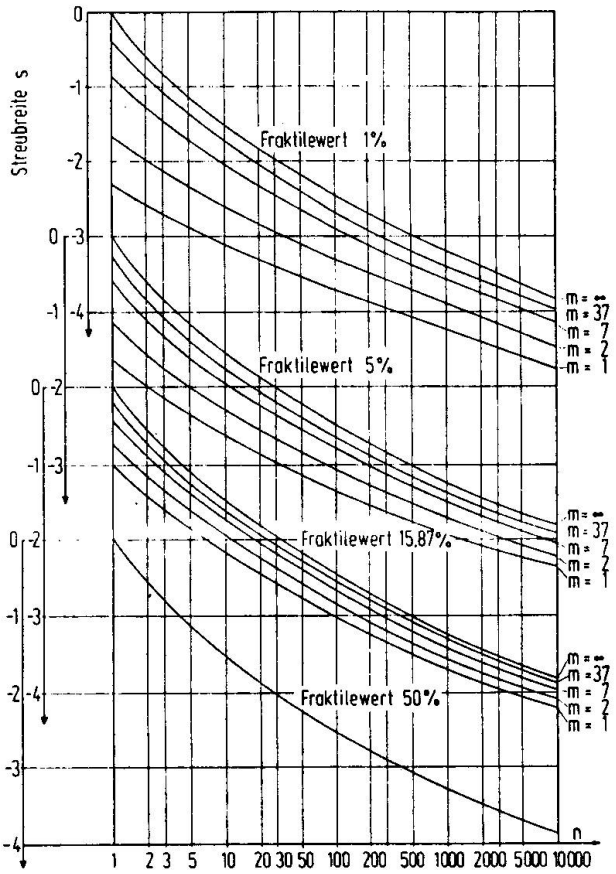

Fig.5 Abnahme von Erwartungswerten an langen und gebündelten Proben für verschiedene Fraktilewerte; berücksichtigt wird die " Hintereinanderschaltung (n)" und die "Parallelschaltung (m)" von Eigenschaften, deren Größe an kurzen Proben ermittelt wurde; die statistischen Größen / = x und s gelten für die kurzen Proben

4. Ermüdung von Drähten

Unter schwingender Belastung können an den Korngrenzen im Bereich mikroskopisch kleiner Inhomogenitäten Rißkeime entstehen, die mit wachsenden Lastwechselzahlen größer werden. Dieses Wachstum kann fortschreiten, einzelne Risse zusammenwachsen und diese können dann als Anriß den Bruch einleiten. Aber es besteht auch die Möglichkeit, daß sich das Werkstoffgefüge stabilisiert d.h.: trotz vorhandener Mikrorisse tritt kein weiteres Wachstum der Risse auf und der Werkstoff wird als dauerfest bezeichnet.

Wenn die angelegte Oberlast größer wird als die Widerstandskraft des Restquer - schnittes, tritt der Bruch ein. Bei kaltgezogenen Stahldrähten werden Anrisse bevorzugt an der Werkstoffoberfläche entstehen und sowohl die Oberflächenrauhigkeit als auch die Grenzstruktur (z.B. Randentkohlung) beeinflussen die Ermüdungsfestigkeit des Stahldrahtes entscheidend.

Die dem Bruch zuzuordnende Lastwechselzahl wird als maßgebliches Resultat für die Erstellung eines Wöhlerfeldes verwendet (Fig. 6), obwohl hier kein direkter Zusammenhang zur kurz vor dem Bruch merklich verminderten statischen Sicherheit berücksichtigt wird.

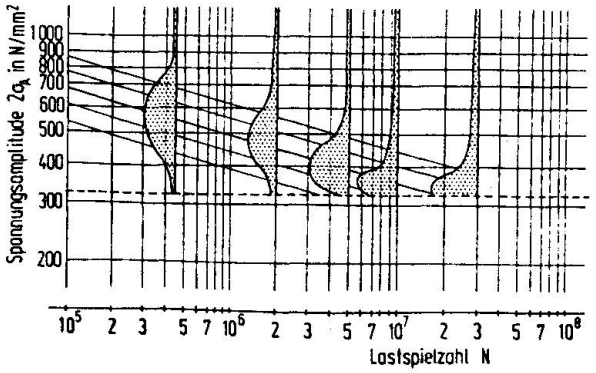

Fig.6 Wöhlerfeld für einen Stahldraht in doppelt logarithmischer Darstellung

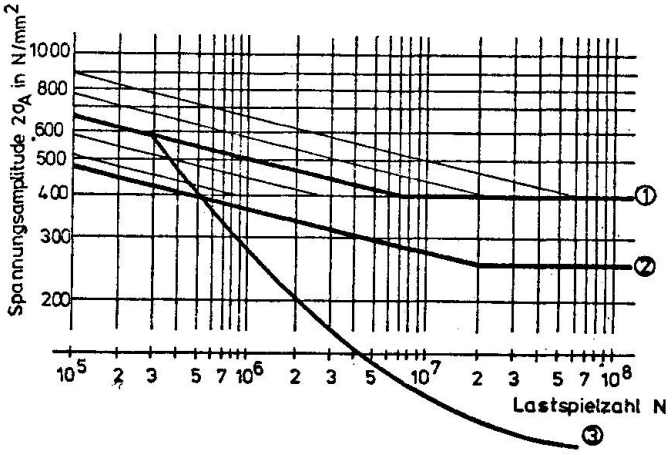

Fig.7 Darstellung der Wöhlerlinien eines an der Luft geschwungenen, ungeschädigten Stahldrahtes 1 mit einem örtlich geschädigten 2 und einem von Reibkorrosion beeinflußten Draht 3.

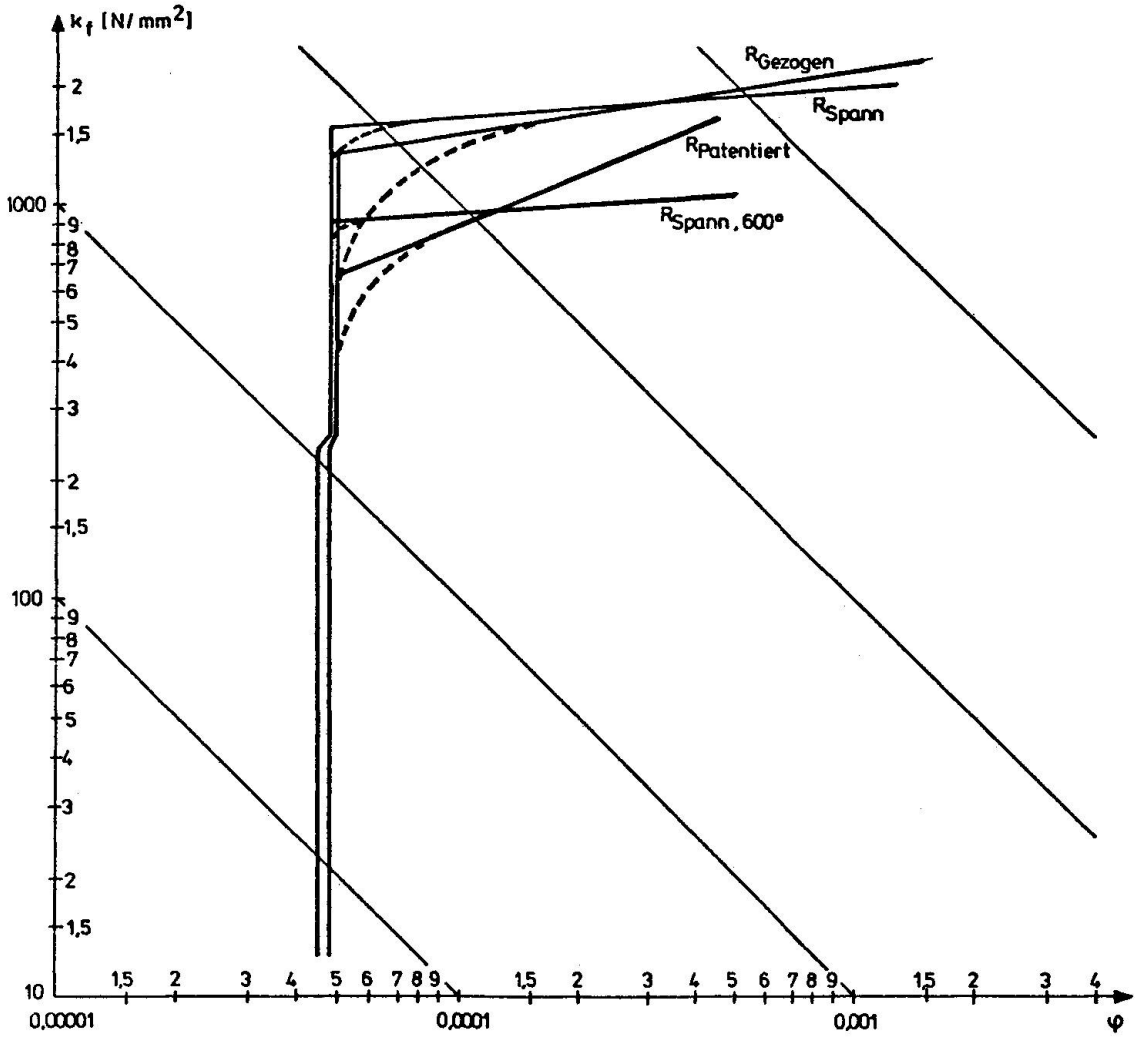

Fig.8 Arbeitslinien von unterschiedlich nachbehandelten, unlegierten Stahldrähten, dargestellt im doppeltlogarithmischen Koordinatensystem mit geschwenkter Ordinate

Aber selbst aufbauend auf den Lastspielzahlen bis zum Bruch der Probe wurde das Wöhlerfeld bisher nur im Bereich der normenmäßig vorgegebenen 2.10^6 Lastwechsel untersucht und die davorliegende Zeitfestigkeit einer intensiven Analyse unterzogen. Im Dauerfestigkeitsbereich ist über die Struktur des Wöhlerfeldes noch sehr wenig bekannt [5] . Das Wissen um diesen Bereich muß aber vertieft werden, wenn von den Ergebnissen an kurzen Proben auf das Verhalten des langen Drahtes geschlossen werden soll, was bisher nur in einzelnen Untersuchungen an Bündeln aus parallelen Drähten geglückt ist.

Das Verseilen der Drähte und die Verankerungssysteme haben Zusatzbeanspruchungen zur Folge und beeinflussen auf diese Weise die Drahtkennwerte. Die Ermüdungsfestigkeit fällt im Bereich von Beanspruchungen, die nur örtlich begrenzte Umformungen erzeugen, auf Mindestwerte ab und Vorgänge, die als Folge von Lastschleifen Energie in den Werkstoff eintragen, wie innere (Gleitungen) und äußere (Reibkorrosion) Reibung, verhindern den stabilen Gefügezustand, der Voraussetzung für die Dauerfestigkeit ist (Fig. 7).

Aufgrund verschiedener Forschungsergebnisse

- -Reines Eisen besitzt keinen Bereich strengelastischen Verhaltens
- -Menge und Art der Legierungsanteile beeinflussen die Ausdehnung des streng elastischen Bereiches [3]
- -Thermische und mechanische Nachbehandlung, die keine Kristallumwandlung bewirken, erweitern den streng elastischen Bereich nicht, sondern schaffen nur eine mehr oder weniger gute quasielastische Erweiterung (Fig. 9)
- -aufgrund von Inhomogenitäten (Kerben, Schweißnähte,...) geschädigte Werkstoffe fallen in der Ermüdungsfestigkeit auf einen bestimmbaren Mindestwert ab, der von der Werkstoffnachbehandlung unabhängig ist und ganz gut mit der Größe des streng elastischen Bereiches übereinstimmt

kann die Behauptung aufgestellt werden, daß sich das dynamische Verhalten eines Werkstoffes mit Hilfe von statischen Feindehnungsmessungen eingrenzen läßt.

5 Einflüsse der Konstruktion

Infolge der Drahtverseilung sowie im Verankerungs- Umlenk -und Querpressbereich der Zugglieder aus hochfesten Drähten treten Zusatzbeanspruchungen auf [4] . Diese zusätzlichen Einflüsse sind zu unterteilen in Schädigungen mechanischer (Kerben, Spannungsspitzen) und energetischer (Reibung, Oxydation) Art. Lokal begrenzte mechanische Einflüsse können die Dauerfestigkeit des Werkstoffes nur bis auf die Grenze des streng elastischen Verhaltens herunterdrücken, die energetischen Einflüsse können die Dauerfestigkeit auslöschen.
Die mechanischen Einflüsse entsprechen Einzelfehlern, wie sie bei der konstruktiven Detailausbildung, dem Transport und der Montage gemacht werden können.
Die energetischen Einflüsse können nur teilweise über die konstruktive Durchbildung reduziert werden, um sie zu bekämpfen, muß für einen einwandfreien Korrosionsschutz gesorgt werden.
Werden Drähte gebündelt und als Probezugglieder in Laborversuchen geprüft, so ergeben sich theoretische Idealwerte, die in der Praxis als Folge einer schlechten Verankerung oder einer Betonumhüllung abgemindert werden.
Sind Drähte verseilt, so werden die Laborversuche an den Seilen immer schlechter ausfallen als die Resultate einer gleichartigen schwingenden Beanspruchung eines einwandfrei korrosionsgeschützen Seiles im Bauwerk.
Am Institut für Massivbau der Universität werden die Kennwerte der heutzutage üblichen Drähte untersucht und mit ihren statistischen Daten festgehalten.
Die Einflüsse der konstruktiven Durchbildung auf diese Werte werden herausgearbeitet und weitgehend mittels konstruktiver Maßnahmen eliminiert. Diese Arbeiten werden im Vortrag angesprochen.

6. Literatur (Einschränkung auf eigene Veröffentlichtungen, welche die aufgestellten Behauptungen verdeutlichen und in denen auf die jeweilige Fremdliteratur verwiesen wurde)

[1] DILLMANN, U., GABRIEL, K., SCHLAICH, J.
Seiltragwerke: Entwurf, Konstruktion und Bauausführung SIA Dokumentation 44, Lausanne 1980

[2] GABRIEL, K. Ebene Seiltragwerke
Merkblatt 496 der Beratungsstelle für Stahlverwenung, Düsseldorf 1980

[3] DILLMANN,U., GABRIEL, K.
Hochfester Stahldraht für Seile und Bündel in der Bautechnik. Eine Folge von bisher acht Berichten, die im Archiv für das Eisenhüttenwesen in den Jahren 1980 bis 1982 veröffentlicht wurden.

[4] GABRIEL, K. SCHLAICH, J. Seile und Bündel im Bauwesen, Berichte zu einer Vortragsveranstaltung von verschiedenen Verfassern, Beratungsstelle für Stahlverwendung, Düsseldorf 1981

[5] GABRIEL, K. Anwendung von statistischen Methoden und Wahrscheinlichkeitsbetrachtungen auf das Verhalten von Bündeln und Seilen aus vielen und langen Drähten.
Vorberichte zum 2. Internationalen Symposium des Sonderforschungsbereiches 64, Universität Stuttgart 1979

Leere Seite
Blank page
Page vide

Fatigue Resistance of Large High Tensile Steel Stay Tendons

Résistance à la fatigue des câbles de fils à haute résistance

Ermüdungswiderstand von Paralleldrahtkabeln grosser Tragfähigkeit

M. BIRKENMAIER
Dipl. Ing. ETH, Dr. h.c.
Bureau BBR Ltd.
Zürich, Switzerland

R. NARAYANAN
M. Sc.,
Stahlton AG
Zürich, Switzerland

SUMMARY
Large parallel wire stay tendons are being increasingly used in major bridge structures. This paper considers the various factors influencing the fatigue resistance of such stay tendons. In the case of HiAm and DINA tendons designed against fatigue according to the "limited damage" concept described in this paper it is possible to guarantee that all tendons in the construction remain intact and serviceable throughout their entire service life.

RESUME
Les câbles à fils parallèles de type HiAm et DINA de grande capacité portante sont de plus en plus utilisés pour la construction des ponts haubannés. Les différents facteurs qui influencent la résistance à la fatigue de tels câbles sont présentés dans cet article. Pour le dimensionnement à la fatigue de ces câbles on a adopté un concept de limitation des dommages, ce qui garantit que tous les câbles HiAm et DINA conservent toute leur capacité portante pendant la durée de vie de l'ouvrage.

ZUSAMMENFASSUNG
HiAm- und DINA-Paralleldrahtkabel grosser Tragfähigkeit sind in letzter Zeit vermehrt im Grossbrükkenbau verwendet worden. Im vorliegenden Beitrag werden die verschiedenen Faktoren beschrieben, welche den Ermüdungswiederstand solcher Grosskabel beeinflussen. Für die Bemessung auf Ermüdung wird ein Schadenbegrenzungs-Konzept vorgestellt, welches garantiert, dass sämtliche HiAm- bzw. DINA-Kabel einer Konstruktion während ihrer Lebensdauer die volle Tragkapazität beibehalten.

1. INTRODUCTION

During the course of the last decade there has been a considerable increase in the number of cable stayed structures which have been designed and erected. This form of construction has enabled the structural engineer to provide elegant solutions to large span construction at an economic cost. Figs. 7, 8 and 9 show examples of recently completed stayed bridges. One of the principal structural elements in such structures is the tensile stay which transmits the main girder loads to the supporting pylon. The types of stay tendons commonly used are built up from parallel strands or parallel wires or locked coil rope. During recent years there has been an increase in the use of high tensile steel parallel wire tendons in stayed structures.

Fig.1 shows a cross-section of a typical parallel wire stay-tendon used in bridge construction. The wire bundle consists of 7 mm dia. cold-drawn, patented high tensile steel wires with ultimate tensile strengths between 1600 and 1800 N/mm^2. Max. bundle sizes of 365 wires 7 mm dia. having an outside diameter of 200 mm have been realised. A robust 3-part protection system is provided through

- a film of anticorrosion fluid coated over the wires during the assembly of the wire bundle,
- a high-density polyethylene duct (wall thickness 8 mm to 11 mm) which also protects the tendon during transport and erection and permits the tendon to be wound on to a bobbin for delivery and erection purposes, and
- a resin-enriched cement grout injected into the polyethylene duct after the final force adjustment in the stay tendon.

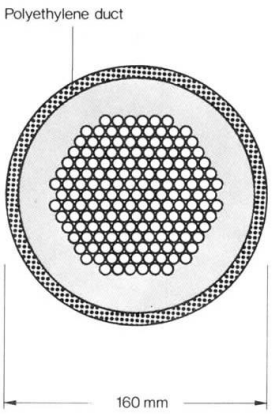

Fig.1

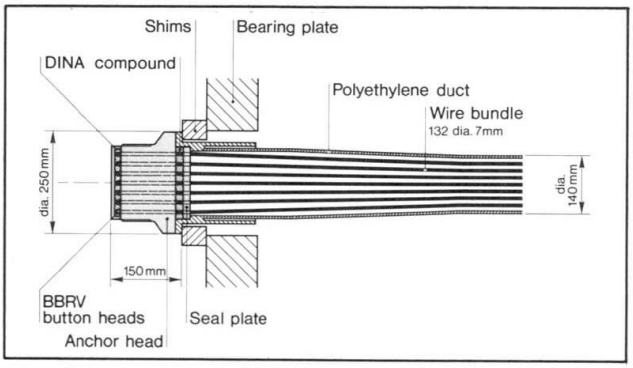

Fig.2

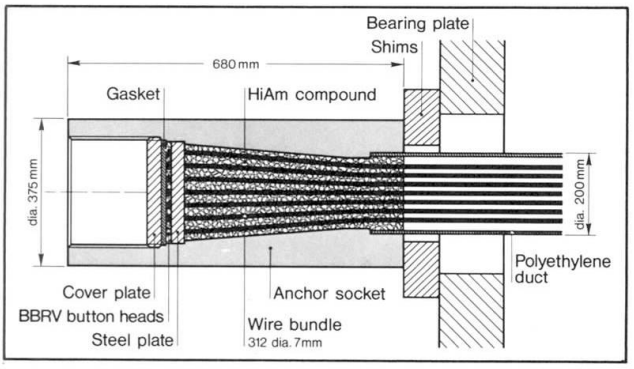

Fig.3

Figs. 2 and 3 show the BBRV-DINA and HiAm anchorages used for such stay tendons.

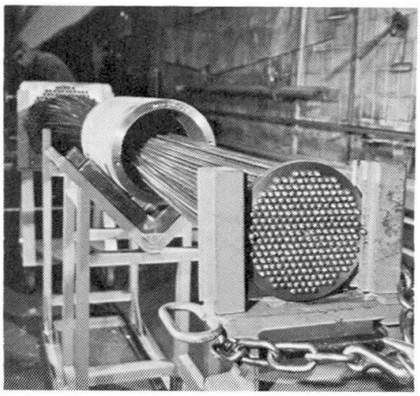

Fig.4

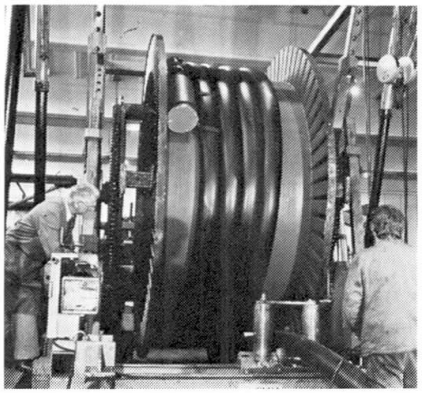

Fig.5

Fig.6

Figs. 4, 5 and 6 show various stages in the manufacture and erection of a HiAm stay tendon [1].

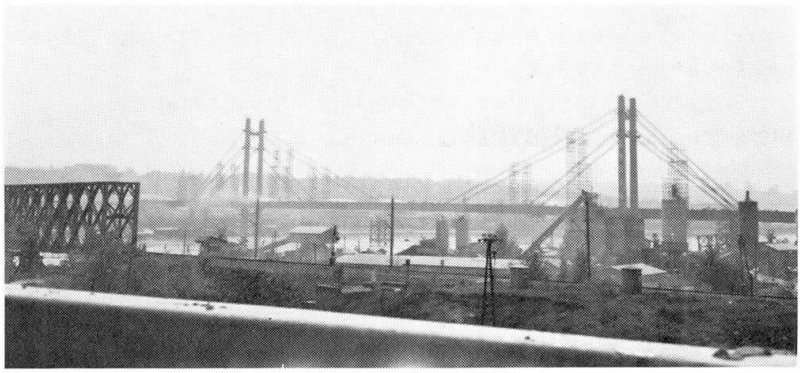

Fig.7

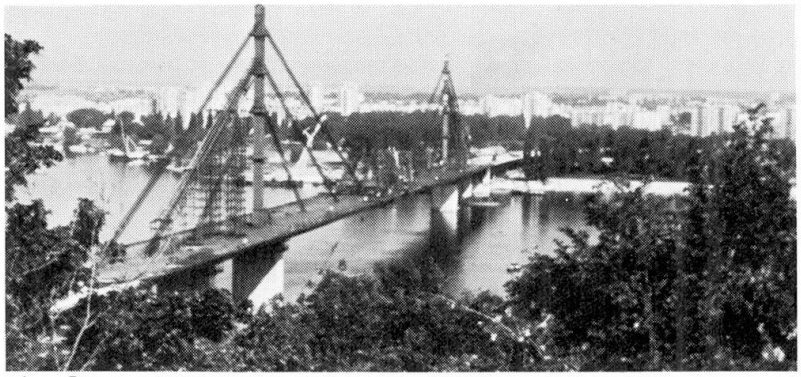

Fig.8

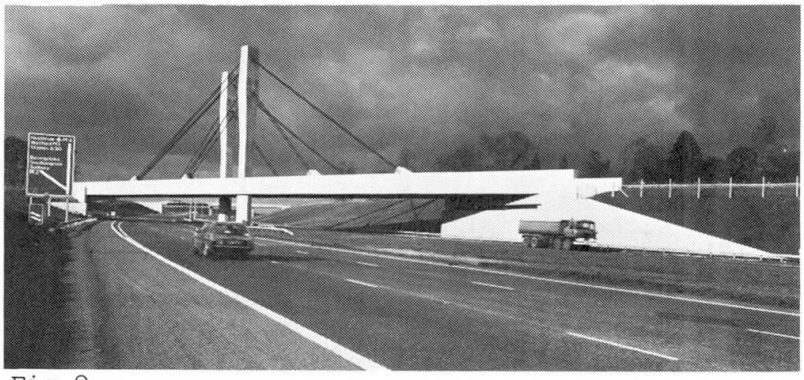

Fig.9

Tendon data for 3 stayed bridges recently completed in Europe are given below.
Save Bridge Belgrade, YUG [2], Fig.7:
for double track railway traffic. Steel box girder with main span of 254 m. Total 64 HiAm tendons clustered in groups of 4. Max. 290 wires 7 mm dia. per tendon. Max. length of tendon 116 m. Tendons arranged in two planes.
Danube Bridge Novi Sad, YUG (3), Fig. 8:
for double track road traffic. Steel box girder with main span of 351 m. Total 48 HiAm tendons clustered in groups of 4. Max. 312 wires 7 mm dia. Max. length of tendon 158 m. All tendons arranged in one plane.
Lyne bridge GB (4), Fig.9:
for double track railway traffic. Prestressed concrete girder with two spans of 54.9 m each. Total 16 DINA tendons with 79 wires 7 mm dia. Max. length of tendon 42 m. Tendons arranged in two planes.

Two typical features of this form of stayed construction are the large tensile forces directly transmitted by the stay tendons and the fluctuation of tensile forces in the tendons caused by the live load.
Table 1 shows the maximum and minimum tensile stresses in the stay tendons on the 3 bridges referred to earlier.

Bridge	Type	Size of tendon with max. stress variation	$\sigma_{max.}$ N/mm^2	$\sigma_{min.}$ N/mm^2	$(\sigma_{max.} - \sigma_{min.})$ N/mm^2
SAVE (YUG)	Rail	4 x 260 dia.7 mm	450	229	221
NOVI SAD (YUG)	Road	4 x 208 dia.7 mm	703	447	256
LYNE (GB)	Rail	79 dia.7 mm	711	587	124

Table 1 Tensile stresses in bridge stay tendons

From these figures it can be seen that the fluctuations of tensile stresses in the stay tendons are quite significant. The stay tendons used for such applica-

tions should therefore not only be in a position to withstand large direct tensile forces but should also be fatigue resistant.
The designer is interested in the following properties of the stay tendons which play an important role in the choice of suitable tendon sizes.

- load-elongation characteristics of tendons
  In indeterminate structures like a stayed bridge, the tendon forces and structural deformations are a function of this characteristic. This characteristic is influenced by the type of wire bundle (i.e. whether parallel wire, parallel strand or locked coil rope), the tendon length and the stress in the tendon. The parallel wire tendon possesses an accurately predictable high value of Young's modulus E which remains constant over an unlimited number of loading and unloading cycles in the stress range encountered in stayed structures.
- ultimate strength of tendons composed of a large number of wires and the fatigue resistance of such tendons. The former property enables the engineer to decide on a suitable cross-section for the tendon so that the maximum tendon forces will be carried safely and the latter property enables him to ensure that at no time in the life of the structure will the repeated loadings cause distress in the tendons.

2. BEHAVIOUR OF PARALLEL-WIRE TENDONS UNDER STATIC AND FATIGUE LOADING

The question associated with these properties is how to accurately forecast and guarantee values for the static and fatigue resistance of stay tendons which could be as long as 200 m and as large as 365 wires 7 mm dia. in cross-section taking into account the numerous factors which can have an influence on these values.

2.1 Basic wire material

One of the most important factors affecting the static and fatigue resistance of tendons is the quality of the basic wire material used in their manufacture. The weight of wire used for tendons on a single project can be quite large. For example, 413 tons of cold drawn high tensile steel wire 7 mm dia. were used for the tendons on the Save Bridge, Belgrade. This material was delivered as 826 wire coils each of 500 kg weight. To assess the static and fatigue properties of such a large wire collective it is important to use the correct testing methods, to devise an adequate sampling procedure, and to employ suitable statistical methods for the evaluation of test results.
Static resistance:
For the Save Bridge project, a minimum of 2 specimens were taken from each wire coil and tested to determine the static tensile strength. In addition the yield stress and elongation after rupture were determined on a limited number of these specimens. Table 2 shows the results.

	Number of tests	Average	Standard deviation
Tensile strength (N/mm^2)	1800	1733	± 33
Yield (0.2 proof limit) (N/mm^2)	361	1548	± 39
Elongation after rupture δ_{10} (%)	361	8.1	± 0.5

Table 2 Results of static tensile tests on wire

These results clearly show the uniformly high quality of this type of wire in respect of its static tensile strength properties.

Fatigue resistance:
In order to define the fatigue behaviour of wire completely it is necessary to possess information in the finite as well as infinite fatigue life range. This can then be represented in the form of a Wöhler curve relating the stress range $\Delta\sigma = 2\sigma_A$ to the number of load cycles N. Since fatigue test results display a large scatter it also becomes necessary to obtain sufficient information from tests to enable the various fractile Wöhler curves to be plotted. In the case of a large wire collective this implies that a large number of specimens have to be tested. There is however a practical limit on the number of test specimens which is imposed by the time to be spent on the tests and the costs incurred on testing. For the Save Bridge project 210 wire specimens were tested, which works out to roughly 1 specimen for every 4 wire coils used. The testing was organized to give a "complete random block". As shown in Fig.10 this was achieved by choosing 5 equally spaced values of stress range $\Delta\sigma = 2\sigma_A$ = 350, 400, 450, 500 and 550 N/mm^2 and testing 42 specimens at each of these values of stress range. Obviously the $\Delta\sigma$ values should be chosen in a range where fatigue failures will occur. Testing was done up to a maximum value of two million load cycles. It was assumed that practically infinite fatigue life is reached when a specimen endures the applied dynamic load for two million load cycles. Specimens which fail below this value of N are said to be in the finite fatigue life range. The values of N at which the specimens ruptured during the test are marked by the vertical dashes in Fig.10. The numerical values against the circles give the number of specimens which did not rupture during the test duration over $N_G = 2 \cdot 10^6$ load cycles. The large scatter of test results is evident from this figure and this characteristic is displayed by the very same wire whose static tensile characteristics are remarkably uniform.

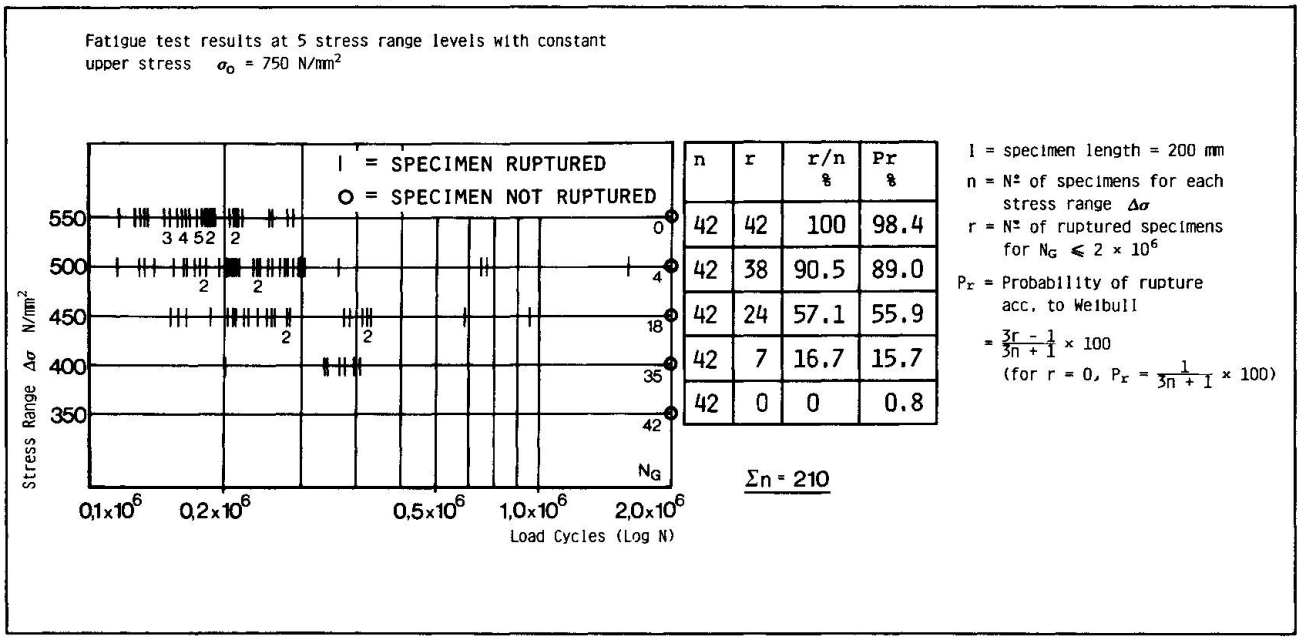

n	r	r/n %	Pr %
42	42	100	98.4
42	38	90.5	89.0
42	24	57.1	55.9
42	7	16.7	15.7
42	0	0	0.8

Σn = 210

l = specimen length = 200 mm
n = N° of specimens for each stress range $\Delta\sigma$
r = N° of ruptured specimens for $N_G \leq 2 \times 10^6$
P_r = Probability of rupture acc. to Weibull
$= \frac{3r - 1}{3n + 1} \times 100$
(for r = 0, $P_r = \frac{1}{3n + 1} \times 100$)

Fig.10

Figs.11 and 12 show the methods employed to derive the various fractile values for the endurance limit ($N_G = 2 \cdot 10^6$ cycles) and the fatigue strengths for finite life. These values have been used to plot the 5 % and 50 % fractile Wöhler curves shown in Fig.13. Ideally it would be desirable to have a Wöhler curve with Pr ≅ 0 which would define the absolute minimum fatigue strength for the wire collective. It is possible to estimate this value using the [arc. sin $\sqrt{Pr}$] Transformation. In the case of the wire used for the Save Bridge such a transformation yields a value of 340 N/mm^2 for the finite fatigue life strength ($N_G = 2 \cdot 10^6$ cycles) compared with the 5 % fractile value of 378 N/mm^2.

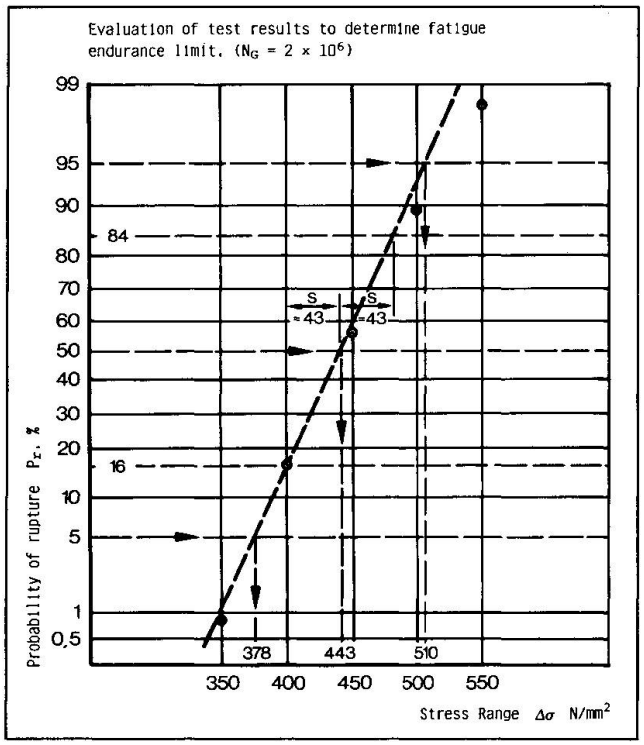

Fig.11

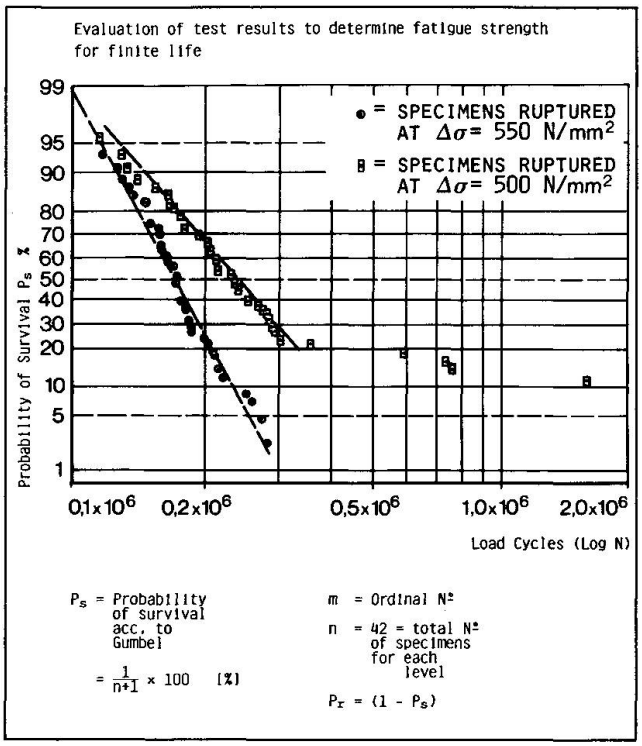

Fig.12

Cases may arise where only a limited number of specimens are available for testing. In such cases the "staircase" method of testing [5] may be adopted to obtain values of infinite fatigue life strength for the material tested (N_G = 2•10^6 cycles). This method is however not as accurate as the complete random block method described earlier. Fig.14 shows the results of an evaluation of such a testing using 25 specimens for each of 2 different lengths l = 200 mm and l = 600 mm. The 2 lines tend to converge to a common point along the line Pr ≅ 0. For the same number of specimens tested the longer specimens include a greater amount of wire material and therefore the Δσ value for Pr = 50 % and the standard deviation S are smaller than the corresponding values for shorter specimens.

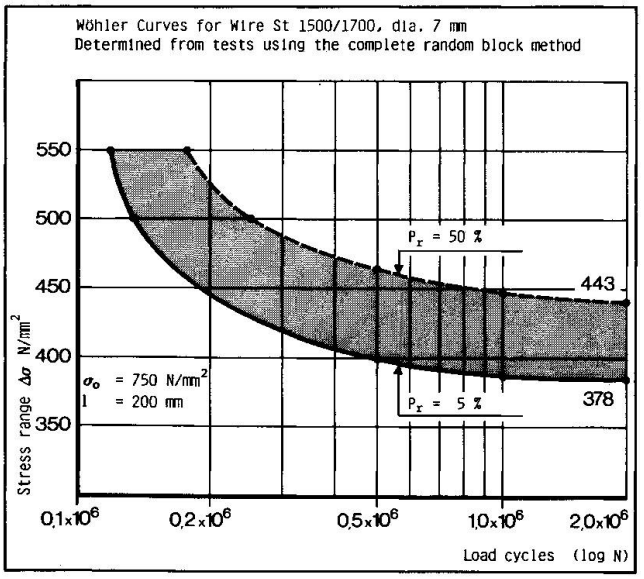

Fig.13

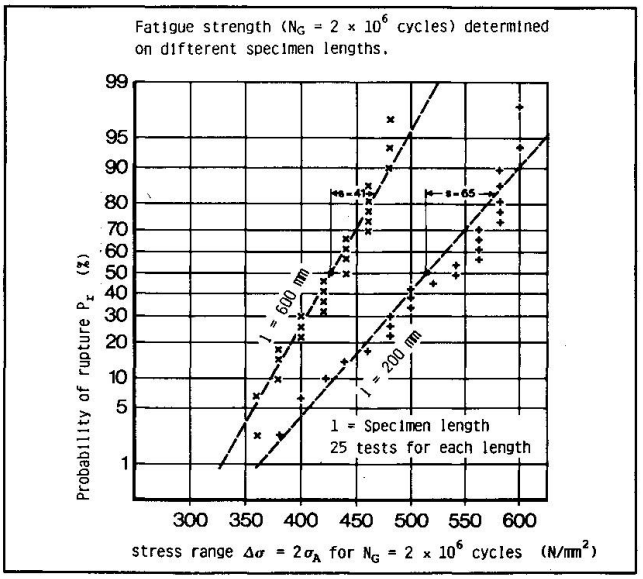

Fig.14

The fatigue resistance properties of wire described above were established from tests on 'as-drawn' wire specimens in a non corrosive environment. The necessity for an absolutely reliable system of protection against wire corrosion is

evident from Fig.15 which shows the fatigue resistance of wires subject to different environments [6]. Specimens tested in sea water show a large reduction in fatigue resistance. The protection system described in an earlier part of this paper ensures that the wires in the tendon are protected from corrosive influences during service life.

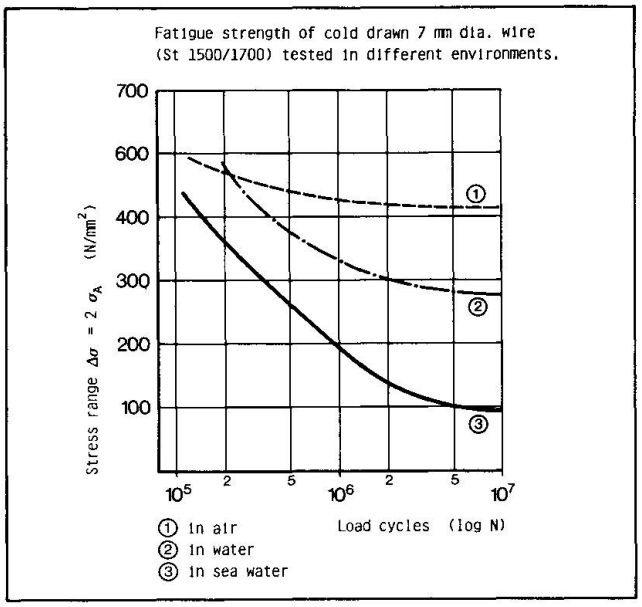

Fig.15

In the search for a reliable corrosion protection system to tendons, the possibility of a primary protection by galvanizing the wire has also been considered. Recent tests on galvanized, cold-drawn high tensile steel St 1500/1700 wire specimens have yielded infinite fatigue life ($N = 2 \cdot 10^6$ cycles) at a stress range $\Delta\sigma = 2\sigma_A$ of at least 450 N/mm^2. These values lie well above those obtained with ungalvanized wire of the same quality.

2.2 Anchored tendon

In all static and dynamic tensile tests on tendons fitted with HiAm or DINA anchorages the wire failure occured in the free length of the tendon. The anchorages did not reduce either the static or the dynamic tensile strength of the tendons. These tendon properties are therefore primarly governed by the corresponding properties of the wire bundle alone. This is reflected in Table 3 which shows the results of static and fatigue tests carried out on various HiAm and DINA tendons. All tendon specimens were subjected to various fatigue loads as shown in the table. On conclusion of the fatigue loading, the tendon specimens were subjected to ultimate static tensile tests to establish the static breaking loads. It was thus possible to establish the damage D caused to the tendons by the foregoing fatigue loading. It is seen that the largest value of damage observed in these tests was 1.3 % or a loss of 3 out of 295 wires in a tendon. Even after $2 \cdot 10^6$ cycles of loading at $\Delta\sigma$ = 20 kp/mm^2 (200 N/mm^2) this tendon was in a position to carry 98.7 % of its static breaking load.

Disposition of Bundle					Fatigue Test					Breaking Test after Fatigue	
TYPE	NUMBER OF WIRES	STEEL GRADE	AVERAGE TENSILE STRENGTH $\bar{\beta}_Z$	CALCULATED BREAKING LOAD z_u	UPPER STRESS σ_u	AMPLITUDE $\Delta\sigma$	NUMBER OF CYCLES	NUMBER OF FAILURES	REDUCTION OF STEEL AREA	MEASURED BREAKING LOAD z_u'	DAMAGE $\frac{z_u - z_u'}{z_u}$
	mm	kp/mm^2	kp/mm^2	Mp	kp/mm^2	kp/mm^2	N	n	%	Mp	%
HiAm	295Ø7	140/160	169	1880	56	20	2×10^6	3	1.0	1856	1.3
HiAm	295Ø7	140/160	178	1980	59	20	2×10^6	1	0.3	1974	0.3
HiAm	19Ø7	150/170	179	128	60	20	2×10^6	0	0	128	0
DINA	102Ø7	150/170	179	688.6	60	20	2×10^6	0	0	688.6	0
DINA	55Ø7	150/170	175	363	110	25	2×10^6	0	0	363	0

Table 3 Results of static and fatigue tests on HiAm and DINA tendons

This is an important characteristic of tensile members composed of a multitude of identically sized and loaded wires. Even after fatigue loading under service, at the most only a small number of the component wires may fail and the member itself is still capable of withstanding pratically the entire original breaking load.

3. DESIGN ASSUMPTIONS

3.1 Static loads

The maximum stresses in the tendons max.σ caused by the design loads should be limited to the permissible value perm.σ laid down in the specifications. In some cases it may be necessary to consider additional stresses caused by angular variations of the tendon in the vicinity of anchorages. In the case of the Save Bridge, Belgrade [7] and the Lyne St. Bridge [8] the maximum stresses in the extreme wire caused by local bending amounted to 10-20 % of the axial stresses. Usual practice is to limit the tendon stresses caused by axial tensions to 0.45 of the ultimate tensile strength of the wire. For cold drawn high tensile steel wire quality St 1500/1700 shown in Table 2 this works out to 765 N/mm^2.
It should be noted that at stress levels of 0.45 β_z in the wire the effects of creep can be neglected and that the tendon may be considered to behave elastically up to the design loads.

3.2 Fatigue loads

Stress variations $\Delta\sigma$, when repeated over a large number of load cycles, lead to a damage of the material so stressed. In the case of stay tendons the damage may sometimes result in a small number of wire breakages. The aim of designing against fatigue in tendons should be to avoid or to limit this damage to a very small value during the life time of a bridge so that the tendon remains largely intact even after being subject to the loading which caused the damage.
The designer will therefore need to have a curve relating the permissible stress range $\Delta\sigma = 2\sigma_A$ to the number of load cycles N for which the damage D $\leqq$ say 5 %. Such a curve is shown in Fig.16 and has been deduced from the 5 % fractile curve (intrinsic fatigue strength) for the basic wire material used for the tendon.

$$\Delta\sigma_{Tendon} = [\Delta\sigma_{Wire} - c]; \qquad c \cong 140 \text{ N/mm}^2$$

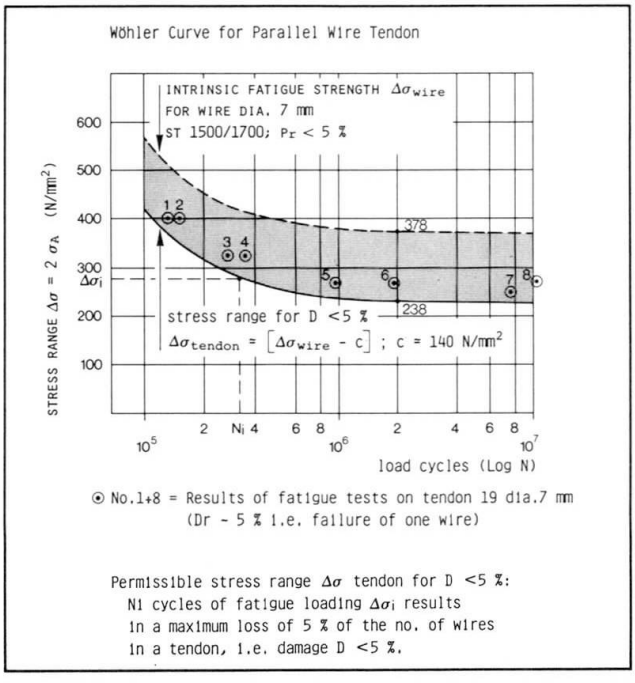

Any fatigue load ($\Delta\sigma$, N) on or below this curve will result in, at the most, a loss of 5 % of the number of wires in a tendon which can subsequently still resist at least 95 % of its original breaking load.
Results of a series of tests on short (l=3000 mm) HiAm tendons are also plotted on this figure. It can be seen that the value of c chosen for these tendons is adequate. It is worth noting in this context that tests on short tendons generally yield lower values of $\Delta\sigma$ since they are very sensitive to small manufacturing tolerances.

Fig.16

The present procedure when designing against fatigue is to determine the max. stress range max.$\Delta\sigma$ in a tendon and to read off the related number of load cycles N from the tendon Wöhler curve. This is compared with a specified value of N. However, this appears a severe condition to be checked for since the value of max.$\Delta\sigma$ is only a peak value in a load collective which occurs during the life time of a bridge.
Using the Palmgren-Miner hypothesis of linear accumulation of damage and the Wöhler curve for constant stress range it is possible to derive a fatigue life curve (max.$\Delta\sigma$, $\overline{N}$) for any desired load collective. Fig.17 shows how the Wöhler curve of Fig.16 drawn to a log-log scale can be represented by 2 straight lines. The curve can be described by the equations

$$N = N_D \cdot \left(\frac{\max.\Delta\sigma}{\Delta\sigma_D} \right)^{-k} \qquad (N < N_D = 10^6)$$

$$\Delta\sigma_D = \text{constant} \qquad (N > N_D = 10^6)$$

and is valid for a load collective p = 1.0, i.e. constant stress range max.$\Delta\sigma$.

A load collective p = 0.5 for a block of 10^6 cycles is also shown in Fig.17. The peak value max.$\Delta\sigma$ of the stress range is the same as for load collective p = 1.0, but occurs only once (10°). The minimum value of the stress range is 0.5•max.$\Delta\sigma$. The procedure [9] for deriving the fatigue life curve for this load collective can best be described with reference to, say, the stress range level max.$\Delta\sigma$ = 350 N/mm^2. The load-collective is described by the continuous curve which dips from a maximum value of 350 N/mm^2 to a minimum value of 0.5 • 350 N/mm^2. This range between 350 and 175 N/mm^2 is divided into a convenient number of steps. For each of these steps the number of load cycles n_i is read off and the partial damage n_i/N_i calculated. Obviously $\Sigma n_i = 10^6$ cycles. The cumulative damage $S = \Sigma n_i/N_i$ related to the block of 10^6 cycles can then be calculated. The Miner condition $\overline{S} = 1.0$ is fulfilled by a value $\overline{N} = 10^6/S$ which gives a point (350, $\overline{N}$) on the fatigue life curve. This procedure is repeated for other values of max.$\Delta\sigma$.

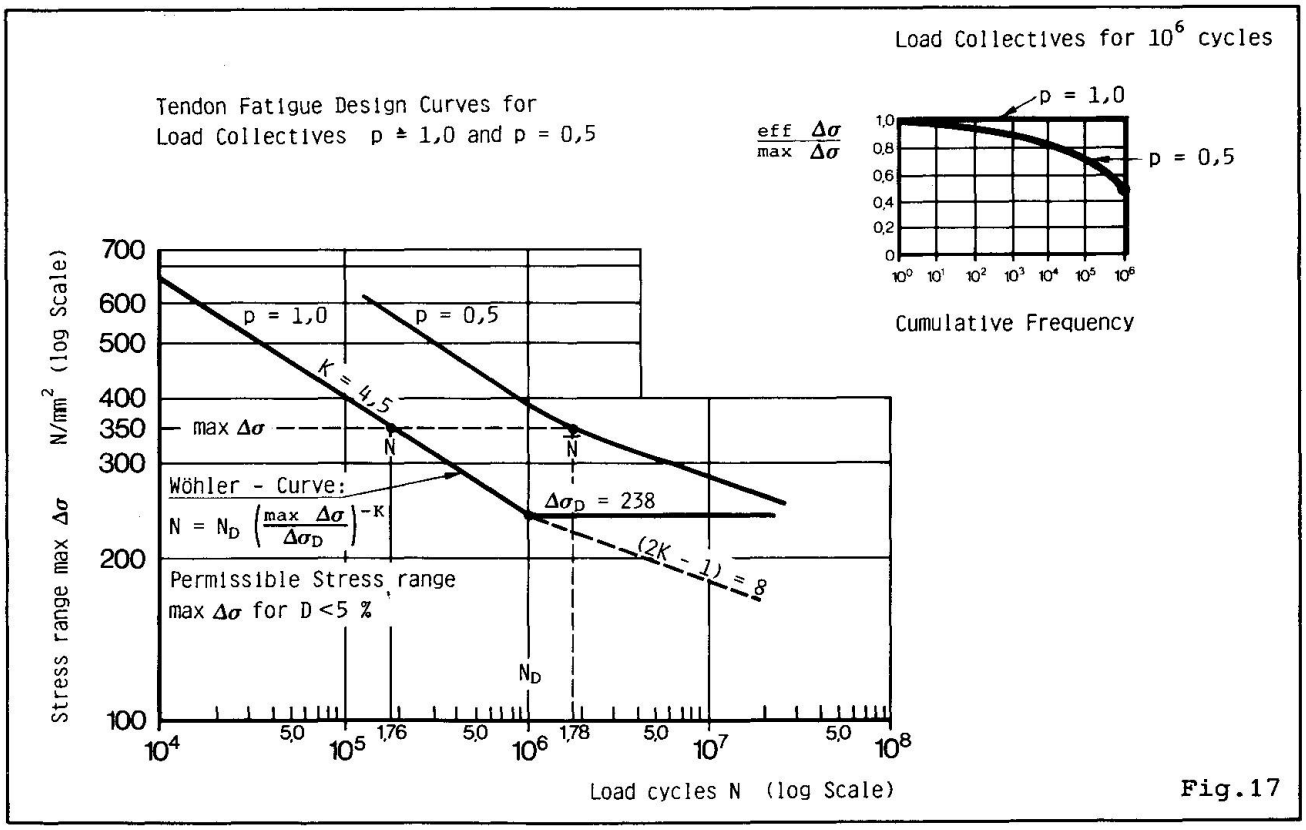

Fig.17

The effect of stress ranges lying below the endurance limit value $\Delta\sigma_D$ has been included by using the fictitious curve shown dashed according to the procedure suggested by Haibach [10]. The fatigue life curve (max.$\Delta\sigma$, $\overline{N}$) shows that for the load collective p = 0.5 shown in Fig.17 values of $\overline{N}$ are obtained which lie considerably above the values of N read off the Wöhler curve p = 1.0.

4. CONCLUDING REMARKS

It is well-known that fatigue loading causes damage to the material on which it acts. When designing stay tendons against fatigue, the principle of limiting such a damage in each tendon to a small value should be adopted and the tendon construction so chosen that a substantial load carrying capacity is still available in it even after the damage has occurred.

The parallel-wire HiAm and DINA tendons fulfil these requirements admirably in that each tendon is composed of a multitude of wires carefully chosen for their high intrinsic fatigue resistance. Using the limited damage concept outlined in this paper it is possible to guarantee that none, or at the most, only a very small number of wires in any tendon cross-section become ineffective under fatigue loads and the tendon as a whole remains intact during the life time of the structure.

REFERENCES

[1] Birkenmaier, M.: Fatigue resistant tendons for cable-stayed construction. IABSE Proceedings P-30/80, May 1980

[2] Hajdin, N., Jevtovic Lj.: Eisenbahnschrägseilbrücke über die Save in Belgrad. Der Stahlbau 47 (1978), Heft 4.

[3] Hajdin, H.: Highway Bridge "23 October" over the Danube at Novi Sad. Proc. 6th Yugoslav Congress of Structural Engineers, Bled 1978. (in Serbo-Croatian).

[4] Concrete Society: All-concrete cable-stayed railway bridge. Concrete Vol. 13, April 1979, No.4.

[5] Deubelbeiss, E.: Dauerfestigkeitsversuche mit einem modifizierten Treppenstufenverfahren. Materialprüfung 16 (1974), No.8.

[6] Nürnberger, U., Wiume, D.: Möglichkeiten des Korrosionsangriffes bei Seilen und Bündeln. Berichtsband aus der Vortragsveranstaltung Seile und Bündel im Bauwesen, Haus der Technik, Essen. September 1981.

[7] Kollbrunner, C. F., Hajdin, N., Stipanic, B.: Contribution to the analysis of cable-stayed bridges, No.48. Institut für bauwissenschaftliche Forschung Stiftung Kollbrunner/Rodio, Zürich, November 1980.

[8] Private communication from K. Kretsis, October 1981.

[9] Schütz, W.: Lebensdauer-Berechnung bei Beanspruchungen mit beliebigen Last-Zeit-Funktionen. VDI Berichte Nr. 268, 1976.

[10] Haibach, E.: Modifizierte lineare Schadensakkumulations-Hypothese zur Berücksichtigung des Dauerfestigkeitsabfalls mit fortschreitender Schädigung. LBF-TM Nr. 50/70.

Verbesserung des Schwingfestigkeitsverhaltens von Spannkabel- und Seilverankerungen

Improvement of the Fatigue Strength of Anchorages for Tendons and Ropes

Amélioration de la résistance à la fatigue des ancrages pour câbles de précontrainte et haubans

W. KÖHLER
Dipl. Ing.
Otto-Graf-Institut
Stuttgart, BRD

U. NÜRNBERGER
Dr. -Ing.
Otto-Graf-Institut
Stuttgart, BRD

ZUSAMMENFASSUNG

Es wird über Untersuchungen zur Verbesserung der Dauerschwingfestigkeit von Keil- und Metallvergussverankerungen berichtet. Massgebend für das Schwingfestigkeitsverhalten ist die Schädigung der Drähte durch Reibkorrosion infolge von Relativverschiebungen unter Querpressung. Als Ergebnis der Untersuchungen werden dynamisch verlustfreie Verankerungen vorgestellt, bei denen entweder die Relativverschiebungen weitgehend ausgeschaltet werden, oder bei denen der Sauerstoff ferngehalten wird. Beide Massnahmen verringern die Reibkorrosion auf ein unbedeutendes Mass, so dass die Dauerschwingfestigkeit der Drähte in den Verankerungen nicht abgemindert wird.

SUMMARY

Investigations were performed in order to improve the fatigue strength of wedge shaped and cast metal anchorages. The fatigue strength is primarily influenced by fretting corrosion of the wires due to relative displacement whilst under lateral pressure. Dynamic, zero-loss anchorages, in which either the relative displacements or the oxygen were eliminated, have been developed as a result of the investigations. Both measures reduce the fretting corrosion to an insignificant level so that the fatigue strength does not diminish in the anchorage.

RESUME

Des études ont été réalisées pour améliorer la résistance à la fatigue des ancrages à clavettes ou coulés. La résistance à la fatigue est essentiellement influencée par l'endommagement des fils causé par la corrosion de frottement due aux déplacements relatifs sous pression transversale. Les ancrages dynamiques, sans perte, dans lesquels les déplacements relatifs ou l'oxygène ont été éliminés, sont présentés comme résultats de ces études. Les deux mesures réduisent la corrosion de frottement à une valeur négligeable de sorte que la résistance à la fatigue des fils dans les ancrages n'est pas diminuée.

1. EINFÜHRUNG

Spannglieder für den Spannbetonbau mit nachträglichem Verbund werden überwiegend in Keil-, Klemm-, Gewinde-, Preßhülsen- oder Köpfchenverankerungen verankert, während Seile für Brücken oder Seilkonstruktionen häufig durch Metall- oder Kunststoffverguß verankert werden (Bild 1).

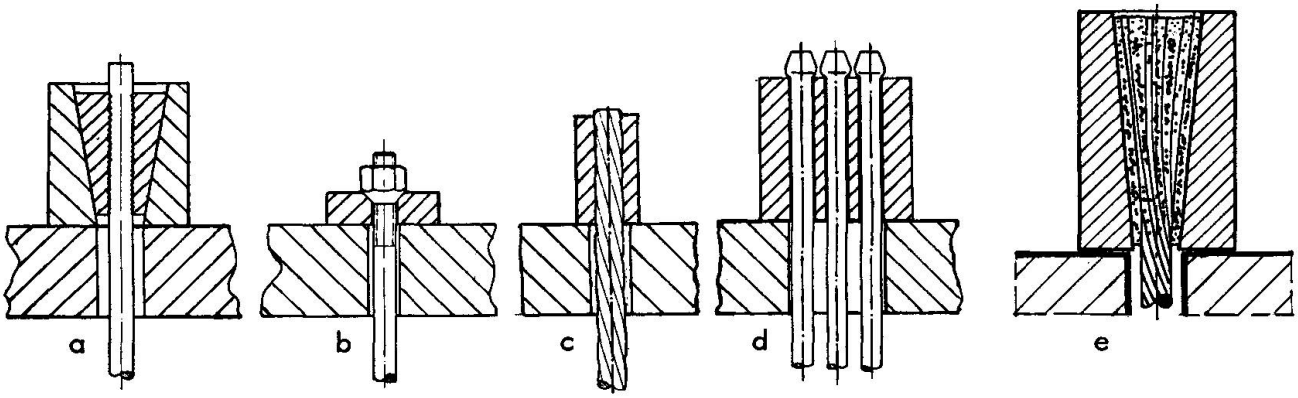

Bild 1. Beispiele für Verankerungen von Spanngliedern und Seilen

In diesen Verankerungen sind entsprechend der hohen Zugfestigkeit der Drähte, Litzen oder Stäbe neben großen statischen Lasten, häufig auch hohe dynamische Lasten zu verankern. So ist z.B. für die Dimensionierung der Abspannseile von Schrägkabelbrücken in der Regel die Dauerschwingfestigkeit der Seilverankerungen maßgebend. Wie aus der Tabelle 1 ersichtlich ist, ist die Dauerschwingfestigkeit der herkömmlichen Spanngliedverankerungen und der Metallvergußverankerungen von Seilen deutlich kleiner als die Dauerschwingfestigkeit der Drähte und Litzen selbst.

Tabelle 1. Dauerschwingfestigkeit von Spanndrähten und Litzen sowie von herkömmlichen Verankerungen

Bauteil	Dauerschwingfestigkeit $2\sigma_A$ in N/mm^2
Spanndrähte (kaltgezogen oder vergütet)	250 - 550
Spanndrahtlitzen	200 - 300
Spanngliedverankerungen nach Bild 1a bis 1d	80 - 150
Metallvergußverankerungen nach Bild 1e	120 - 140

In den folgenden Ausführungen werden die Ursachen für die relativ niedrigen Dauerschwingfestigkeiten der Keil- und Metallvergußverankerungen aufgezeigt sowie Vorschläge für Verankerungen mit verbesserter Dauerschwingfestigkeit gemacht. Diesen Ausführungen liegen umfangreiche Grundsatzuntersuchungen zugrunde, die im Otto-Graf-Institut durchgeführt wurden.

2. KEILVERANKERUNGEN

Es herrschte bisher die Meinung vor, daß die Dauerschwingfestigkeit der Keilverankerungen in erster Linie beeinflußt wird durch die Kerben, die von den Keilzähnen in den Spannstahl eingeprägt werden, und durch die hohe Querpressung am Beginn der Verankerung. Entsprechend werden bei den bekannten Keilverankerungen die Zähne an der Keilspitze stumpf ausgebildet. Außerdem ist die Keilspitze durch abnehmende Zahnhöhe ausgerundet oder abgefast (Bild 2a). Dadurch daß die Keilneigung etwas größer gewählt wird als die Konusneigung des Ankerkörpers, erreicht man eine Begrenzung der Querpressung an der Keilspitze und damit eine gleichmäßigere Kraftübertragung über die gesamte Keillänge. Auch eine große Keillänge führt zu kleinerer Querpressung.

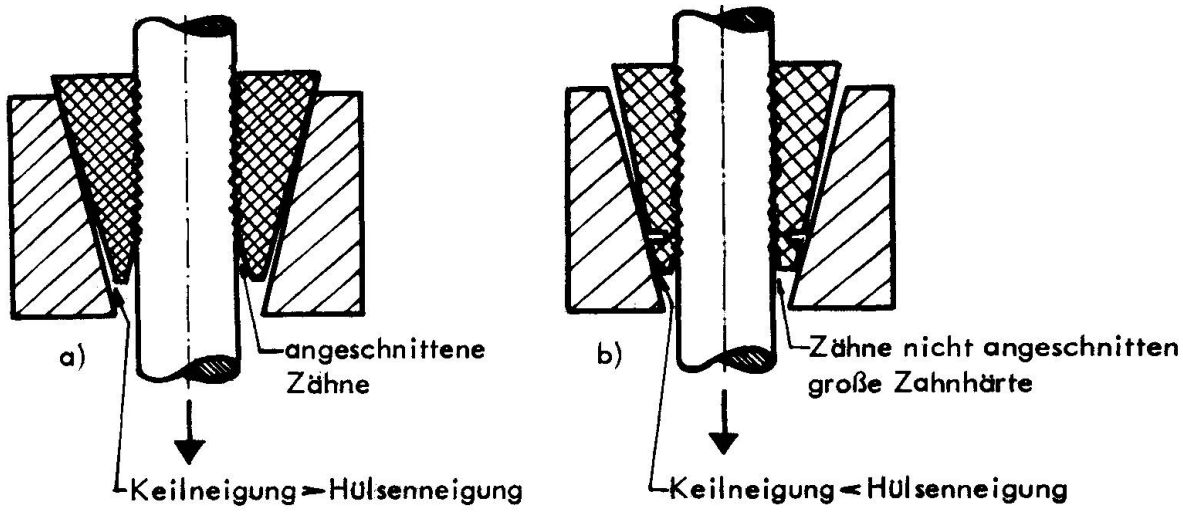

Bild 2. Herkömmliche (a) und dynamisch verlustfreie (b) Keilverankerung

Um den Einfluß von Querpressung, Kerbwirkung und Reibkorrosion (Relativverschiebung bei gleichzeitiger Querpressung) auf die Dauerschwingfestigkeit einzeln untersuchen zu können, wurden die im folgenden beschriebenen Versuchsreihen durchgeführt. Das Bild 3 zeigt die verwendeten Versuchsanordnungen. Die Querpressung wurde jeweils durch angeklemmte gleichartige Drähte erzeugt. Der Einfluß der Querpressung allein wurde durch zwei Versuchsvarianten (Bilder 3a und 3b) untersucht. Im Falle des längs angepreßten Drahtes betrug die

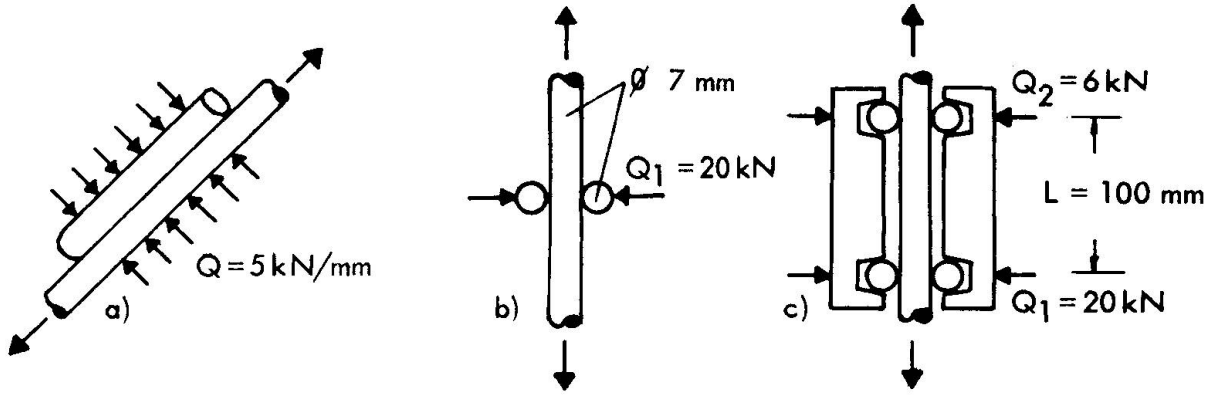

Bild 3. Versuchsanordnungen für die Dauerschwingversuche mit Längspressung (a), mit Querpressung (b) und mit Relativverschiebungen bei gleichzeitiger Querpressung (c)

Querkraft 5 kN/mm und im Falle der quer angepreßten Drähte betrug die Querkraft 20 kN. Die so gepreßten Drähte wurden im Zugschwellversuch ($\sigma_o = 0{,}55\ R_m$) geprüft. Es zeigte sich, daß die Drähte die hohen, bereits zu merklichen plastischen Verformungen der Drahtoberfläche führenden Querpressungen ohne wesentliche Abminderung der Dauerschwingfestigkeit ertragen können.

Der Einfluß von Relativverschiebungen bei gleichzeitiger Querpressung wurde durch Versuche nach Bild 3c untersucht. Hier wurden Drähte, die im Abstand von 100 mm in einem starren Rahmen gehalten wurden, mit unterschiedlich großen Querkräften von 6 bzw. 20 kN quer angepreßt, so daß sich der Prüfdraht im Dauerschwingversuch relativ zu den mit der kleineren Querkraft angepreßten Drähten verschieben konnte. Infolge der sich hier einstellenden Reibkorrosion nahm die Dauerschwingfestigkeit um mehr als 50 % gegenüber jener des unbeeinflußten Drahtes ab. Die Abminderung der Dauerschwingfestigkeit ist kleiner, wenn die Reibung durch Schmieren vermindert wird oder wenn die Beilagedrähte z.B. galvanisch verzinkt oder cadmiert sind.

Der Einfluß von Kerben bei gleichzeitiger Querpressung wurde wie folgt untersucht. Von quergezahnten Keilen (Zahnwinkel 90°, Radius der Zahnspitze 0,03 mm, Oberflächenhärte ca. 900 HV 1) zur Verankerung von Drähten Ø 12 mm wurden sämtliche Zähne mit Ausnahme des mittleren Zahns abgearbeitet. Zwei dieser Keile wurden dann gegenüberliegend mit 20 bzw. 80 kN Querkraft auf Drähte Ø 12 mm aufgepreßt. Dabei entstanden Kerben von ca. 0,1 bzw. 0,3 mm Tiefe. Die Drähte wurden dann mit den aufgepreßten Keilen im Dauerschwingversuch geprüft. Die Drähte brachten unbeeinflußt durch die Kerben in der freien Drahtlänge. Das günstige Ergebnis ist darauf zurückzuführen, daß der Drahtwerkstoff beim Einpressen des Keilzahns im Kerbgrund verfestigt wird. Diese Verfestigung und Gefügeverdichtung verhindert das Entstehen von Dauerschwinganrissen.

Werden die gleichen einzahnigen Keile derart verkantet auf die Drähte aufgepreßt, daß ein Keilende die Drahtoberfläche berührt und beim Dauerschwingversuch dort reibt, so brechen die Drähte an diesen Reibstellen (Bild 4). Die Abminderung der Dauerschwingfestigkeit infolge dieser Reibkorrosion beträgt bis zu 50 %.

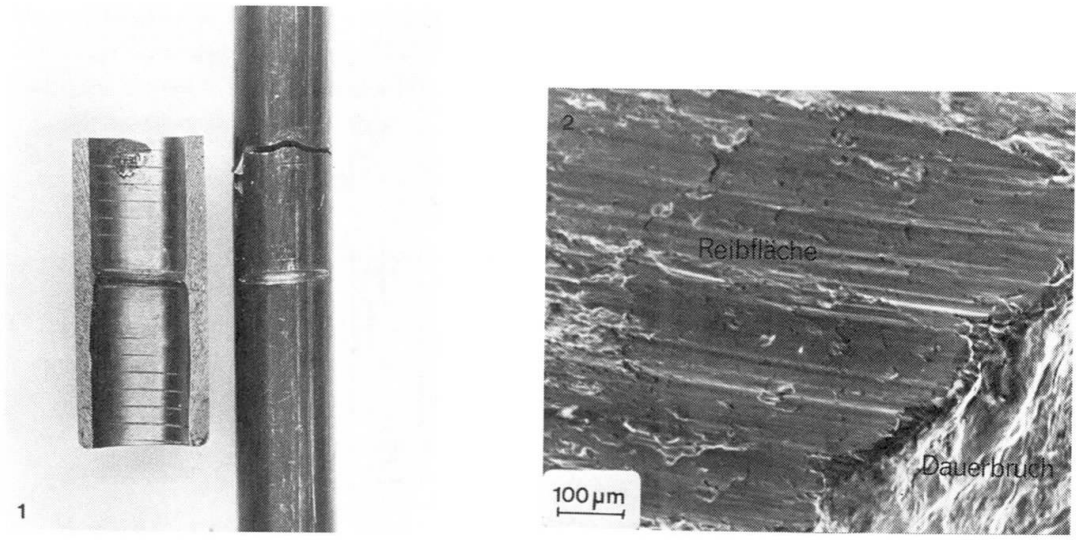

Bild 4. Dauerschwingversuch mit verkantet aufgesetztem einzahnigen Keil. Dauerbruch an der Reibstelle

Ähnlich ungünstig verhalten sich herkömmliche Keilverankerungen. Das Bild 5 zeigt die Verhältnisse für einen 44 mm langen Keil auf einem Draht Ø 12 mm. Da die Keilneigung größer war als die Konusneigung, gruben sich die Zähne an der Keilspitze nur ungenügend in den Draht ein. Entsprechend bildete sich dort während des Dauerschwingversuchs Reibkorrosion aus mit entsprechend ungünstigem Dauerschwingverhalten.

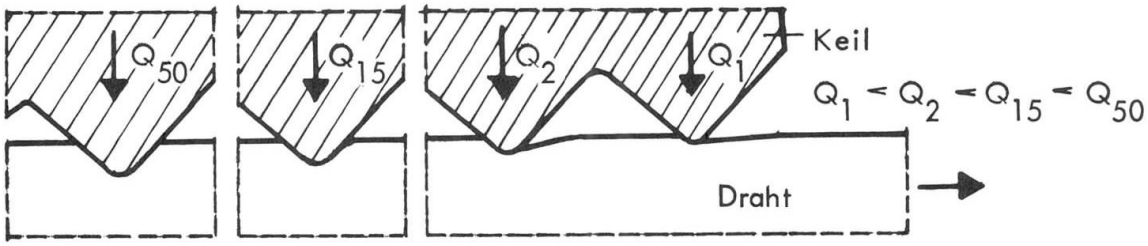

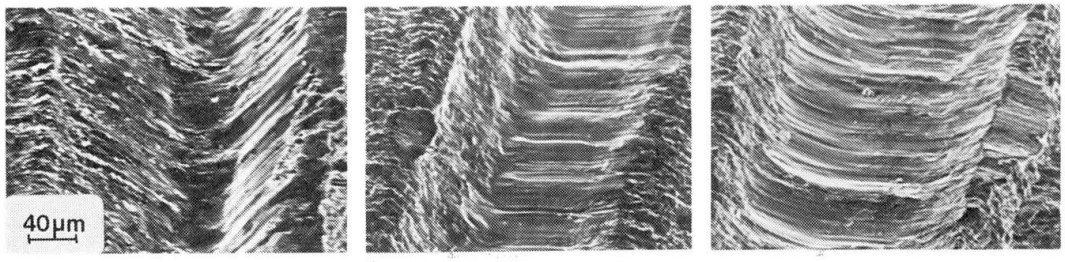

50. Zahneindruck 15. Zahneindruck 2. Zahneindruck

Bild 5. Eindrücke von Keilzähnen im Spanndraht Ø 12 mm

Zusammenfassend ist zu den hinsichtlich ihres Einflusses auf die Dauerschwingfestigkeit von Keilverankerungen untersuchten Faktoren festzustellen:

- Die durch die Keilzähne in die Drahtoberfläche eingeprägten Kerben beeinflussen die Dauerschwingfestigkeit nicht.
- Die Höhe der Querpressung und das Spannungsgefälle längs des Keiles beeinflussen die Dauerschwingfestigkeit im Gebrauchslastbereich nur unwesentlich.
- Die Dauerschwingfestigkeit wird überwiegend durch Relativverschiebungen zwischen Spannstahl und Keil und der daraus resultierenden Reibkorrosion abgemindert. Diese Abminderung der Dauerschwingfestigkeit ist bedingt durch Anrisse in der Drahtoberfläche und eine sich unterhalb der Reibfläche einstellende Zerrüttungszone.

Unter Reibkorrosion ist definitionsgemäß eine Schädigung von Werkstoffen zu verstehen, deren Oberflächen bei gleichzeitig wirkender Normalkraft Scheuerbewegungen kleinsten Ausmaßes gegen einen starren Reibkörper ausführen. Bei metallischen Werkstoffen ist die Schädigung durch Reibkorrosion um so ausgeprägter, je höher die Flächenpressung und je größer der Reibweg ist. Die Frequenz der Reibbewegungen ist ebenfalls zu beachten. Mit abnehmender Frequenz nimmt der Einfluß der Reibkorrosion auf die Dauerschwingfestigkeit zu, da dann der Korrosionseinfluß stärker zum Tragen kommt. D.h. unter praxisnahen Bedingungen ist eher mit Reibkorrosion zu rechnen als bei der Prüfung im Labor. Die Bilder 6 und 7 zeigen zwei Beispiele von durch Reibkorrosion geschädigten Drahtoberflächen. Die Pfeile verweisen auf Anrisse, die senkrecht zur Reibrichtung verlaufen.

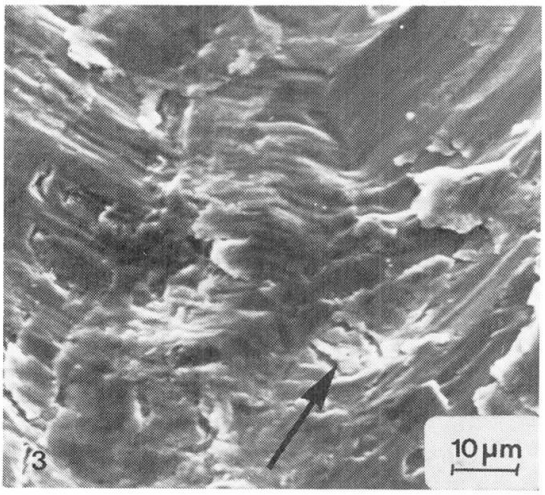

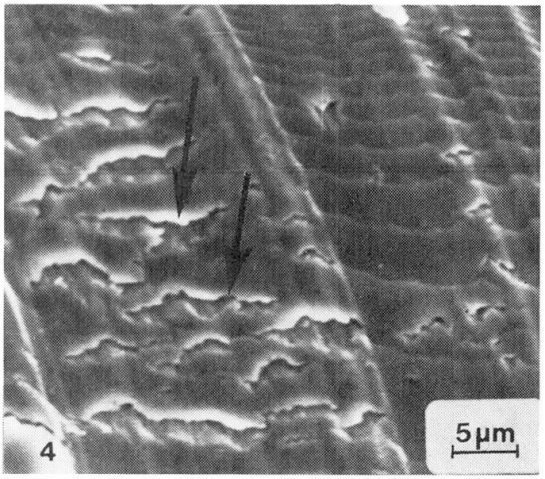

Bilder 6 und 7. Reibkorrosion auf kaltgezogenem Spanndraht

Nach den vorstehenden Ausführungen kann die Dauerschwingfestigkeit von Keilverankerungen durch Maßnahmen verbessert werden, die die Relativverschiebungen und damit die Reibkorrosion beseitigen oder zumindest auf ein unbedeutendes Maß reduzieren. Dazu müssen die Keilzähne an der Keilspitze tief in den Draht eindringen und auf Dauer in dieser Lage gehalten werden. Wie Bild 2b zeigt, kann dies durch folgende Maßnahmen erreicht werden:
- Die Keilzähne müssen an der Keilspitze scharfkantig und in voller Höhe ausgebildet sein,
- große Oberflächenhärte der Keilzähne,
- hohe Querpressung an der Keilspitze, diese wird erreicht durch nicht zu große Keillänge, geringe Reibung zwischen Keilrücken und Konusfläche und durch eine gegenüber der Konusneigung geringfügig kleinere Keilneigung,
- der erste tragende Zahn muß ausreichend abgestützt sein, d.h. der Keil muß vor dem ersten Zahn noch einen kurzen ungezahnten Bereich aufweisen, der den Draht jedoch nicht berühren darf.

Durch zahlreiche Versuche konnte nachgewiesen werden, daß nach diesen Grundsätzen gestaltete Keilverankerungen dynamisch verlustfrei arbeiten: in Dauerschwingversuchen mit derart verankerten Drähten brachen die Drähte unbeeinflußt durch die Verankerungen in der freien Drahtlänge.

Insbesondere bei Litzen und dünnen Drähten zeigte sich, daß durch derartige Verankerungen die statische Tragfähigkeit infolge der Kerbwirkung und hohen Querpressung im Krafteinleitungsbereich abgemindert wird [3] . Hier wurden mit herkömmlichen Keilen hohe Dauerschwingfestigkeiten erzielt, wenn die gesamte Keilverankerung mit einem auch bei dynamischer Beanspruchung gut haftendem Kunststoff verfüllt und abgedichtet wird [1]. In diesem Fall wurde der für die Reibkorrosion notwendige Luftsauerstoff ferngehalten.

3. METALLVERGUSSVERANKERUNGEN

Als Ursache für das schlechte Dauerschwingverhalten der Metallvergußverankerungen wurden bisher angesehen
- Gefügeveränderungen durch die Temperaturbeanspruchung beim Vergießen,
- plastische Verformung der Drähte beim Herstellen des Seilbesens,
- Aufrauhung der Drahtoberfläche durch das Beizen,
- die spröde Hartzinkschicht der verzinkten Drähte,

- die hohe Querpressung und die plötzliche Krafteinleitung am Eintrittsbereich des Seils in die Hülse,
- Relativverschiebungen zwischen Draht und Vergußmetall und
- Reibkorrosion.

In Dauerschwingversuchen mit auf 400°C angelassenen, hin- und zurückgebogenen, gebeizten bzw. feuerverzinkten Spanndrähten zeigte sich keine Verschlechterung der Dauerschwingfestigkeit gegenüber dem unbeeinflußten Spanndraht. In den Fällen des Anlassens und Feuerverzinkens war sogar eher eine Verbesserung der Dauerschwingfestigkeit festzustellen. Auch hohe Querpressungen und eine plötzliche Krafteinleitung wirken sich nicht nachteilig auf die Dauerschwingfestigkeit aus, wie im Abschnitt 2 bereits dargelegt wurde. Als dominierender Einfluß auf die Dauerschwingfestigkeit ist die Reibkorrosion infolge der Relativverschiebungen zwischen den Drähten und dem Vergußmetall unter Querpressung anzusehen.

Der Einfluß von Relativverschiebungen unter Querpressung wurde mit der im Bild 8 dargestellten Vorrichtung untersucht. Infolge der großen Dehnsteifigkeit der Vorrichtung entstehen Relativverschiebungen zwischen Draht und Reibkörpern bei Spannungsänderungen im Draht.

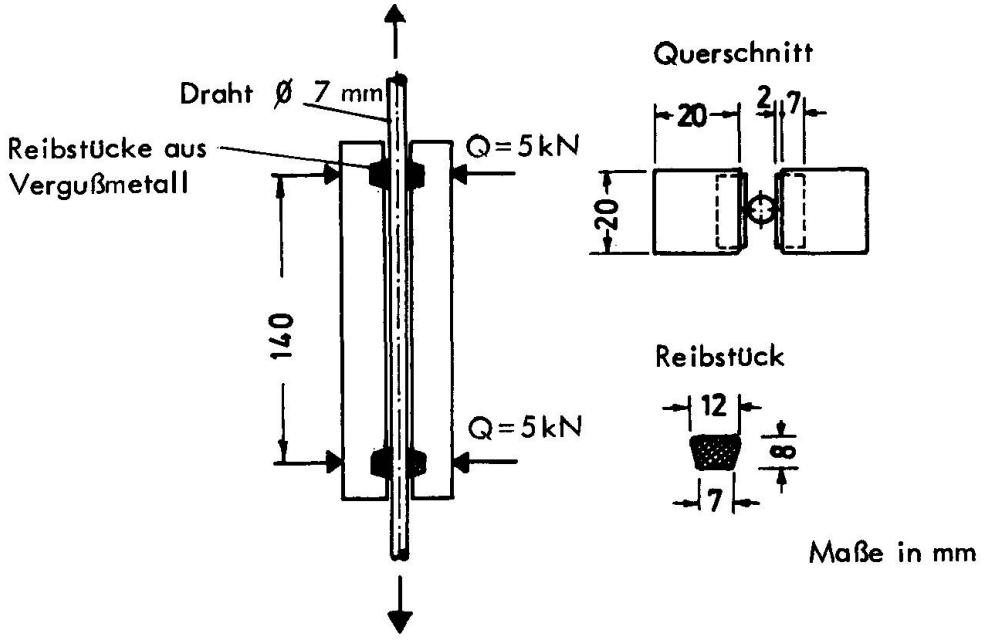

Bild 8. Versuchsanordnung für die Dauerschwingversuche mit Reibkörpern aus Vergußmetall

Es wurden Reibkörper aus einer Bleilegierung (PbSn 10Sb 10) und einer Zinklegierung (ZnAl6Cu1) untersucht. Bei der Verwendung von Reibkörpern aus der Bleilegierung wurde keine Abminderung der Dauerschwingfestigkeit festgestellt, während die Zinklegierung eine etwa 50 %ige Abminderung der Dauerschwingfestigkeit bewirkte. An den geprüften Drähten zeigte sich, daß die Reibkörper aus der Bleilegierung am Draht keine oder nur eine sehr geringe Reibkorrosion bewirkten. Dieses günstige Verhalten ist im wesentlichen auf die guten Schmiereigenschaften der Bleilegierung und auf die geringe Härte der entstehenden Bleioxide zurückzuführen. Hinzu kommt, daß sich die Drähte in die weiche Bleilegierung besser einbetten konnten, so daß die spezifische Pressung bei konstanter Querkraft Q kleiner war als bei der härteren Zinklegierung. Dieser günstige Einfluß wird in wirklichen

Verankerungen weniger ausgeprägt sein, da dort das Vergußmetall weniger gut ausweichen und daher höhere Pressungen übertragen kann. Die Reibkörper aus der Zinklegierung bewirkten dagegen eine erhebliche Reibkorrosion.

Diese Zusammenhänge wurden für eine Metallvergußverankerung mit hoher Dauerschwing- und Dauerstandfestigkeit wie folgt angewendet (Bild 9): Der Eintrittsbereich der Drähte in die Hülse wird auf wenige cm Länge mit einer Bleilegierung vergossen, die keine Reibkorrosion bewirkt. Die übrige Verankerung wird dann mit einer Zinklegierung vergossen, die eine ausreichende Dauerstandfestigkeit besitzt. Versuche mit derart vergossenen Litzen und Paralleldrahtbündeln ergaben bei hohen Schwingbreiten Dauerbrüche in der freien Länge außerhalb der Verankerungen. Die hohe Dauerschwingfestigkeit des zweischichtigen Vergusses gegenüber dem üblichen Verguß mit Zinklegierung ist darauf zurückzuführen, daß der Bleiverguß den Sauerstoff der Atmosphäre von den Reibstellen zwischen Draht und Zinkverguß fernhält. Eine Oxidation des Drahtes und Zinks mit Bildung harter Zinkoxide ist nicht möglich. Somit ist die Schädigung des Drahtes durch Reibkorrosion ganz wesentlich kleiner. Der Eintrittsbereich kann an Stelle der Bleilegierung auch mit einem Kunststoffverguß, z.B. Polyurethan-Zinkchromat oder Epoxidharz-Zinkstaub, abgedichtet werden.

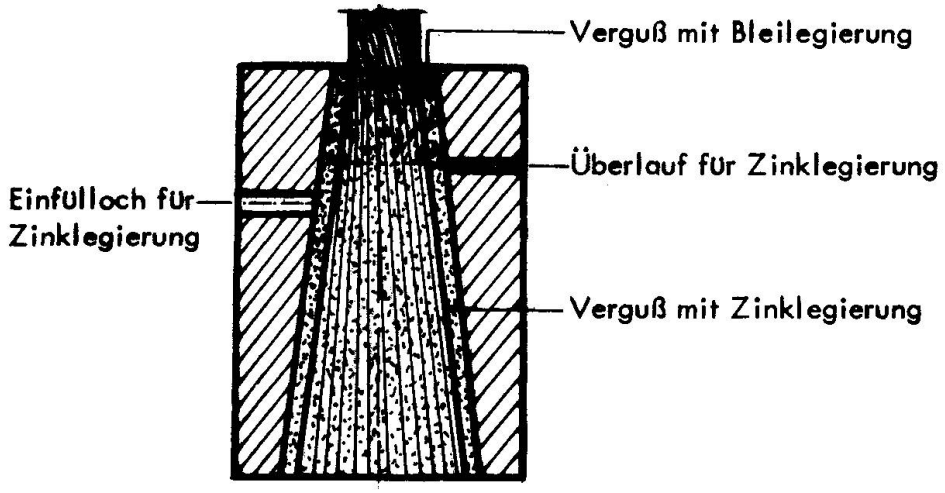

Bild 9. Zweischichtige Metallvergußverankerung

LITERATURVERZEICHNIS

[1] NÜRNBERGER, U; PATZAK, M: Metallische Verankerungen für dynamisch beanspruchte Zugglieder. Mitteilungen 44/1978, SFB 64, Universität Stuttgart.

[2] REHM, G.; NÜRNBERGER, U.; PATZAK, M.: Keil- und Klemmverankerungen für dynamisch beanspruchte Zugglieder aus hochfesten Drähten. Bauingenieur 52 (1978), 287-298.

[3] NÜRNBERGER, U.: Verhalten von Spannstählen in Keilverankerungen unter statischer Belastung. Bauingenieur 56 (1981), 25-32.

[4] PATZAK, M.; NÜRNBERGER, U.: Grundlagenuntersuchungen zur statischen und dynamischen Belastbarkeit von metallischen Drahtseilvergüssen (Vergußverankerungen). Mitteilungen 45/1978, SFB64, Universität Stuttgart.

[5] REHM, G., PATZAK, M., NÜRNBERGER, U.: Metallvergußverankerungen für Zugglieder aus hochfesten Drähten. Draht 28 (1977), 134-141.